University of California, Davis
Atmospheric Boundary Layer Wind Tunnel Facility
Department of Mechanical and Aeronautical Engineering
One Shields Avenue, Davis, California 95616-5294

FINAL REPORT

A WIND-TUNNEL MODEL OF WIND EFFECTS ON AN AIR COOLING CONDENSER

Bruce R. White, Professor

Daeseong Kim, Research Manager

John Christopher Bachman, Undergraduate Associate

Prepared for :

Electric Power Research Institute
3420 Hillview Avenue, P.O. Box 10412,
Palo Alto, California 94303

December 2009

TABLE OF CONTENTS

INTRODUCTION

There will be increasing competition for fresh water supplies in the future, due to several key demographic, technical, and regulatory factors. These factors include; (1) rapid population growth in the United States (U.S.), particularly in the southwestern states; (2) the resulting growth of electricity demand and water consumption for power generation and other uses; (3) periodic drought conditions that may increase in severity as a result of global climate change; and, (4) regulatory requirements that limit thermal emissions and restrict both water supplies and effluent quality. Since the water consumption of thermoelectric power plants and the electricity demand are highly linked, it is imperative to develop a new power plant that can effectively utilize a minimal amount of water.

Thermoelectric power plants, such as nuclear, and many types of fossil fuel plants are equipped with a cooling system. Typical and efficient cooling systems include a once-through cooling system and an evaporative wet cooling tower. However, once-through cooling systems withdraw significant volumes of water to cool the condenser and is subject to Sections 316a (thermal) and 316b (fish impingement and entrainment) of the U.S. Clean Water Act. Wet cooling towers consume 85% to 90% of the water withdrawn via evaporation and would be unfavorable in a water-constrained environment. The direct dry cooling systems are somewhat less effective than once-through cooling systems, although are a good alternative when trying to minimize water consumption.

An air cooling condenser (ACC) is the core of any direct dry cooling system. The air cooling condenser shown in Figure 1 uses space saving A-frame fin tubes. The steam exhausted from the turbine flows through the steam header on top of the A-frame and then flows diagonally down through finned tubes. Cool air is then drawn by fan units upward across the heat exchanging tubes and condenses the steam. In a typical ACC system, a significant number of these fans and A-frame fin tubes are usually installed on a rectangular platform hundreds of feet above the ground. The number of fans and tubes depends on the plant's capacity. The ACC platform can be installed on the top of the boiler house, if the plant is small. At large power plants, the ACC platforms are located near the boiler house in various forms: single line, two lines, or in two-dimensional grid formations.

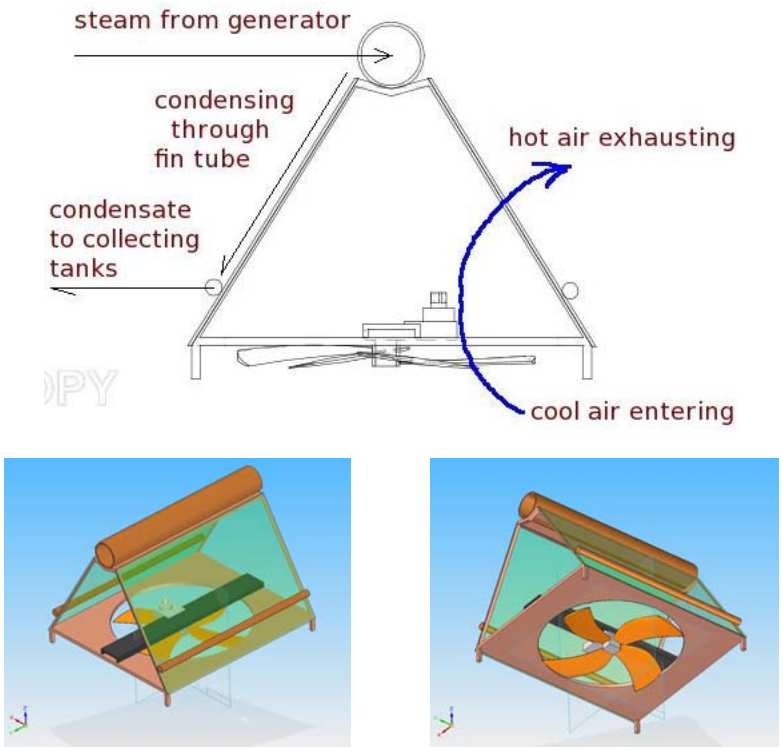

Figure 1 Schematic Drawing of an Air Cooling Condenser Cell

Under stable conditions with no wind, the backpressure can be easily controlled by changing the air flow rate through the ACC unit. In reality, the wind blows a majority of the time and a number of studies have argued that the wind, in general, negatively affects the performance of ACC systems. As it is shown in Table-1, many experimental and computational studies have investigated the wind effects on ACC systems and the possible mitigation plans. However, an investigation of practical wind effect is scarce due to the ACC unit's site specific meteorological conditions. The varying meteorological conditions make it impractical to apply one case to another.

The objective of the present study is to physically model an air cooling condenser and to assess potential mitigation measures to reduce the impact of the wind on the ACC's performance. The present study supports Electric Power Research Institute (EPRI)'s participation in the Electricite de France-EPRI Advanced Cooling Technology Partnership, which is to assess and develop advanced power plant cooling technology concepts for a water-constrained future. A parallel contract will extend EPRI report 1005358, "Comparison of Alternative Cooling Technologies for U.S. Power Plants: Economic, Environmental, and Other Tradeoffs," to nuclear

power plants and evaluates advanced power plant cooling concepts for thermoelectric power plants.

The work scope of the present study includes: (1) development and construction of simplified scale models of power plants with both single-unit and dual-unit ACCs; (2) wind-tunnel testing of the scale models to assess high wind impacts on air-flow around and within ACC cells; (3) wind-tunnel testing of mitigation measures to reduce wind impacts on ACC performance; and, (4) applying the field data to the wind tunnel study results.

Table 1 Summary of the present and previous investigations

author(s)	year	study type	u_e/U range	cooling tower type	fan array	study parameters※
Present	2009	experimental	0.89~4.61	mechanical draft A-frame modules	6×5	re-circulation ratio ($R \equiv \dot{m}_i / \dot{m}_e$)
Gu *et al*.	2007	experimental	0.07~1 (revised)	mechanical draft A-frame modules	4 of 8×7	re-circulation ratio ($R \equiv C_R / \overline{C}_R$)
Zhai & Fu	2006	experimental & numerical	0.24, 0.26, & 0.36 (revised)	natural draft round	1×2	total heat exchange rate ($Q_{w/w} - Q_{w/nw} / Q_{nw} - Q_{w/nw}$)
Bornoff	2001	numerical	2.3 (revised)	mechanical draft round tower	1×1, 1×2, 2×1	non-dimensional temperature
Duvenhage & Kroger	1996	numerical	3.3~6.3 (revised)	mechanical draft flat frame bank	2×16	re-circulation effectiveness $\left(e_r \equiv (T_{mao} - T_{mai}) / (T_{ao} - T_{ai})\right)$
Derksen *et al*.	1996	experimental	0.82 (revised)	mechanical draft flat frame	1×2	flow speed at air intake $\left(T^* \equiv \frac{C - C_a}{C_0 - C_a} = \frac{T - T_a}{T_0 - T_a}\right)$
du Preez & Kroger	1993	experimental & numerical	U = 0~11 m/s	natural draft round	Scattered 6 cells	temperature differences $\left(\Delta T = (T_{wo} - T_{ai})_w - (T_{wo} - T_{ai})\right)$
Hitchman & Slawson	1987	experimental	0.3~1.6	mechanical draft flat frame	1×1 & 1×2	re-circulation ratio $\left(R \equiv (T_w - T_a) / (T_j - T_a)\right)$
Slawson & Sullivan	1981	experimental	0.5~3.5	mechanical draft flat frame	4 row & 2 row	re-circulation ratio $\left(R_i \equiv (T_{wi} - T_a) / (T_j - T_a)\right)$
Kennedy & Fordyce	1974	experimental	0.3~4 (revised)	mechanical draft round	1×2 & 2×1	re-circulation ratio $\left(R \equiv (T_w - T_a) / (T_j - T_a)\right)$

※ Nomenclatures for each parameter are declared in the corresponding literatures.

WIND TUNNEL MODELING

In order to simulate an atmospheric boundary-layer flow field in a wind tunnel several important similarity criteria have to be met. It is also necessary to consider dynamic and thermal parameters to accurately model the natural processes of flow and diffusion in the atmosphere. Detailed consideration of the criteria and parameters for the present wind-tunnel model includes;

Atmospheric Flow Similarity

Wind-tunnel models of a particular test site are typically several orders of magnitude smaller than full-scale. In order to simulate atmospheric winds in a wind tunnel, certain flow parameters must be satisfied between the model and its corresponding full-scale equivalent. Similitude parameters can be obtained by non-dimensionalizing the equations of motion, which build the starting point for the similarity analysis. Fluid motion can be described by the following time-averaged equations.

Conservation of mass:

$$\frac{\partial \overline{U}_i}{\partial t_i} = 0 \text{ and } \frac{\partial \rho}{\partial t} + \frac{\partial (\rho \overline{U}_i)}{\partial x_i} = 0$$

Conservation of momentum:

$$\frac{\partial \overline{U}_i}{\partial t} + \overline{U}_j \frac{\partial \overline{U}_i}{\partial x_j} + 2\varepsilon_{ijk}\Omega_j \overline{U}_k = -\frac{1}{\rho_0}\frac{\partial \overline{\delta P}}{\partial x_i} - \frac{\overline{\delta T}}{T_0} g\delta_{i3} + \nu_0 \frac{\partial^2 \overline{U}_i}{\partial x_j} + \frac{\partial (\overline{-u_j u_i})}{\partial x_j}$$

Conservation of energy:

$$\frac{\partial \overline{\delta T}}{\partial t} + \overline{U}_i \frac{\partial \overline{\delta T}}{\partial x_i} = \left[\frac{\kappa_0}{\rho_0 c_{p_0}}\right] \frac{\partial^2 \overline{\delta T}}{\partial x_k \partial x_k} + \frac{\partial (-\overline{\theta u_i})}{\partial x_i} + \frac{\overline{\phi}}{\rho_0 c_{p_0}}$$

Where the mean quantities are represented by capital letters while the fluctuating values are represented by lower-case letters. In the momentum equation, δP, ρ_0, T_0, and ν_0 are the deviation of pressure, density, temperature, and kinematic viscosity in a neutral atmosphere, respectively. In the energy equation, ϕ is the dissipation function, $\overline{\delta T}$ is the deviation of temperature from the temperature of a neutral atmosphere, κ_0 is the thermal diffusivity, and c_{p_o} is the heat capacity.

Applying the Boussinesq density approximation, application of the equations is then restricted to fluid flows where $\overline{\delta T} << T_0$. By defining the following non-dimensional quantities

$$\overline{U}_i' = \overline{U}_i' / U_0 \; ; \; u_i' = u_i / U_0 \; ; \; x_i' = x_i / L_0 \; ; \; t' = tU_0 / L_0 \; ; \; \Omega_j' = \Omega_j / \Omega_0 \; ; \; \overline{\delta P}' = \overline{\delta P} / \rho_0 U_0^2 \; ;$$
$$\overline{\delta T}' = \overline{\delta T} / \delta T_0 \; ; \; g' = g / g_0 \; ; \; \overline{\varphi}' = \overline{\varphi} / \varphi_0$$

and then substituting them into the above equations yield the following dimensionless form of the equations of motion.

Continuity Equation:

$$\frac{\partial u_i'}{\partial x_i'} = 0 \text{ and } \frac{\partial \rho'}{\partial t'} + \frac{\partial (\rho' u_i')}{\partial x_i'} = 0$$

Momentum Equation:

$$\frac{\partial \overline{U}_i'}{\partial t'} + \overline{U}_j' \frac{\partial \overline{U}_i'}{\partial x_j'} + \frac{2}{Ro} \varepsilon_{ijk} \overline{U}_k' \Omega_j' = -\frac{\partial \overline{\delta P}'}{\partial x_i'} + \frac{1}{Fr^2} \overline{\delta T}' \delta_{3i} + \frac{1}{Re} \frac{\partial^2 \overline{U}_i'}{\partial x_j' \partial x_j'} + \frac{\partial (\overline{-u_j' u_i'})}{\partial x_j'}$$

Turbulent Energy Equation:

$$\frac{\partial \overline{\delta T}'}{\partial t'} + \overline{U}_i' \frac{\partial \overline{\delta T}'}{\partial x_i'} = \Pr \cdot \frac{1}{Re} \frac{\partial^2 \overline{\delta T}'}{\partial x_k' \partial x_k'} + \frac{\partial (-\overline{\theta' u_i'})}{\partial x_i'} + \frac{1}{Re} \cdot Ec \cdot \overline{\varphi}'$$

The continuity equation requires geometric similarity from non-dimensionalizing and coefficients from the other two equations provide the following similarity parameters.

1. Rossby number: $R_0 \equiv U_0 / L_0 \Omega_0$
2. Densimetric Froude number: $Fr \equiv U_0 / (g L_0 \delta T_0 / T_0)^{1/2}$
3. Prandtl number: $\Pr \equiv \rho_0 c_{p_0} \nu_0 / \kappa_0$
4. Eckert number: $Ec \equiv U_0^2 / c_{p_0} \delta T_0$
5. Reynolds number: $Re \equiv U_0 L_0 / \nu_0$

In the dimensionless momentum equation, the Rossby number is extracted from the denominator of the third term on the left side. The Rossby number represents the ratio of advective acceleration to Coriolis acceleration due to the rotation of the earth. If the Rossby number is large, Coriolis accelerations are small. In nature, the rotation of the earth influences the upper layers of the atmosphere; thus, the Rossby number is small and becomes important to match, and the corresponding term in the momentum equation is sustained. However, typical wind tunnels are not rotating and the Rossby number is infinite, allowing the corresponding term in the dimensionless momentum equation to approach zero. Most modelers have assumed the Rossby number to be large, thus, neglecting the respective term in the equations of motion and ignoring the Rossby number as a criterion for modeling. Snyder (1981) showed that the characteristic length scale, L_0, must be smaller than 5 km in order to simulate diffusion under neutrally stable conditions in relatively flat terrain. Since the UC Davis wind tunnel produces a boundary layer with a height of roughly one meter, the surface layer extends 20 cm above the floor of the wind tunnel. In this region the velocity spectrum is accurately modeled. The Rossby number can then be ignored in this region. Because the testing is limited to the lower 10% to 15% of the boundary layer, the length in longitudinal direction, which can be modeled, has to be no more than a few kilometers.

Derived from the denominator of the second term on the right side of the dimensionless momentum equation, the square of the Froude number represents the ratio of inertial forces to buoyancy forces. High values of the Froude number infer that the inertial forces are dominant. For values equal or less than unity, thermal effects become important. Since the conditions inside the UC Davis wind tunnel are inherently isothermal, the wind tunnel generates a neutrally stable boundary layer; hence, the Froude number is infinitely large, allowing the respective term in the momentum equation to approach zero.

The third parameter is the Prandtl number, which is automatically matched between the wind-tunnel flow and full-scale winds if the same fluid is used.

The Eckert number criterion is important only in compressible flow, which is not of interest in a low-speed wind tunnel. Because the testing speed in the present study did not exceed 11.5 ft/s, the Eckert number was negligible.

Reynolds number represents the ratio of inertial to viscous forces. The reduced scale of a wind-tunnel model results in a Reynolds number several orders of magnitude smaller than in full

scale. Thus, viscous forces are more dominant in the model than in nature. No atmospheric flow could be modeled if strict adherence to the Reynolds number criterion was required. However, several arguments have been made to justify the use of a smaller Reynolds number in a model. These arguments include laminar flow analogy, Reynolds number independence, and dissipation scaling. With the absence of thermal and Coriolis effects, several test results have shown that the scaled model flow will be dynamically similar to the full-scale case if a critical Reynolds number is larger than a critical independence value(Snyder; 1981). The gross structure of turbulence is similar over a wide range of Reynolds numbers. Nearly all modelers use this approach today.[Derksen *et al*. (1992, 1996), Gu *et al*. (2007), Hitchman & Slawson (1987), Kennedy & Fordyce (1974), and Slawson & Sullivan (1981)]

Boundary Layer Similarity

Wind-tunnel simulation of the atmospheric boundary layer, under neutrally stable conditions, also must meet non-dimensional boundary-layer similarity parameters between the scaled-model flow and its full-scale counterpart. The most important conditions are:

1. The normalized mean velocity, turbulent intensity, and turbulent energy profiles.
2. The roughness Reynolds number, $\mathrm{Re}_z = z_0 u_* / \nu$.
3. Jensen's(1958) length-scale criterion of z_0/H.
4. The ratio of H/δ for H greater than $H/\delta > 0.2$.

In the turbulent core of a neutrally stable atmospheric boundary layer, the relationship between the local flow velocity, U, versus its corresponding height, z, may be represented by the following velocity-profile equation.

$$\frac{U}{U_\infty} = \left(\frac{z}{\delta}\right)^{\alpha}$$

U_∞ is the mean velocity of the inviscid flow above the boundary layer, δ is the height of the boundary layer, and α is the power-law exponent, which represents the upwind surface conditions. Wind-tunnel flow can be shaped such that the exponent α will closely match its

corresponding full-scale value, which can be determined from field measurements of the local winds. The required power-law exponent, α, can then be obtained by choosing the appropriate type and distribution of roughness elements over the wind-tunnel flow-development section. According to Table 1, the power-law exponent for the atmospheric wind profile of the El Dorado Power Plant was selected to be 0.15 based on the geometric conditions, which is a desert playa with small bushes covering the area. This condition was closely matched in the UC Davis Atmospheric Boundary Layer Wind Tunnel (ABLWT) by systematically arranging a pattern of 9/16-inch nuts along the entire surface of the flow-development section. The pattern generally consisted of alternating sets of four and five nuts in one row.

Table 2 The Power-law Exponents for Various Terrain Conditions

Terrain Description	**The Power-law Exponent**
Calm open sea	0.1
Desert or natural snow surface	0.11~0.13
Fairly level grass plains	0.14~0.16
Farmland	0.16~0.2
Sub-urban area or wooded country	0.2~0.26
Small town	0.26~0.3
Large city	0.3~0.35

In the lower 20% of the boundary-layer height, the flow is then governed by a rough-wall or "law-of-the-wall" logarithmic velocity profile.

$$\frac{U}{u_*} = \frac{1}{\kappa} \ln\left(\frac{z}{z_o}\right)$$

where, u_* is the surface friction velocity, κ is von Karman's constant, and z_o is the roughness height. This regime of the atmospheric boundary layer is relatively unaffected by the Coriolis force, thus being the only regime that can be accurately modeled by the wind tunnel (i.e., the lowest 150 to 300 ft of the atmospheric boundary layer under neutral stability conditions). It is desirable to have the scaled-model buildings and its surroundings contained within this layer.

The geometric scale of the model should be determined by the size of the wind tunnel, the roughness height, z_o, and the power-law index, α. With a boundary-layer height of 3 ft in the test section, the surface layer would be 0.7 ft deep for the U.C. Davis ABLWT. For the present study, this boundary layer height and the surface layer depth correspond to full-scale length of 853 ft and 171 ft, respectively. Since the highest elevation of the site investigated is about 92 ft full-scale, the entire testing model is contained in the surface layer.

Due to scaling effects, a good simulation of the boundary-layer profiles only can be attained in wind tunnels with long flow-development sections. For full-scale matching of the normalized mean velocity profile, an upwind fetch of approximately 10 to 25 boundary-layer heights is desired. To fully simulate the normalized turbulent intensity and energy spectra profiles, the flow-development section needs to extend to about 50 and 100 to 500 times the boundary-layer height, respectively. These profiles must at least meet full-scale similarities in the surface-layer region. However, with the addition of spires and other flow tripping devices, the flow development length can be reduced to less than 20 boundary layer heights for most engineering applications. In the U.C. Davis ABLWT, the maximum values of turbulent intensity near the surface range from 35% to 40%, similar to that in full scale. Thus, the turbulent intensity profile, u'/u versus z, should agree reasonably with full-scale, particularly in the region where testing is performed.

The second boundary-layer condition involves the roughness Reynolds number, Re_z. According to the criterion given by Sutton (1949), Reynolds number independence is attained when the roughness Reynolds number is defined as follows.

$$Re_z = \frac{u_* z_0}{\nu} \geq 2.5$$

u_* is the friction speed, z_0 is the surface roughness length, and ν is the kinematic viscosity. Re_z larger than 2.5 ensures that the flow is aerodynamically rough. Therefore, wind tunnels with a high enough roughness Reynolds numbers are able to simulate full-scale aerodynamically rough flows exactly. To generate a rough surface in the wind tunnel, roughness elements are placed on the wind-tunnel floor. The height of the elements must be larger than the height of the viscous sub-layer in order to trip the flow. The UC Davis ABLWT satisfies this condition, since the roughness Reynolds number is about 40, when the wind-tunnel free-stream velocity, U_∞, is equal

to 12.5 ft/s, the friction speed, u_*, is 0.79 ft/s, and the roughness height, z_o, is 0.1 inch. Thus, the flow setting satisfies the Re number independence criterion and dynamically simulates the flow. This validity sustains for various testing condition in the present study.

To simulate the pressure distribution on objects in the atmospheric wind, Jensen (1958) found that the surface roughness to object-height ratio in the wind tunnel must be equal to that of the atmospheric boundary layer, i.e., z_o/H in the wind tunnel must match the full-scale value. Thus, the geometric scaling should be accurately modeled.

The third boundary layer condition is the characteristic scale height to boundary layer ratio, H/δ. There are two possible ranges for this ratio. If H/δ is larger than or equal to 0.2, then the ratios must be matched. If $(H/\delta)_{\text{Full Scale}}$ is smaller than 0.2, then of $(H/\delta)_{\text{Wind Tunnel}} < 0.2$. Using a logarithmic profile equation, instead of the power-law velocity profile, this constrains the physical model to 10% to 15% of the wind-tunnel boundary-layer height.

Along with these conditions, two other constraints have to be met. First, the mean stream wise pressure gradient in the wind tunnel must be zero. Even if high- and low-pressure systems drive atmospheric boundary-layer flows, the magnitude of the pressure gradient in the flow direction is negligible compared to the dynamic pressure variation caused by the boundary layer. The other constraint is that the model should not take up more than 5% to 15% of the cross-sectional area at any downwind location. This assures that local flow acceleration affecting the stream wise pressure gradient will not distort the simulation flow. It will be shown later in this report that the present testing model takes less than 5% cross-sectional area.

U.C. Davis ABLWT is not capable of simulating unstable boundary layer flows. In fact, simulation of unstable boundary layer flows could be a disadvantage due to the artificial secondary flows generated by the heating, which dominate and distort the longitudinal mean-flow properties, thus, invalidating the similarity criteria. However, this is not considered to be a major constraint, since the winds that produce an annual average dispersion are sufficiently strong, that for flow over a complex terrain, the primary source of turbulence is due to mechanical shear and not due to diurnal heating, or cooling effects in the atmosphere.

Scaled Model Design and Construction

Although the main objective of the present study is to develop a general model of an ACC system, it is necessary for comparison purposes to select an existing unit and to construct the scaled model with the geometric conditions of that unit. Considering the accessibility of field data and detailed geometry of the plant supplied by EPRI and the present research team, the El Dorado Power Plant in Nevada was selected for the scaling. As shown in Figures 2 and 3, the El Dorado plant is located approximately 25 miles southeast of Las Vegas and has 480 MW of power generating capacity. The plant is a combined cycle natural gas power plant.

The El Dorado plant primarily consists of two boiler houses, a generator building, and 30 fans arrayed in a five by six ACC unit. This ACC unit is aligned on exact north and the turbine buildings are located to the north of the ACC unit. The five 28 feet tall A-frames, with six-fans on each line, are mounted on a platform 63 feet from ground. Thirty fans with a diameter of 34 feet can draft up to 1.3 million cubic feet per minute at full speed. The maximum axial speed of the flow reaches 24 feet per second at full power. In order to reduce negative wind effects and to improve air intake, there are four 27.5 feet tall windbreaks on each side of the platform and two sets of wind screens beneath the platform.

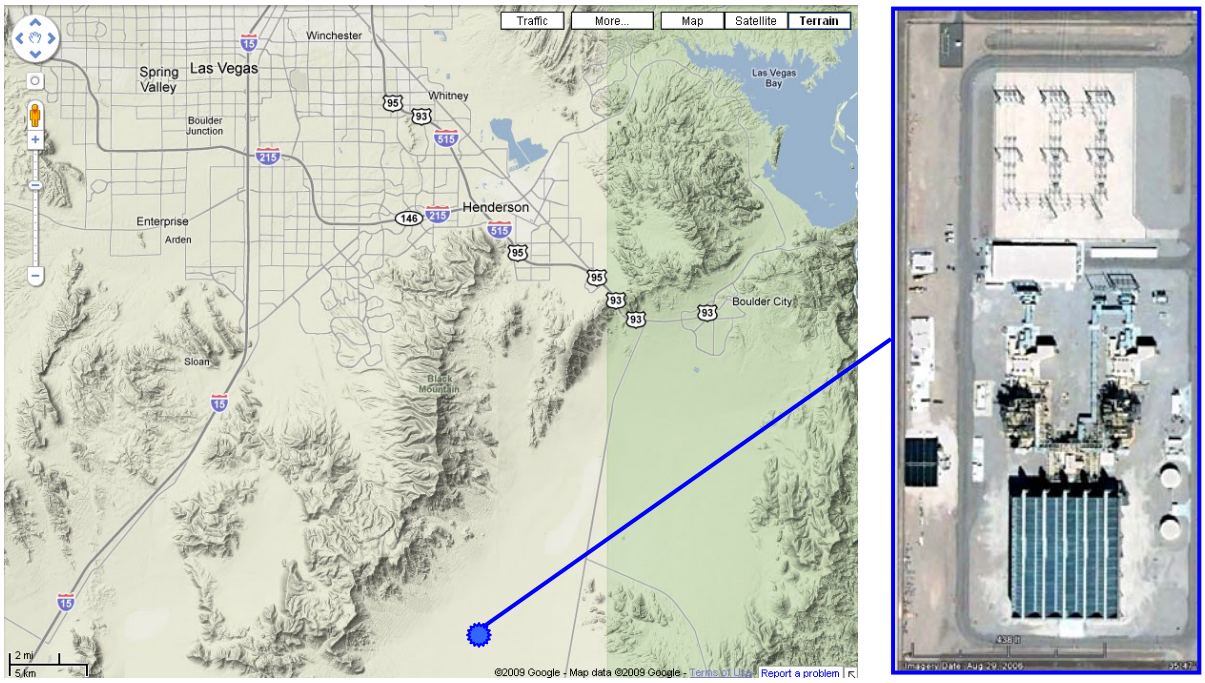

Figure 2 The Location of the El Dorado plant and ACC Configuration on Google® Maps

Figure 3 Side Views of the El Dorado Power Plant

Due to the limited sizes of micro fans, the fan size became the highest priority in deciding the scale of the model. The micro fans used in the study are originally used for cooling laptop computers and have a diameter of 4 cm (≈ 1.6 inch). The scale factors of the fans were 1 to 260 with a fan diameter of 34 feet in full scale. A series of verifications were done to check if this scale factor meets previously presented scaling criteria.

Once the model is installed in the test section of the wind tunnel, the model shrinks the flow area and accordingly increases the speed. The blockage effect of the model can be estimated by the ratio of cross-sectional area of the model to the cross sectional area of the test section. Compensating for this effect is difficult, as pointed out by Isyumov and Tanaka (1979). Isymuov and Tanaka reported that the flow distortion is negligible with a blockage ratio less than 5%. Therefore, the scaled model cross-sectional area has to be less than 5% of the cross sectional area of the test section to meet the Isyumov criterion. Considering the cross-sectional area of the UC Davis wind tunnel (3.9 ft by 5.2 ft) and the area of the ACC unit of the El Dorado plant (233 ft by 28 ft), any scale ratio larger than 79 meets the Isyumov criterion. The model of ACC with a scale factor of 260 will provide a blockage ratio of approximately 0.5%.

The typical atmospheric boundary layer thickness is known to be 1,200 ft over suburban terrain, 900 ft over open area, and 700 ft over ocean. The ratio of atmospheric boundary layer

thickness to the thickness of the simulated boundary layer represents another scale factor. Considering the test section height of the U.C. Davis ABLWT (5.5 ft) and the possible disturbance at the top of the boundary layer, caused by the traversing mechanism, a scale factor between 220 and 270 should be applied to simulate the atmospheric boundary layer over desert terrains. The scale factor of 260 also meets this condition.

For the construction of the model, a majority of the buildings were made of Styrofoam and cardboard. Other materials used were plastic plate, wires, and dowels. The model was built on a turn table so that any wind direction easily could be tested. As shown in Figure 4, the configuration of the ACC unit was carefully set in the center of the test section for all the directions tested. The platform supports were inserted in the turn table and the simulated wind screens were mounted between the posts. The porosity of the windscreen in the El Dorado ACC unit was simulated with nylon screen.

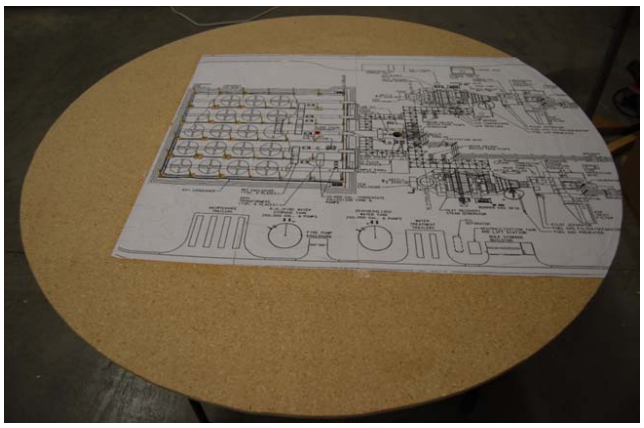

Figure 4 ACC Model Layout and Turn table Base

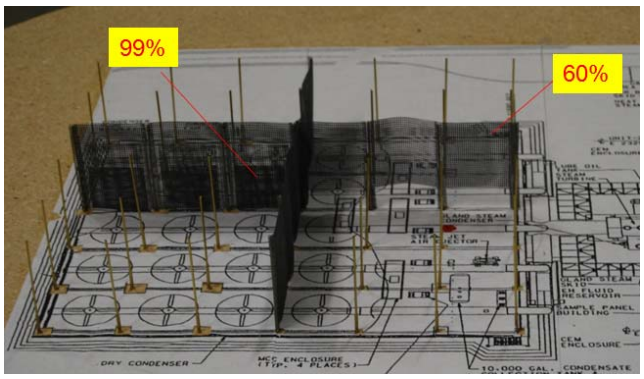

Figure 5 Installation of Platform Supports and Wind Screens

The micro fans were mounted on a plastic platform and the adjacent buildings were glued as shown in Figure 6. Several holes for running the electric wires and gas tubes through the turn table were drilled at this stage. A-frame models were mounted on the platform and two layers of Nylon screens were installed on each fan unit to simulate the heat exchanger. After the smaller details were added to the buildings and the ACC unit, the electric wires and gas tubes were properly connected to each fan cell for testing. In order to minimize the flow disturbance by the wires and tubes, they were hidden inside the hollow steam headers and condensing pipes. The wires and tubes ran through the wind tunnel floor and were connected to the custom designed control box shown in Figure 7. The final outlook of the model is presented in Figure 8. Several views of the model are compared with the real plant in Figure 9 to show the geometric similarity of the model.

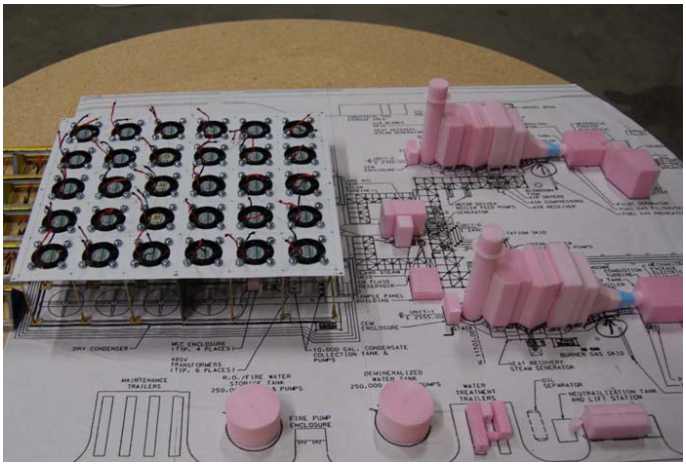

Figure 6 Installation of Fans and Adjacent Buildings

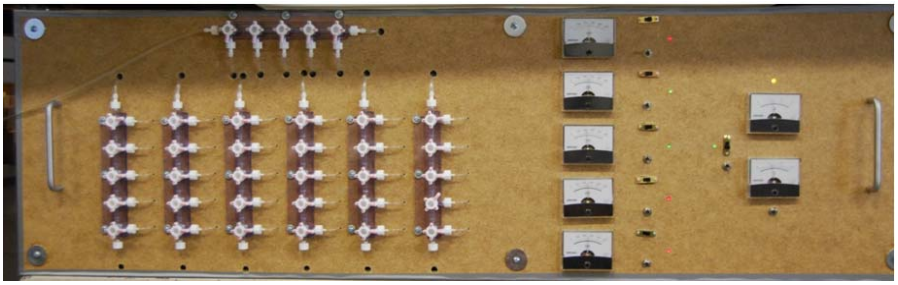

Figure 7 Front View of the Control Box Panel

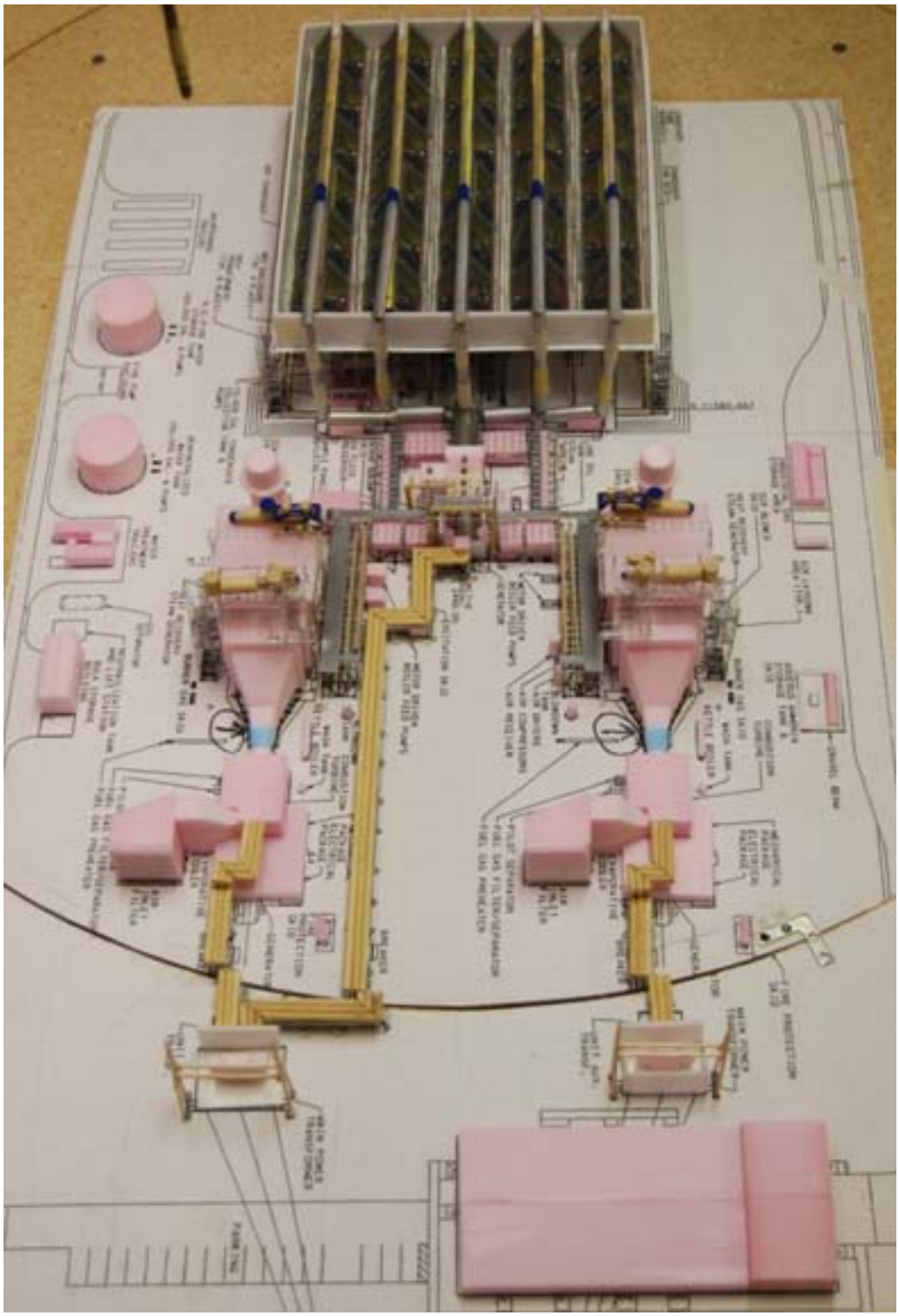

Figure 8 Aerial View of the El Dorado Power Plant Model

Figure 9 Verification of Model Geometry by Comparison with Full Scale

TESTING FACILITIES

The Atmospheric Boundary Layer Wind Tunnel at UC Davis

In the present investigation, the Atmospheric Boundary Layer Wind Tunnel (ABLWT) located at University of California, Davis was used (Figure 10). Built in 1979 the wind tunnel was originally designed to simulate turbulent boundary layers comparable to wind flows near the surface of the earth. In order to achieve this effect, the tunnel requires a long flow-development section that produces a mature boundary-layer flow at the test section. The wind tunnel is an open-return tunnel with an overall length of 70 feet and is composed of five sections: the entrance, the flow-development section, the test section, the diffuser section, and the fan and motor section.

The entrance section is elliptical with a smooth contraction area that minimizes the free-stream turbulence of the incoming flow. Following the contraction area is a commercially available air filter that reduces large-scale pressure fluctuations in the flow and filters larger-size particles out of the incoming flow. Behind the filter, a honeycomb flow straightener is used to reduce undesired large-scale turbulence.

The flow development section is 40 ft long with an adjustable ceiling to control the longitudinal pressure-gradient. For the present study, the ceiling was diverged so that a zero-pressure-gradient condition was formed in the stream wise direction. At the leading edge of the section following the honeycomb flow straightener, four triangularly shaped spires are stationed on the wind-tunnel floor to provide favorable turbulent characteristics in the boundary-layer. Roughness elements are then placed on the floor to artificially thicken the boundary layer. For a free-stream wind speed of 13 ft/s, the wind-tunnel boundary layer grows to a height of one meter at the test section. With a thick boundary layer, larger models can be tested and measurements can be made with higher resolution.

Dimensions of the test section are 8 feet in the stream wise direction, 5.5 feet high, and 3.9 feet wide. Similar to the flow-development section, the test section ceiling also can be adjusted to obtain the desired stream wise pressure gradient. Experiments can be observed from both sides of the test section through framed Plexiglas windows. One of the windows can be slid open to allow access into the test section. When closed, twelve clamps distributed over the top and bottom of the window are used to seal the sliding window. Inside the test section, a three-

dimensional probe-positioning system is installed in the ceiling to provide fast and accurate sensor placement. The traversing scissors, which provide vertical motion to the probe, are made of aerodynamically shaped struts to minimize flow disturbances.

The diffuser section is 7.8 ft long and has an expansion area that provides a continuous transition from the rectangular cross-section of the test section to the circular cross-sectional area of the fan. To eliminate upstream swirl effects from the fan and avoid flow separation in the diffuser section, fiberboard and honeycomb flow straightener are placed between the fan and the diffuser section.

The fan consists of eight constant-pitch blades, 6 feet in diameter, and is powered by a 56 kW (75 hp) variable-speed DC motor. A dual belt and pulley drive system is used to couple the motor and the fan.

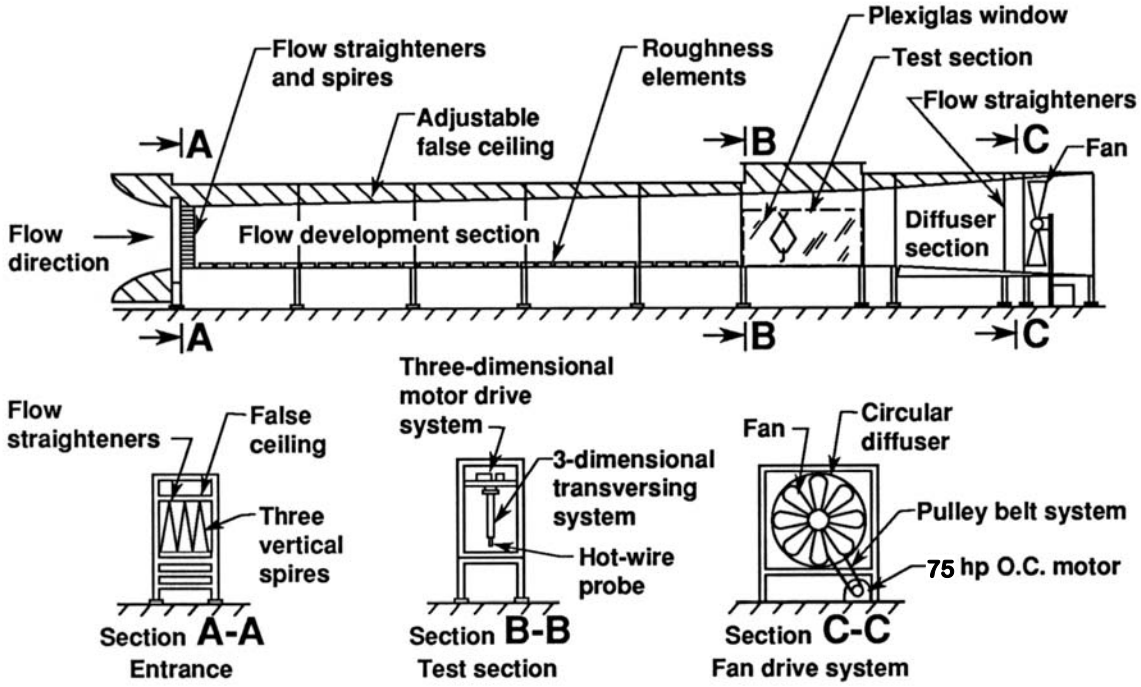

Figure 10 Schematic Diagram of the UC Davis Atmospheric Boundary Layer Wind Tunnel

Instrumentation and Measurement System

Wind-tunnel measurements of the mean velocity and turbulent characteristics were performed using hot-wire anemometry. A Thermo Systems Inc. (TSI) single hot-wire sensor model 1210-60 was used to measure the wind quantities. The sensor was installed at the end of a TSI 1150 50-cm probe support, which was secured to the support plate of the three-dimensional sensor positioning system in the U.C. Davis ABLWT test section. A 50-ft shielded tri-axial cable was used to connect the probe support and sensor arrangement to a TSI IFA 100 constant temperature anemometry unit with signal conditioners.

Hot-wire sensors were calibrated in the ABLWT test section over a range of velocities in the wind-tunnel boundary layer. Signal-conditioned voltage readings of the hot-wire sensor were then matched against the velocity measurements from a pitot-static tube connected to a Meriam 34FB2 oil micro-manometer, which has a resolution of 1/1,000 inch of oil. The specific gravity of the oil in the oil micro-manometer was 0.934. The pitot-static tube was secured to an aerodynamically shaped stand and was positioned so that its flow-sensing tip is normal to the flow and situated near the volumetric center of the test section. Normal to the flow, the end of the hot-wire sensor was then traversed to a position 4 inch next to the tip of the Pitot-static tube.

Using a LabVIEW data acquisition system, all the data was acquired and digitally recorded for each point at a sampling rate of 1000 Hz for 30 seconds, which is equivalent to one hour of field measurement with 20 MPH wind speeds at a height of 520 ft. This yielded 30,000 voltage readings from the anemometer transducer that were individually converted to instantaneous wind speeds by applying a calibration curve, which was acquired prior to the testing. The 30,000 samples were then statistically analyzed to produce a single average wind speed and the standard deviation (turbulent intensity). The resulting mean speeds and turbulent intensities represent one-hour of full-scale measurements of time averaged wind speeds and fluctuations.

In order to measure the recirculation rate of exhausted gas, concentrations of an ethane tracer gas were measured with the use of a Rosemount Analytical 400A hydrocarbon analyzer. This instrument uses flame-ionization detection to determine trace concentrations of hydrocarbons in the air. The ethane-air samples are iso-kinetically aspirated into a burner where the sample is burned with a mixture of medical-rated air (40% hydrogen and 60% nitrogen).

Figure 11 displays a schematic of the concentration measurement system. Copper refrigeration-grade tubing, 1/4 inch in diameter and 12 inches in length, covered with a layer of filter at the end, was used as a gas-analyzer sensing probe. This probe was secured to the traverse-system mounting plate, where an additional length of Nylon tubing was used to connect the probe to a pressure-regulated vacuum pump, which sends samples into the analyzer at a constant pressure of 5 psig.

Prior to calibration, the analyzer voltage output was first mechanically zeroed using a sample of pure air (hydrocarbon-free). Calibration of the hydrocarbon analyzer system was accomplished with either of two known samples of ethane-air mixtures, one certified with 52.4 parts per million (ppm) and the other with 524.8 ppm. Calibration gas samples were accurate to less than 0.5% of the stated value. The error of the gas analyzer at full scale is lower than 1%.

Ethane tracer gas emissions, from the nozzles atop the fan in the A-frames, were controlled by a model B-250-1 ball-type flow meter. The flow meter was calibrated by measuring the time elapsed for ethane to fill a container of known volume. Since the ethane mixture was virtually invisible, the gas level needs to be monitored by using a visible substance such as water. This was done by completely submerging the calibration container in a water tank, then allowing ethane into the container through the flow meter to displace a known quantity of water. Elapsed times are collected for three height settings on the flow meter. Dividing these times by the known volume gives a volumetric flow rate for a corresponding flow meter setting.

"Raw" voltage data sets of hot-wire velocity measurements and of tracer gas concentrations were digitally collected using a LabVIEW data acquisition system, which was installed in a Gateway personal computer with a Pentium 166Mhz processor. Voltages corresponding to gas concentration were collected from the hydrocarbon analyzer analog output. Hot-wire voltages were obtained from the signal conditioner output of the IFA 100 anemometer. The two outputs were connected to a multi-channel daughter board linked to a United Electronics Inc. (UEI) analog-to-digital (A/D) data acquisition board, which is installed in one of the ISA motherboard slots of the Gateway PC. LabVIEW software was used to develop virtual instruments (VIs) that would initiate and configure the A/D board, then collect the voltage data given by the measurement equipment, display the converted results on the computer screen, and save the "raw" voltage data into a designated filename.

Since velocity and concentration measurements were individually performed, a VI was developed for each type of acquisition. For the hot-wire acquisition, the converted velocity data and its histogram is displayed along with the mean voltages, mean velocity, root-mean-square velocity, and turbulent intensity. In the concentration VI, the converted concentration data is shown with the corresponding mean voltage and mean concentration. For both programs, the raw voltage data can be saved on the computer hard drive. For both hot-wire and gas concentration acquisition, 30,000 samples were collected at a sampling rate of 1000 Hz. This acquisition setting satisfies the Nyquist sampling theorem, requiring that the average tunnel turbulence signal is 300 Hz.

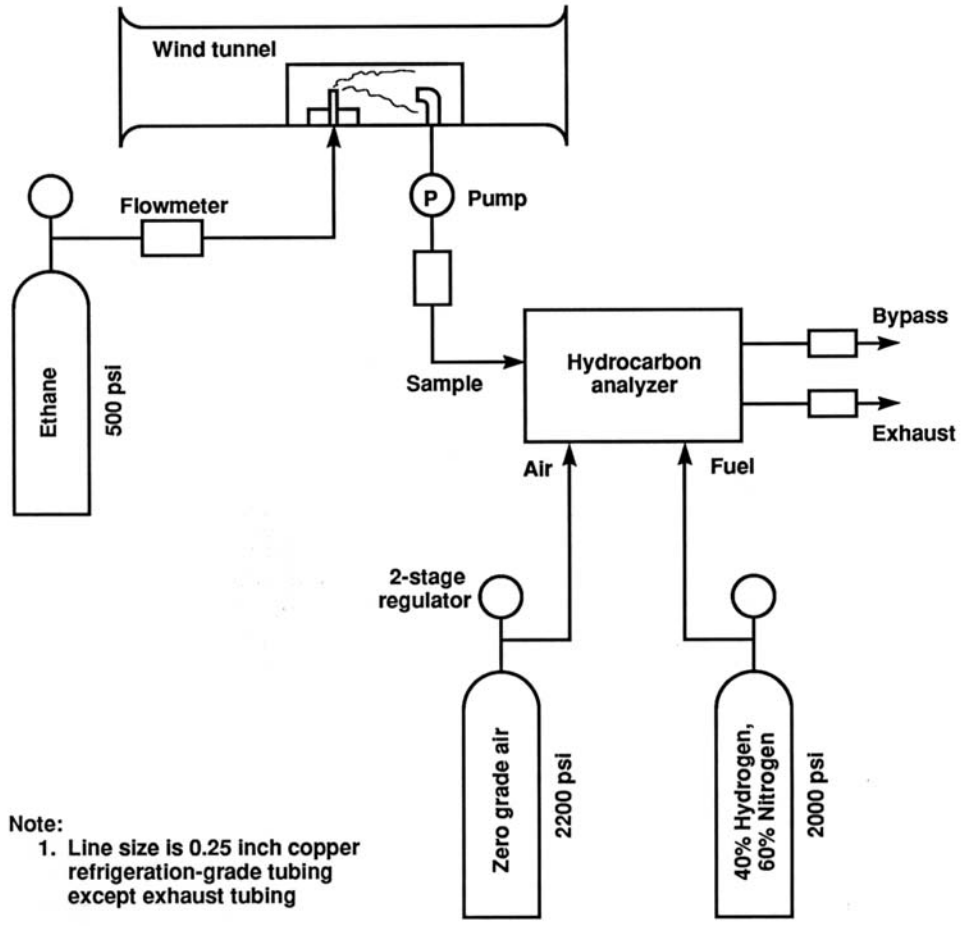

Figure 11 Schematic Diagram of Gas Dispersion Concentration Measurement System

TESTING METHODOLOGY

The El Dorado power plant is located in a basin with surrounding low brush, the 'power-law exponent,' mentioned earlier, accordingly was estimated to be 0.15 (refer Table 2). In order to simulate the boundary layer flow of the El Dorado site in the U.C. Davis ABLWT, 9/16 inch nuts were systematically placed on the flow development section of the wind tunnel. Figure 12 shows the boundary-layer profile generated in the wind tunnel along with an ideal pattern of the boundary layer with a power-law exponent of 0.15. By comparing the two profiles in Figure 12, it was verified that the wind tunnel properly simulates the El Dorado boundary layer up to 10 inches in model scale, which corresponds to over 200 feet in full scale. In regard to the height of the real ACC unit, which is 93 feet including the steam header, the size of the wind tunnel boundary layer is adequately high to simulate the wind effect at the El Dorado power plant. To ensure the simulation quality of boundary layer characteristics, turbulent intensity profiles and power spectrums also were examined.

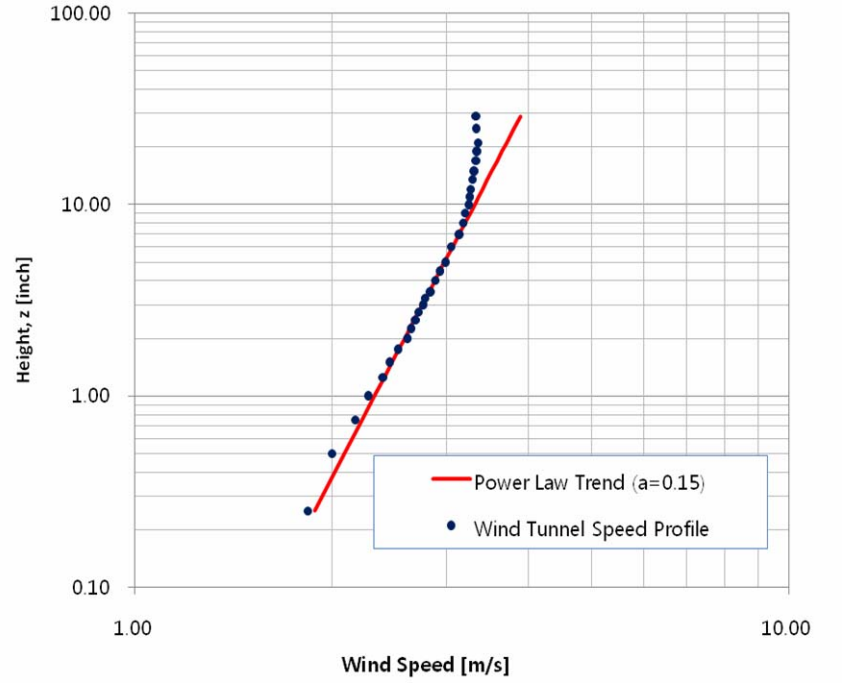

Figure 12 Simulated Boundary Layer Profile in the U.C. Davis ABLWT

Due to the large number of fans in the ACC unit, special attention was given to ensure the consistency of performance between each model fan. All thirty fans were individually tested for flow rate, prior to the final assembly of the model. Figure 13 shows the cross-sectional flow pattern of nine fans operated at full speed. The flow speed measurements were made at a height of 2 inches above the fan. Further, measurements were taken at the center of the fan to one fan-diameter in length away from the center. Similar to the other speed measurements in the present study, model-fan flow-speeds were measured with a single hot wire with a constant temperature anemometer. Each color of dots in Figure 13 display the cross sectional flow profile for each fan and, as seen in the figure, the speed profile of the fans are reasonably consistent. A curve fit of the profile was constructed by averaging all of the profiles. The flow in the center of the fan is restricted by the rotor hub and accordingly shows low speeds. The flow speed between the hub and fan frame accordingly is much higher. For the nine micro fans presented in Figure 13, the average total flow rate was found to be 13.2 CFM with a standard deviation of 0.39 CFM. Thus, the fan performance was within 2.9% uncertainty.

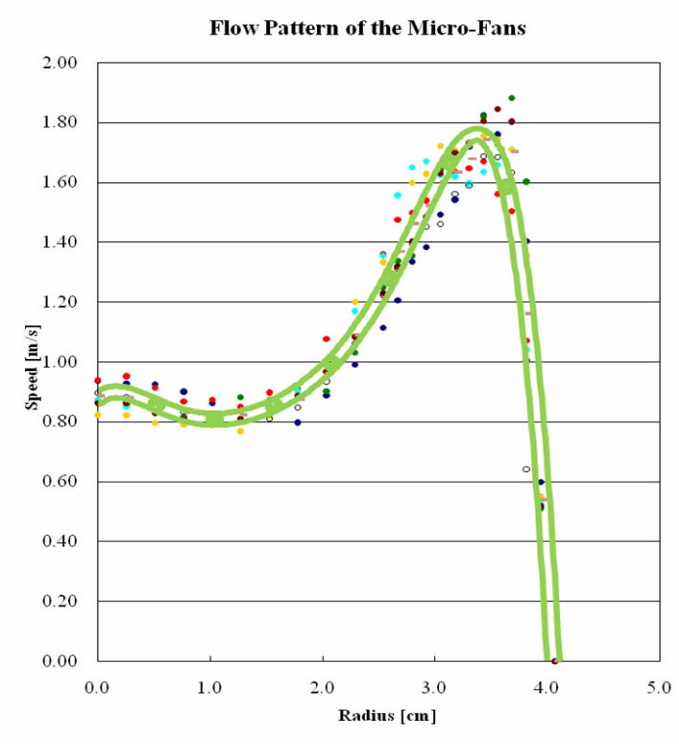

Figure 13 Cross-sectional Flow Pattern of Nine Micro-fans at a Height of 2 inches

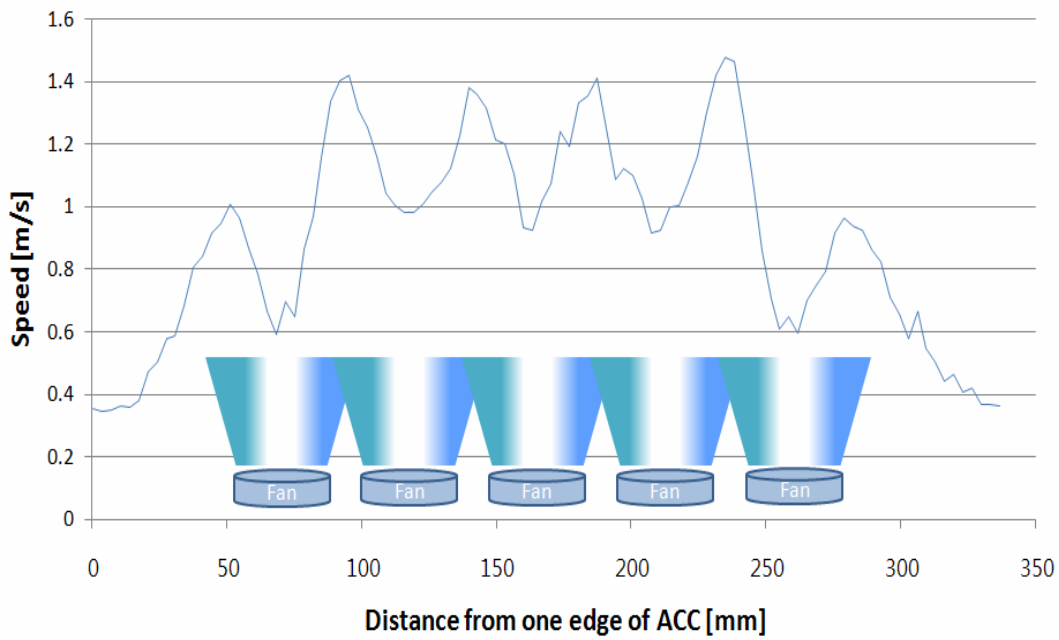

Figure 14 Flow distribution of a Fan Array Measured at 1-D Above the Steam Header

After the fans were completely assembled on the model ACC platform, flow distribution along the centerline of five fans, on an array, was measured at 1 fan diameter above the steam header. Shown in Figure 14, the air flow exhausted from each fan is combined, resulting in higher flow speeds, or flow rates, in the middle than the outer boundaries of the fan array. The valley patterns between peaks of the flow speed represent the lack of flow by blockage of the steam headers, shown in Figure 13.

Since the full scale Reynolds number, Re_R, is substantially high, the exhaustion and dispersion of hot air from the ACC unit in full scale are turbulent.

$$\mathrm{Re}_R = \frac{U_f L_f}{\nu} = \frac{24\,ft/s \times 34\,ft}{1.63\times10^{-4}\,ft^2/s} \approx 5\times10^6$$

Where, U_f, L_f, and ν are fan speed, characteristic length, and dynamic viscosity of air, respectively. In order to ensure similarity, the Reynolds number must match between full scale and the model. Because the model fan speed is scaled to approximately half that of the real fan and the geometric length is reduced by a scale factor of 260, the model scale Reynolds number should be less than the full scale Reynolds number by several orders of magnitude. Although matching the Reynolds numbers of the model to full scale is impractical, the wind-tunnel

simulation is still considered to be adequate if the exhaust flow from the model is turbulent (Snyder, 1981). This condition is generally achieved (for neutral stability conditions) for model Reynolds number, Re_M, greater than:

$$\mathrm{Re}_M = \frac{U_M D_M}{\nu} = \frac{U_M \times 1.57 inch}{1.63\times10^{-4}\, ft^2/s} > 2300$$

Due to this constraint, the model fan speed has to exceed 2.9 ft/s (≈0.8 m/s). It will be shown in the following chapter that the Reynolds number in the present study is between 15,000 and 40,000 depending on the wind speed setting and meets this Reynolds number criterion.

Besides the Reynolds number, the ratio of exhaust air speed, u_e, to the upstream wind speed, U, has to be maintained correctly for adequate simulation [Isyumov and Tanaka (1980)].

$$\left(\frac{u_e}{U}\right)_R = \left(\frac{u_e}{U}\right)_m$$

Where, R and m represent real scale and model scale, respectively. At the real power plant, the upstream speed is uncontrollable and only the fan speed can be adjusted upon the level of back pressure in steam line. For the full-scale speed ratio the fan air speed was assumed to be the total air flow without any displacement caused by back pressure from the heat exchanger tubes and fins. Although the fan is set to one of only three speeds (zero, half, or full speed), the continuous variation of natural wind speeds yield an indefinite number of the speed ratio cases in full scale. In order to estimate the upstream wind effect on the ACC unit, the meteorological data at the site was analyzed and divided into five categories that evenly spread the statistical occurrence of wind speeds. Table 3 shows the upstream wind speed categories and the combinations of model fan speed and wind-tunnel speed used to meet the wind-speed ratios of the full-scale plant. In order to properly control the model fan speed, a calibration between the fan speed and power input was done prior to testing. The wind-tunnel speed also was calibrated to the power frequency settings. In order to accurately model the fan air speed, the flow rate of tracer gas issued atop the fan was taken into account. The $(u_e)_m$ values in Table 3 represent the total exhaust flow speed. The proper upstream wind speed and exhaust speed were then achieved by controlling the respective power settings.

Table 3 Wind Speed Ratio Settings and the Definition of Upstream Wind Speed Categories

Category	Calm	Mild	Moderate	Strong	Extreme
Speed Ratio	77.7	4.61	2.66	1.46	0.89
U_R [m/s]	0.096	1.61	2.81	5.10	8.37
$(u_e)_R$ [m/s]	7.45	7.45	7.45	7.45	7.45
U_m [m/s]	0.03	1.065	1.845	3.36	2.645
$(u_e)_m$ [m/s]	2.33	4.91	4.91	4.91	2.33

Figure 15 shows the distribution of wind speed occurrence in sixteen azimuthal wind directions, in the form of a wind rose, taken from the El Dorado site. The original data of Figure 15 was acquired by Dr. Maulbetsch during the period of August 2001 through October 2004.(Maulbetsch, 2008) The southwesterly wind is dominant at the site while the northwesterly wind is very rare. The speed categories shown in Table 3 were chosen to evenly distribute testing speed through the speed range observed in Figure 15.

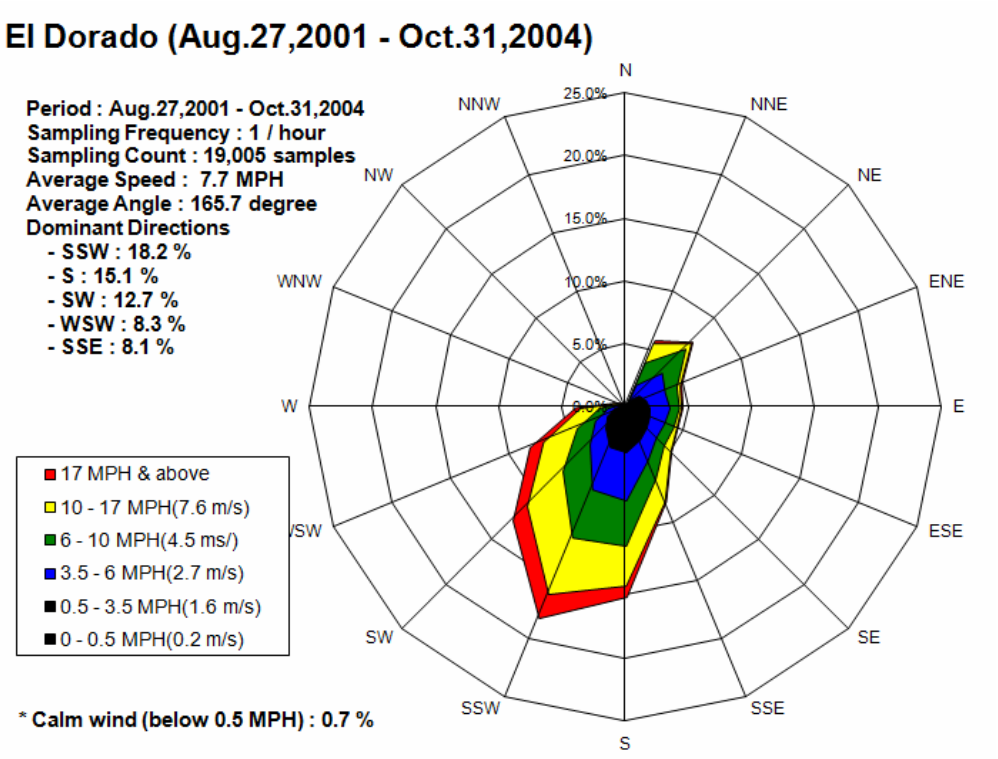

Figure 15 Wind Rose for the El Dorado Power Plant Site (from cited data sampled by Dr. Maulbetsch)

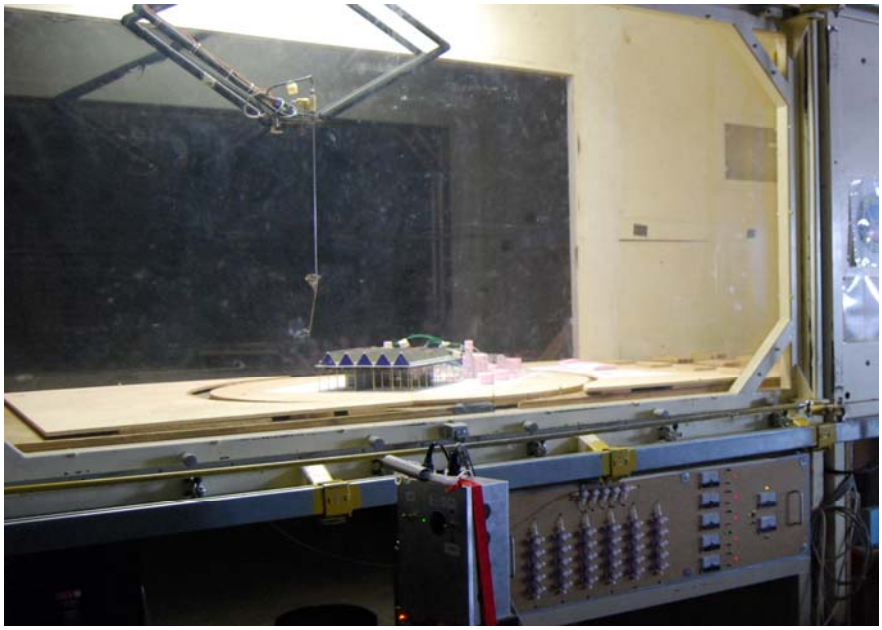

Figure 16 Scaled El Dorado Power Plant Model Centered in the Wind Tunnel

Ideally all sixteen wind directions would be tested and analyzed. However, due to the large number of measurement points and the time constraint, the wind directions tested were reduced to four cases; North (N), South (S), South-west (SW), and West (W). By considering the pseudo symmetric geometry of the plant and the ACC unit, the testing results of the west wind direction also was used as the east wind direction results later in the analysis. Using the same concept, the southwest results were used as the southeast results. The remaining minor wind direction results were acquired by interpolating between the measured wind directions. Although the north wind is rare at the site, the north wind direction had to be tested because of the expected high recirculation of exhausted air caused by the adjacent buildings on the north side.

Once the wind-tunnel model was completed and the testing conditions were selected, the scaled model was centered in the wind-tunnel as shown in Figure 16. During the tests, the model was mounted on a turntable on the floor of the wind-tunnel test section for easy positioning to any wind direction. The UCD ABLWT can only simulate a neutrally stable atmosphere while the exhausted air from the real ACC is either stable or unstable. However, the differences have a relatively small effect on the flow compared to the wakes generated by adjacent structures such as the ACC platform and turbine buildings and accordingly is ignored. After the micro fan speed

and wind-tunnel speed were set to the values given in Table 3 and the model is set to the desired wind direction, wind speeds were measured using hot-wire anemometry. The winds effect on the efficiency of an ACC system is due to its effect on the rate of air indigested into the fans, the exhaust air dispersion, and the recirculation of hot exhausted air. The recirculation due to wind effects plays a critical role in the negative effects of the wind on ACC efficiency as Gu *et al*. (2007) pointed out. The present study focused on the wind's effect on the recirculation. Although the relationship between the recirculation level and the efficiency of ACC is not completely understood, it is obvious that under a specific wind direction and speed, ambient temperature, and fan-flow rate, the ACC efficiency must be inversely proportion to the recirculation level. Because of this, the relationship between the recirculation level and the efficiency of the ACC system was not taken into account in the study, but the recirculation level itself was presented throughout the report to quantitatively understand the wind's effect.

In order to quantify the recirculation level, it was necessary to distinguish the exhausted air from the air surrounding the ACC unit. This study used ethane (C_2H_6) gas as a tracer gas, since the density of ethane is close to air. Additionally, a hydrocarbon analyzer can distinguish it from air. The ethane gas was released at a controlled flow rate through a nozzle mounted atop each micro fan. Released ethane gas was then mixed in each A-frame unit with air blown up by the fan. The air-ethane mixture then passed through the porous heat exchanger model. By measuring the ethane flow rate out of the nozzle and returning back to the fan unit, the recirculation level may be determined. Figure 17 illustrates the re-entrainment of exhausted air and the evaluation procedure. Since the ethane issued through nozzle was completely mixed in

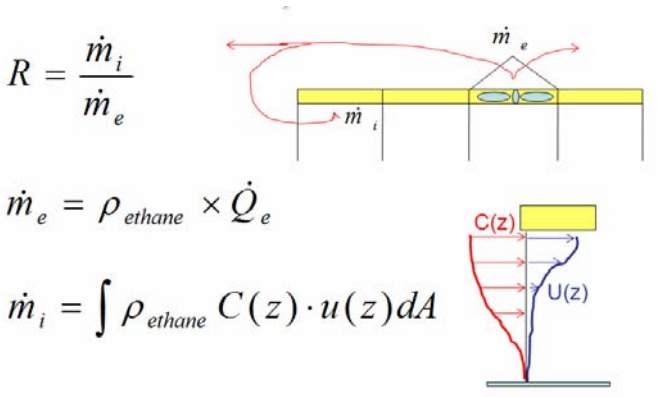

Figure 17 The Schematic Diagram of Re-entrainment Flow and the Calculation of the Re-entrainment Rate

the A-frame and exhausted through several layers of screen, the ethane exhaust rate, Q_e, was assumed to be uniform. The exhaust rate can be monitored by the flow meter at the gas distributor and the mass flow rate of ethane exhaust can be calculated. Re-entrainment flow, however, is not uniform in speed or concentration at the entrance plane and accordingly is more complicated to calculate. As shown in Figure 17 and Figure 18, since the entering flow speed and concentration of the ethane gas are functions of height, both profiles of speed and concentration are needed to calculate the ethane inlet rate, Q_i. After the ethane concentration profile and flow speed profile at the entrance plane of the ACC cells were measured, integration of the mass flow rate of ethane was calculated to give the volumetric flow rate re-entering the ACC unit. The ratio of the re-entered ethane mass flow rate to the exhausted ethane mass flow rate is the re-entrainment rate at the cell as it is defined in Figure 17. The total re-entrainment rate, R_T, can be determined by integrating the local re-entrainment rates, R_n, at all the cells along the outer boundary of ACC platform;

$$R_T = \sum_N R_n$$

When the ethane gas was issued from one nozzle at a time, the local re-entrainment rate was determined for each fan unit. The individual contribution of each fan on total re-entrainment rate can then be evaluated. However, when considering the number of fans, sampling locations, wind-speed categories, and wind directions, the concentration measurements would take over

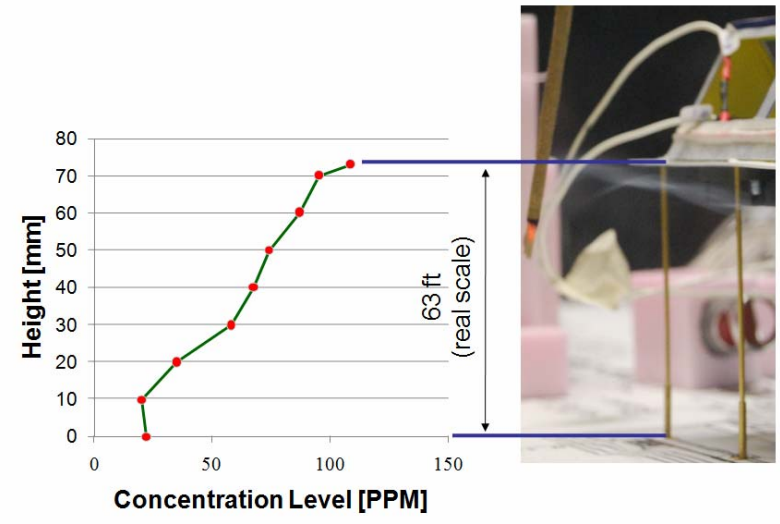

Figure 18 Vertical Profile of Ethane Concentration and the Flow Visualization of the Entering Flow at a Corner of the ACC Platform for a Southerly Mild Wind

500 hours. Due to the time constraint, for most of the testing cases all the nozzles were controlled to issue the same rate of ethane gas simultaneously and accordingly the local re-entrainment rate values represent the total contribution of all the fan units. The individual contribution of each fan was only examined for the worst case.

The sampling number of vertical profile flow speeds and concentration levels also was limited in the present study. As shown in Figure 18, three measurements were made from the middle of the platform height, and one-sixth the platform height from ground and one-sixth the platform height down from the platform. Each of these three values represented one-third of the sampling surface in the re-entrainment calculation.

Figure 19 shows the testing concepts and flow schematics at the ACC units. In order to measure wind speeds or concentrations, a hot-wire probe or a gas sampling tube was attached to the traversing mechanism.

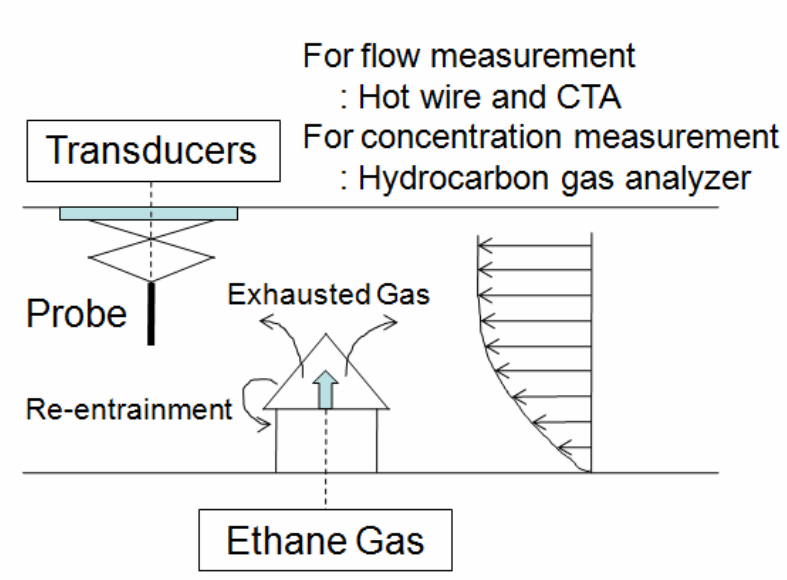

Figure 19 Schematic Diagram of Testing Apparatus and Air Flow at the ACC Unit

SINGLE UNIT MODEL ANALYSIS

Wind-tunnel Testing Results

The air cooling condenser at the El Dorado power plant consists of 30 fan units in a six by five grid as shown in Figure 20. Three turbine buildings, boiler houses, and other facilities are located north of the ACC unit. Five-steam headers run from north to south, each centered on a row of fans, atop of A-frames. In the present study, the series of A-frame under each steam header was named Row-1, Row-2, and repeating to Row-5. The name of Column-A through Column-F were given to the first through sixth fan unit in each row. With this notation, all the fans in Row-1, Row-5, Column-A, and Column-F are at the outer boundary of the ACC unit. As mentioned previously, the re-entrainment ratio was measured only at the outer boundaries. The testing surfaces were named #1 through #16 starting from the north side of fan A-1 going clockwise around the ACC unit. The El Dorado ACC has two screens installed beneath the platform between Row-2 and Row-3 and between Column-C and Column-D to enhance the fan performance. The testing surfaces were selected to cover the corners of the platform and points neighboring the screen, as displayed in Figure 20. The re-entrainment rates at the spaces between the testing surfaces were numerically interpolated in the analysis. The testing conditions and the settings were described in previous chapters.

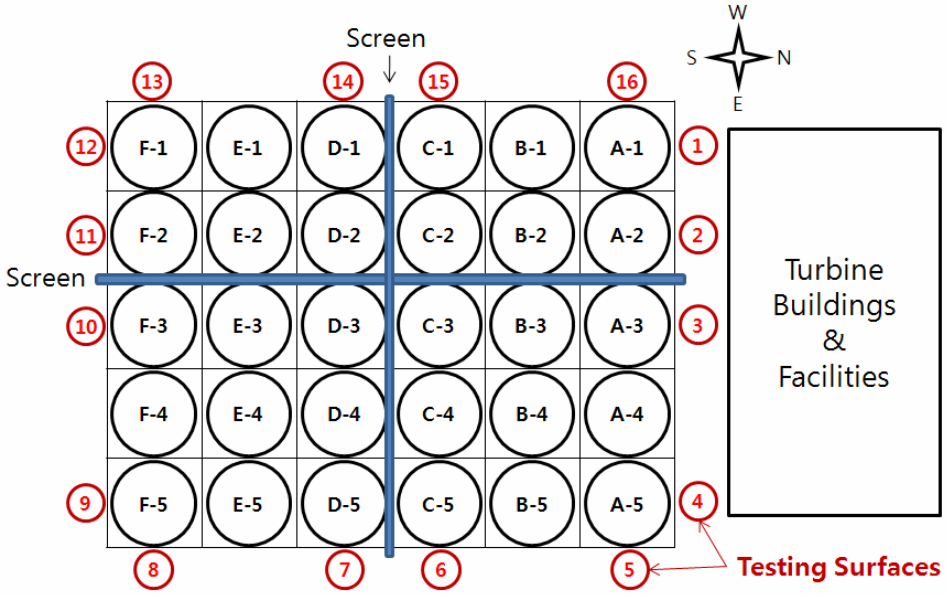

Figure 20 ACC Model Configuration and Testing Surface Locations

Figure 21 shows a sample of the worksheet used to calculate the re-entrainment rate and to display the results. The first row indicates the wind speed category, defined in Table 2, the direction of the setting, and the purity of ethane gas. In the data table, the first column lists the testing surface numbers and the next three columns provide geometric information of the testing surfaces. The next six columns show three sets of concentration and flow speed readings. T, M, and B stand for Top-section, Middle-section, and Bottom-section, indicating the sampling heights. The next three sets of data indicate the ethane flux re-entering through each section of the testing surface. The ratio of the re-entering flux to the exhausted flux yields the re-entrainment rate, shown in the next three columns. The last column in the table indicates the total re-entrainment rate of each testing surface. By summing the local re-entrainment rates from all the testing surfaces, the total re-entrainment rate may be evaluated and is shown at the bottom of the table. Relatively high values, among the re-entrainment rate values in the table, were highlighted. Vertical distributions of re-entrainment rates measured from the top, middle, and bottom section of each testing surface are displayed in the lower left corner. The lower right corner shows estimated contours of re-entrainment rates for all the fan units. In between, re-entrainment rates are plotted along the outer boundary of the ACC unit. A total of twenty worksheets, like Figure 21, were made from five wind speeds and four wind directions. Appendix-A contains the twenty worksheets.

Figure 22 compares the trends of re-entrainment rate distributions for different speed and direction settings. Each column in Figure 22 represents a wind speed setting while the rows show the wind direction setting. Figure 22 indicates that the re-entrainment of the ACC unit is greatly affected by both wind speed and direction, along with the interference of adjacent buildings and the ACC. For the calm wind speed, most of the re-entrainment occurred at the opposite side from the incoming wind. This trend indicates that the platform generates a wake by distorting the wind and that the exhausted “hot" air and wake was drawn by the fans on the backside of the platform. This trend was sustained for all the wind directions. The effect of the wind and the adjacent buildings on the flow was not strong enough to stretch the wake away from the platform.

Wind Strength Moderate **Wind Direction** N **Ethan Purity** 98.5

	X	Y	width	Concentration [PPM]			Speed [m/s]			Flux (times million)			Re-Entrainment Rate (%)			
	[cm]	[cm]	[cm]	T	M	B	T	M	B	T	M	B	T	M	B	SUM
1	0	-1.77	5.5	1.90	0.40	0.15	2.38	1.82	1.63	0.0061	0.0010	0.0003	0.0084	0.0014	0.0004	0.0102
2	0	-7.27	5.5	10.21	3.04	2.84	2.69	2.35	0.58	0.0373	0.0097	0.0022	0.0509	0.0132	0.0030	0.0672
3	0	-12.77	5.5	8.41	6.51	6.79	2.72	2.11	0.75	0.0310	0.0186	0.0069	0.0424	0.0254	0.0095	0.0773
3-4	0	-19.25	5.5	8.54	7.52	7.73	2.19	1.62	1.02	0.0254	0.0165	0.0107	0.0347	0.0225	0.0146	0.0718
4	0	-25.73	5.5	8.68	8.53	8.66	1.66	1.12	1.29	0.0196	0.0130	0.0151	0.0268	0.0177	0.0207	0.0652
5	-2.7	-27.5	5.4	13.52	9.35	8.60	1.14	0.59	0.72	0.0205	0.0074	0.0083	0.0280	0.0101	0.0113	0.0494
5-6	-8.1	-27.5	5.4	145.38	11.96	9.26	1.38	0.90	0.82	0.2678	0.0143	0.0101	0.3657	0.0195	0.0138	0.3990
6	-13.5	-27.5	5.4	277.24	14.57	9.91	1.63	1.20	0.92	0.6008	0.0233	0.0121	0.8205	0.0318	0.0165	0.8688
7	-18.9	-27.5	5.4	404.40	50.95	10.50	1.77	1.66	1.48	0.9526	0.1124	0.0207	1.3009	0.1534	0.0282	1.4825
7-8	-24.3	-27.5	5.4	624.72	215.80	23.64	1.62	1.67	1.53	1.3488	0.4810	0.0481	1.8419	0.6568	0.0656	2.5644
8	-29.7	-27.5	5.4	845.04	380.66	36.78	1.47	1.69	1.58	1.6583	0.8573	0.0772	2.2646	1.1707	0.1054	3.5407
9	-32.4	-25.73	5.5	626.68	491.96	89.69	0.75	0.81	1.27	0.6347	0.5421	0.1540	0.8667	0.7403	0.2103	1.8173
9-10	-32.4	-19.25	5.5	480.32	379.20	131.36	0.76	0.79	0.89	0.4964	0.4074	0.1592	0.6779	0.5564	0.2174	1.4517
10	-32.4	-12.77	5.5	333.97	266.45	173.04	0.78	0.77	0.52	0.3521	0.2790	0.1222	0.4809	0.3810	0.1669	1.0288
11	-32.4	-7.27	5.5	300.50	222.23	155.13	1.12	0.89	0.51	0.4551	0.2675	0.1083	0.6214	0.3653	0.1479	1.1346
12	-32.4	-1.77	5.5	500.26	372.23	159.71	0.65	1.09	1.25	0.4381	0.5509	0.2703	0.5983	0.7523	0.3691	1.7197
13	-29.7	0	5.4	585.45	366.91	85.35	1.36	1.66	1.49	1.0604	0.8090	0.1693	1.4481	1.1047	0.2311	2.7839
13-14	-24.3	0	5.4	495.00	291.56	58.08	1.45	1.60	1.39	0.9560	0.6203	0.1073	1.3055	0.8471	0.1466	2.2992
14	-18.9	0	5.4	404.55	216.21	30.81	1.54	1.54	1.29	0.8298	0.4433	0.0528	1.1332	0.6054	0.0721	1.8107
15	-13.5	0	5.4	352.96	113.08	19.06	1.31	1.19	0.93	0.6140	0.1787	0.0237	0.8385	0.2440	0.0324	1.1149
15-16	-8.1	0	5.4	190.55	62.66	16.51	1.18	0.84	0.77	0.2993	0.0704	0.0169	0.4087	0.0961	0.0231	0.5280
16	-2.7	0	5.4	28.15	12.25	13.95	1.05	0.50	0.61	0.0395	0.0082	0.0113	0.0539	0.0111	0.0154	0.0804
		height		6.2	3.7	1.2	6.2	3.7	1.2				Total Re-Entrainment (%)			24.97

* Inlet area is 63' (74mm in model scale) tall and 45, 46' (54, 55mm) wide

Vertical Distributions of Re-Entrainment Rate

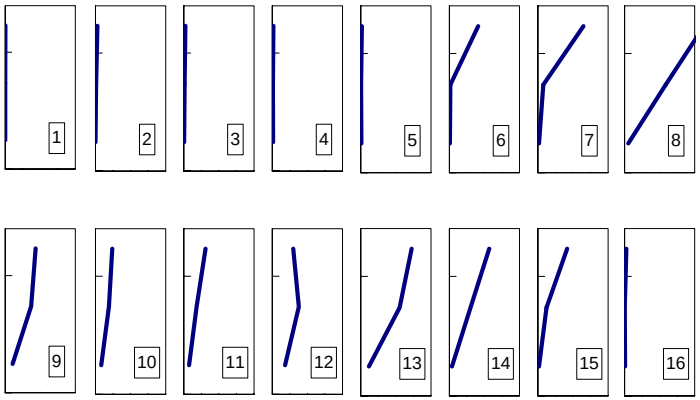

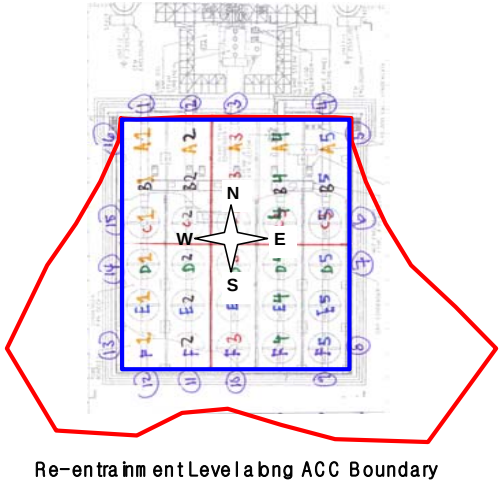

Re-entrainment Level along ACC Boundary

Estimated Contour of R

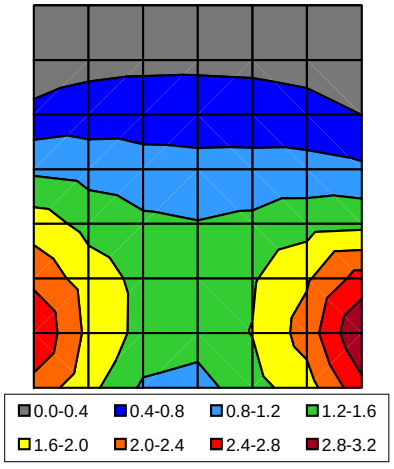

Figure 21 Wind Tunnel Model Testing Results for Moderate Northerly Wind

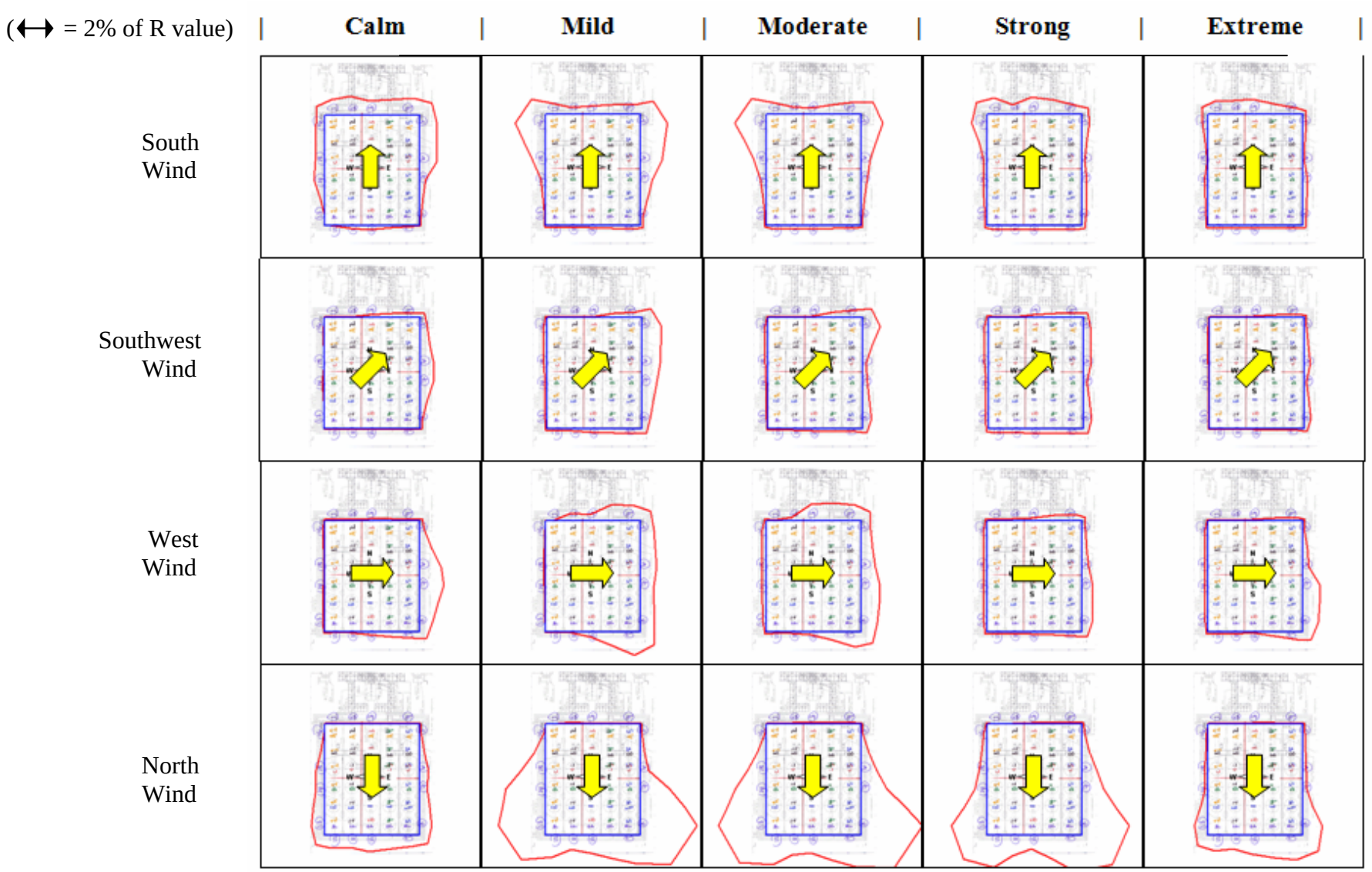

Figure 22 Re-entrainment Rate Distributions along the ACC Boundaries for Five Wind Speeds and Four Wind Directions

However, increasing wind speed significantly changes this trend. As wind speed increases, the wake size increases. When the wind is strong enough to pull the exhausted hot air from ACC, the re-entrainment accordingly decreases. Accordingly, highest recirculation is occurred at mid-level of upstream wind speed. This dependency of re-entrainment on wind speed also was reported by experimental study of Gu *et al*. (2007), Slawson & Sullivan (1981), and Hitchman & Slawson (1987) as well as Duvenhage and Kroger's computational study (1996). However, Kennedy and Fordyce (1974) have reported that strong wind speed stretches exhausted plume long enough to reach air-inlet of the fan cells and accordingly increases recirculation. Kennedy and Fordyce(1974) also showed the effect of wind speed on recirculation varies to the densimetric Froude number. Because of the differences in modeling conditions for experimental and numerical simulation of flow and heat transfer, the present and previous results show somewhat different value of peak recirculation level and corresponding wind speed. However, it is clearly agreed through all the research studies that wind speed strongly affects on the recirculation process.

The size of the wake and according recirculation also are significantly affected by geometric condition such as cooling tower configuration against wind and the space between adjacent buildings and cooling tower. The dependency of re-entrainment on wind direction was reported by Kennedy and Fordyce (1974) and Gu *et al*. (2007). They stated that the wind blowing in the direction of the major axis of a heat exchanger results in a high recirculation of hot plume. The north wind case in the present study showed the highest re-entrainment distribution while the west and south-west directions resulted in much lower re-entrainment rates.

Figure 23 was presented in order to evaluate how the total re-entrainments rate depends on the wind speed and direction. The wind speed in Figure 23 was converted from the category values in Table 3 to meteorological tower height speeds. North wind has a significantly higher re-entrainment rate than the rest of the wind directions. This is probably due to the power plant buildings and facilities being located directly upwind of the ACC in the North wind direction case. The peak values of total re-entrainment for the north wind direction were found in the mild

and moderate speed categories. For the south wind direction, although the buildings are downwind of the ACC, they still played a role in enhancing the re-entrainment. However, the overall magnitude of the total re-entrainment rate was much lower in the south wind case than the north wind case. Figure 23 also shows relatively higher R_T values along the gap between the ACC platform and buildings for the west wind direction case. Gu *et al*. (2007) stated that the adjacent building did not much affecting on the recirculation rates. However, their case considers the effect of building diagonally locating from the ACC module and is different to the present testing condition. Slawson and Sullivan (1981) and Hitchman and Slawson (1987) showed that re-circulation is strongly affected by separation distance between towers and the configuration.

Figure 23 indicates the west wind does not cause significant re-entrainment. However, the building affects on the recirculation and the southeast side of platform showed a higher re-entrainment rate than northeast corner. For the southwest wind direction, the ACC unit forms a wedge shaped projection to the incoming wind. Since the wake is weaker with such a condition, the R_T values are low for all southwesterly wind speeds.

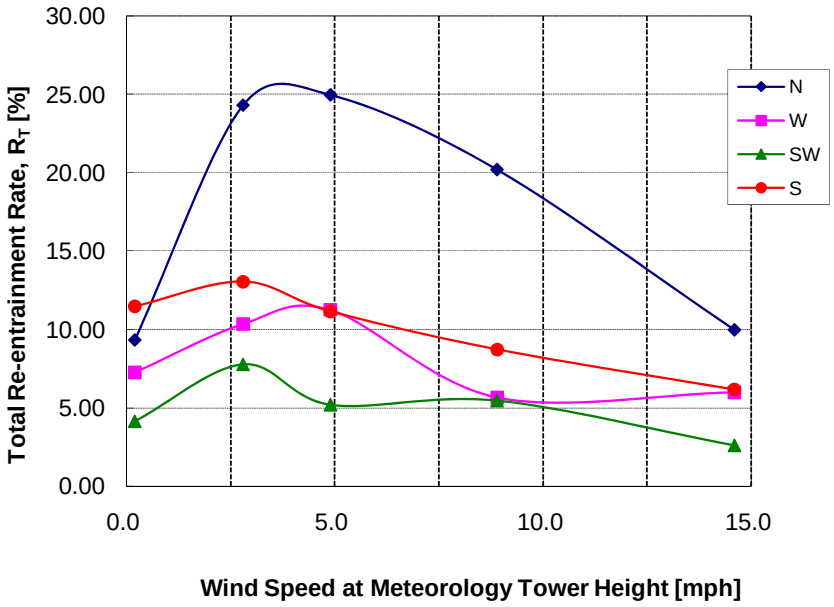

Figure 23 Effect of Wind Speed and Direction on the Total Re-entrainment Rate of the Base Model

Application of Meteorological Data

Although the testing results shown in Figures 21, 22, and 23 are useful to understand the recirculation phenomenon around the ACC platform, they however are not what is actually observed at the El Dorado site. This is because each of the result points was determined under ideal conditions of a single wind direction and single wind speed, yet the real atmosphere generally is much more complex than the ideally uniform wind-tunnel wind condition. Natural wind at a particular location, such as El Dorado in this study, usually has a pattern that can be found by analyzing meteorological data accumulated over a substantial period of time. Figure 15 displays this pattern in a wind rose and Table 3 shows the meteorological data. The left side of Table 3 shows the total hourly count of each wind direction in the corresponding speed range out of a total of 19,005 hours of observation including calm 127 hours. This hourly count can be converted into the occurrence percentage as shown on the right side of Table 3. It is obvious from the meteorological data that south-westerly wind is very dominant at the El Dorado site while north-westerly wind is scarce.

Table 4 Wind Data Collected by Maulbetsch (2008) Between 2001 and 2004 at the El Dorado Plant Meteorology Tower

		Hourly Count						Annual Occurrence [%]					
Speed	Low	0.2	2.8	4.9	8.9	14.6		0.2	2.8	4.9	8.9	14.6	
Range	High	2.8	4.9	8.9	14.6	& higher		2.8	4.9	8.9	14.6	& higher	
Direction	Azimuth	3554	3613	5246	4313	2279	Total	18.7%	19.0%	27.6%	22.7%	12.0%	Total
N	0	10	7	18	4	0	37	0.1%	0.0%	0.1%	0.0%	0.0%	0.2%
NNE	22.5	87	166	420	334	92	1092	0.5%	0.9%	2.2%	1.8%	0.5%	5.8%
NE	45	197	315	688	172	28	1395	1.0%	1.7%	3.6%	0.9%	0.1%	7.4%
ENE	67.5	229	257	319	66	19	879	1.2%	1.4%	1.7%	0.3%	0.1%	4.7%
E	90	263	256	262	43	18	831	1.4%	1.3%	1.4%	0.2%	0.1%	4.4%
ESE	112.5	286	222	236	72	8	813	1.5%	1.2%	1.2%	0.4%	0.0%	4.3%
SE	135	340	215	200	184	10	941	1.8%	1.1%	1.1%	1.0%	0.1%	5.0%
SSE	157.5	374	355	354	389	70	1534	2.0%	1.9%	1.9%	2.0%	0.4%	8.1%
S	180	473	595	885	572	341	2858	2.5%	3.1%	4.7%	3.0%	1.8%	15.1%
SSW	202.5	460	564	902	892	632	3447	2.4%	3.0%	4.7%	4.7%	3.3%	18.2%
SW	225	301	329	515	796	480	2404	1.6%	1.7%	2.7%	4.2%	2.5%	12.7%
WSW	247.5	247	174	280	485	392	1571	1.3%	0.9%	1.5%	2.6%	2.1%	8.3%
W	270	141	93	124	243	170	761	0.7%	0.5%	0.7%	1.3%	0.9%	4.1%
WNW	292.5	67	50	26	36	9	180	0.4%	0.3%	0.1%	0.2%	0.0%	1.0%
NW	315	56	10	11	14	6	88	0.3%	0.1%	0.1%	0.1%	0.0%	0.5%
NNW	337.5	23	5	6	11	4	47	0.1%	0.0%	0.0%	0.1%	0.0%	0.3%

In order to evaluate the actual re-entrainment level of the ACC, the wind occurrence percentage data should be applied to the wind results of the wind-tunnel modeling. The application of meteorological data is especially important in order to integrate the actual non-ideal winds on site with the results of the tunnel modeling.

Figure 24 displays the dependency of the total re-entrainment rate of the El Dorado site on wind speed and direction. Although the base model showed that the north wind direction has the highest re-entrainment rate, Figure 24 indicates that the re-entrainment caused by northerly wind is low at the El Dorado plant probably due to the low occurrence of northerly wind. Instead, southerly wind induces much higher re-entrainment. Despite the low contribution of southwest wind to the base model, Figure 24 shows that the southerly wind provides the highest re-entrainment due to its high occurrence. Figure 24 also shows a slightly different dependency on wind speed from the base model results shown in Figure 23. However, the highest re-entrainment rate did not occur at the highest wind speeds, but once again at moderate speeds.

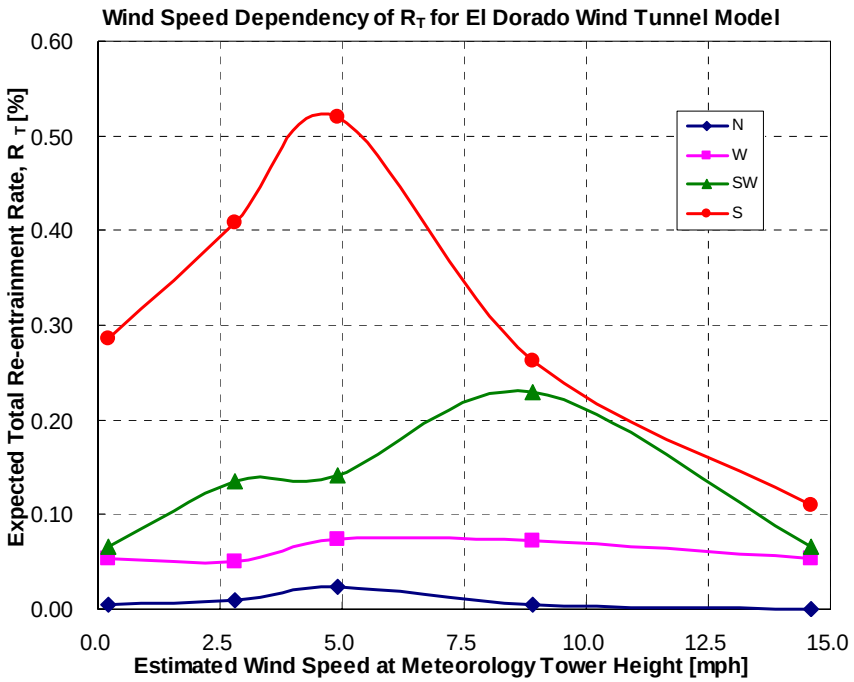

Figure 24 The Wind Speed and Direction's Effect on the Total Re-entrainment Rate of The El Dorado Air Cooling Condenser

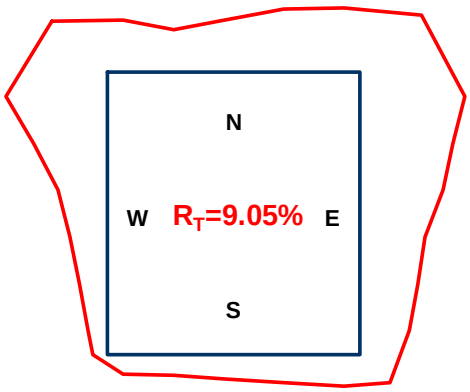

Figure 25 Annual Total Re-entrainment Rate of the El Dorado Site and the Distribution Along the Platform Boundary

Figure 25 displays the annually estimated total re-entrainment rate, R_T, in the local distribution profile along the platform boundary. The rectangle in the figure represents the ACC platform and the curve around the platform shows the magnitude of re-entrainment rate at the boundary cells. The highest re-entrainment was found on the northeast corner of the ACC closely followed by northwest corner and east edge. This local distribution is strongly affected by the characteristics of the El Dorado meteorological wind data, which has dominant wind coming from the southwesterly direction as shown in Figure 15 and Table 3.

Individual Contribution of Fan Cells

In order to find out the individual contribution of the fan cells on the total re-entrainment rate additional testing was done on the worst case of the previous results. Based on Figure 24, moderate south wind was found to cause the worst re-entrainment. For this additional testing, only one nozzle at a time was tested and released the ethane tracer gas. Then the ethane concentration levels were measured around the outer boundary of the ACC platform. Accordingly, a total of thirty sets of re-entrainment rate were measured and evaluated for each single nozzle. Due to the time constraint, the measurements were made at only the top one third portion of the testing surface. Figure 26 shows the thirty sets of correlation between each fan cell and the boundary testing surface recirculation. Each of the thirty charts is displayed at the

location of the corresponding fan cell on the ACC platform and the testing surface numbers identify the location of measurement. In the charts, the magnitude of re-entrainment caused by the fan cell to each testing surface was plotted in a red solid bar.

Figure 26 shows that the most significant contribution was made by the two corner edge cells onto the fans on the same side edge. The individual contribution of the fans along both side edges was higher than the fans in the middle. This suggests that a wedge shaped wake is generated from the front corners of the ACC and the wake spires along the side edges. In addition to the two edge wakes along the platform, the wake atop the fans also develops and mixes with the exhausted air. This mixing causes a cross sectional contribution of some fans to the testing surfaces on the other side as shown in Figure 26. For instance, the E1 fan re-circulates to the number-5 surface.

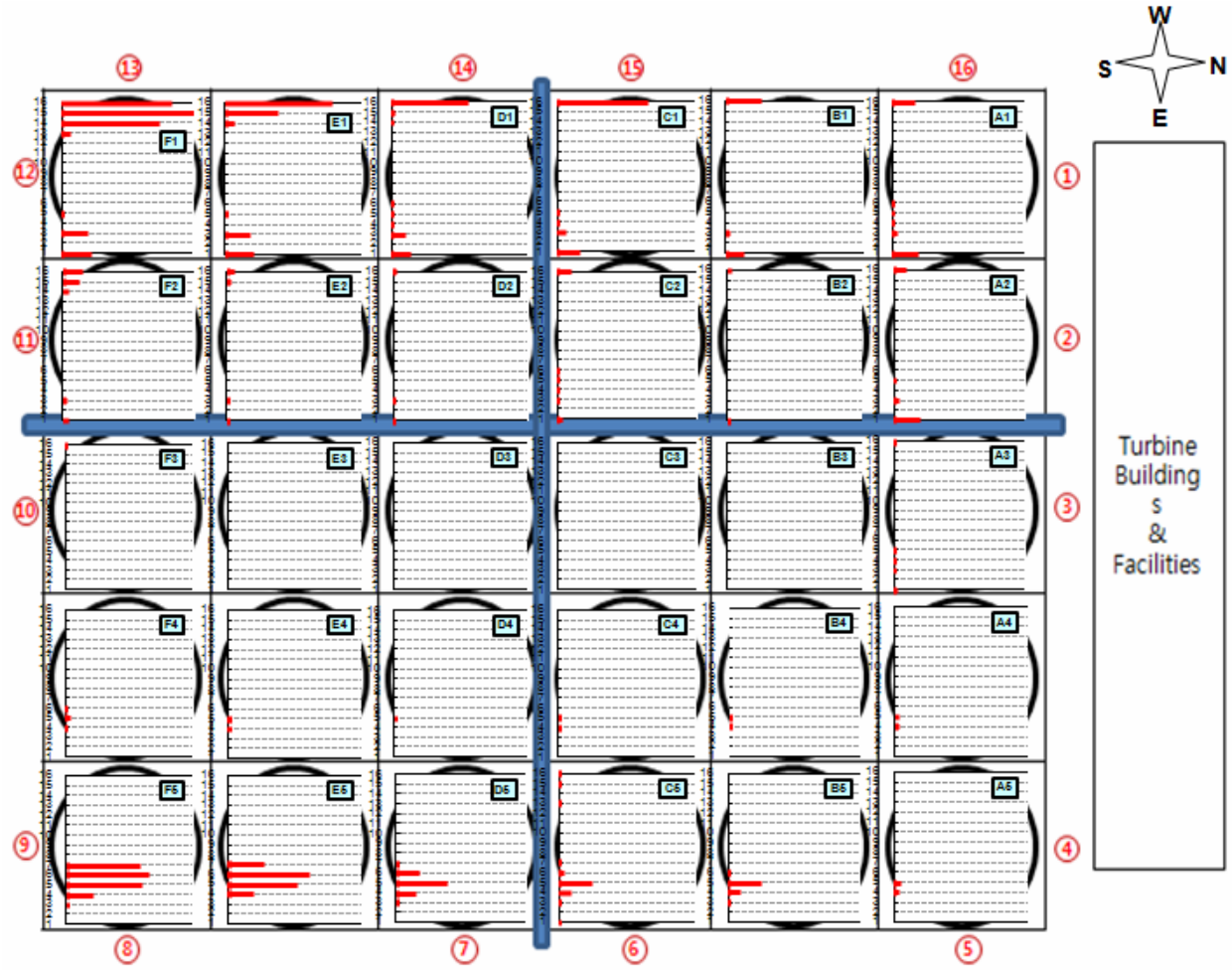

Figure 26 Individual Contribution of ACC Fans on Re-entrainment Rate for Southerly Moderate Wind

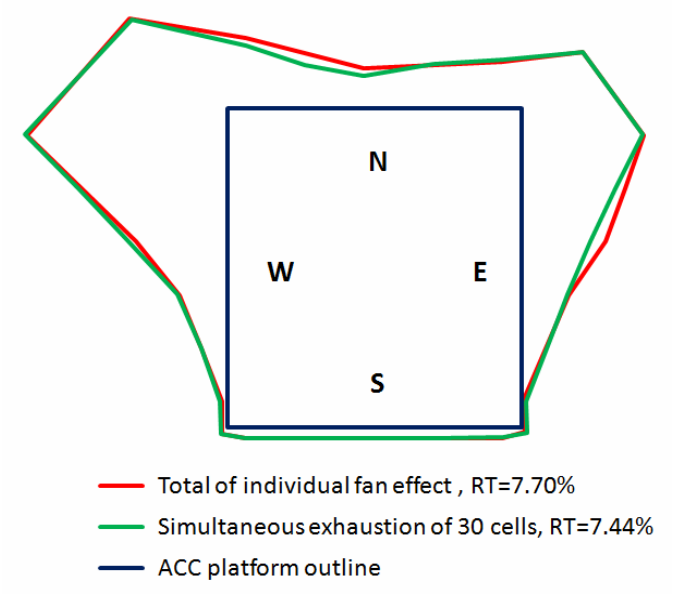

Figure 27 Comparison of Total Re-entrainment Rate Between Individual and Simultaneous Measurements

Figure 27 shows the local re-entrainment rate distributions of the individual contribution testing results and the simultaneous exhaust case results. Ideally, both results should be identical. Figure 27 shows slight differences between both results, however, the distribution trends and the values of total re-entrainment rates are reasonably well matched within the uncertainty range.

Mitigation Plans

In order to extend the understanding of ACC flow characteristics, four different modifications were applied on the ACC platform and were evaluated. As Hitchman and Slawson (1987), Bender et al. (1996a, 1996b), and Zhai and Fu (2006) have indicated, simple structures on or near cooling tower platform could improve cooling efficiency of the unit by changing flow pattern of the tower. Figure 28 shows the schematics of the proposed mitigation plans. Plan 1 utilizes a 15 feet extended horizontal skirt, from the walkway, around the platform. The skirt was assumed to be solid unlike the walkway. Plan 2 uses an extra downward 15 feet solid wall from the platform on all four sides. Plan 3 substituted the vertical windbreak with a 70 degree slanted wall up same height to the windbreak. Plan 4 employs a downward 9 feet long vertical wall similar to Plan 2. Figure 28 shows the individual contribution of each fan on the re-entrainment for the four mitigation plans.

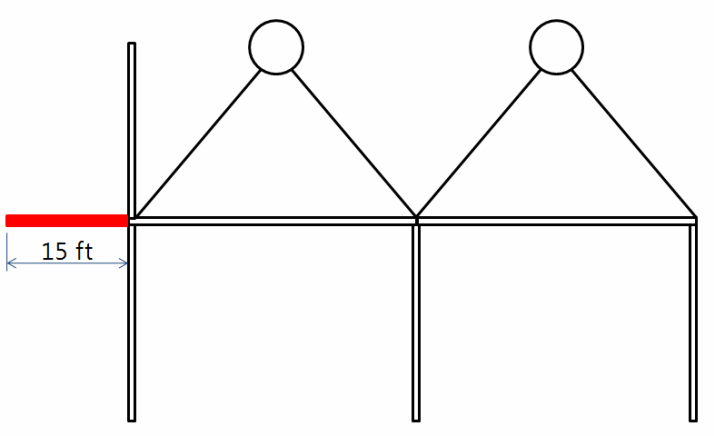

(a) Plan 1: 15 ft horizontal skirt

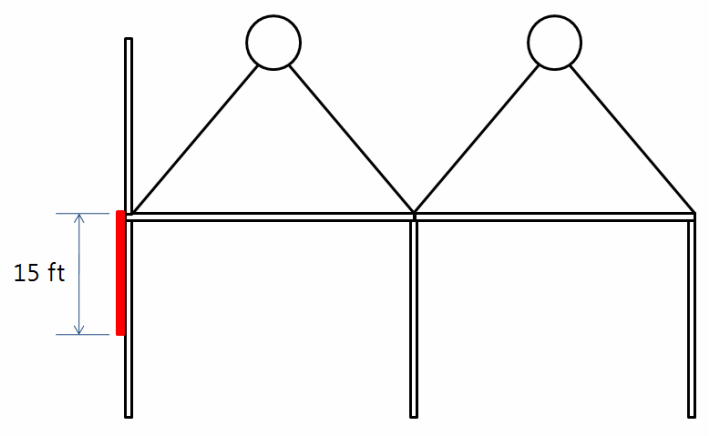

(b) Plan 2: 15 ft vertical windbreak

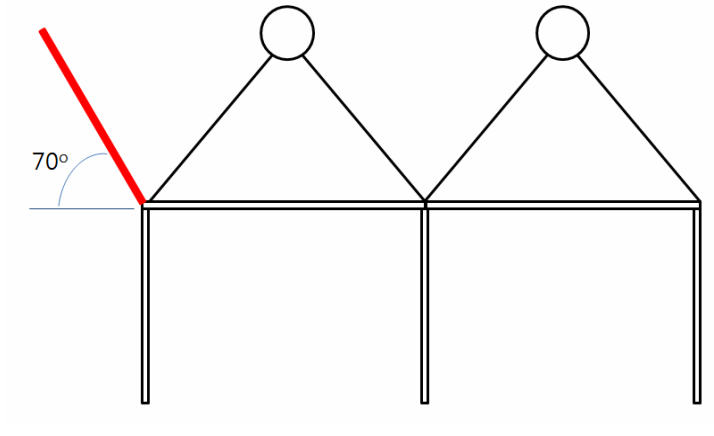

(c) Plan 3: 70 degree slanted wall without current windbreak

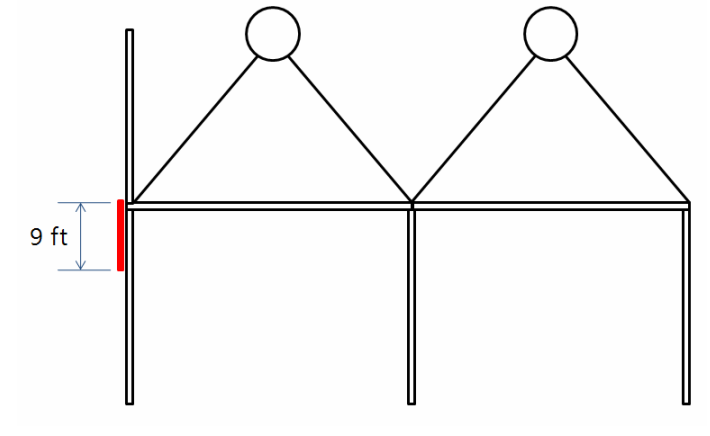

(d) Plan 4: 9 ft vertical windbreak

Figure 28 Schematic Diagrams of Tested Mitigation Plans

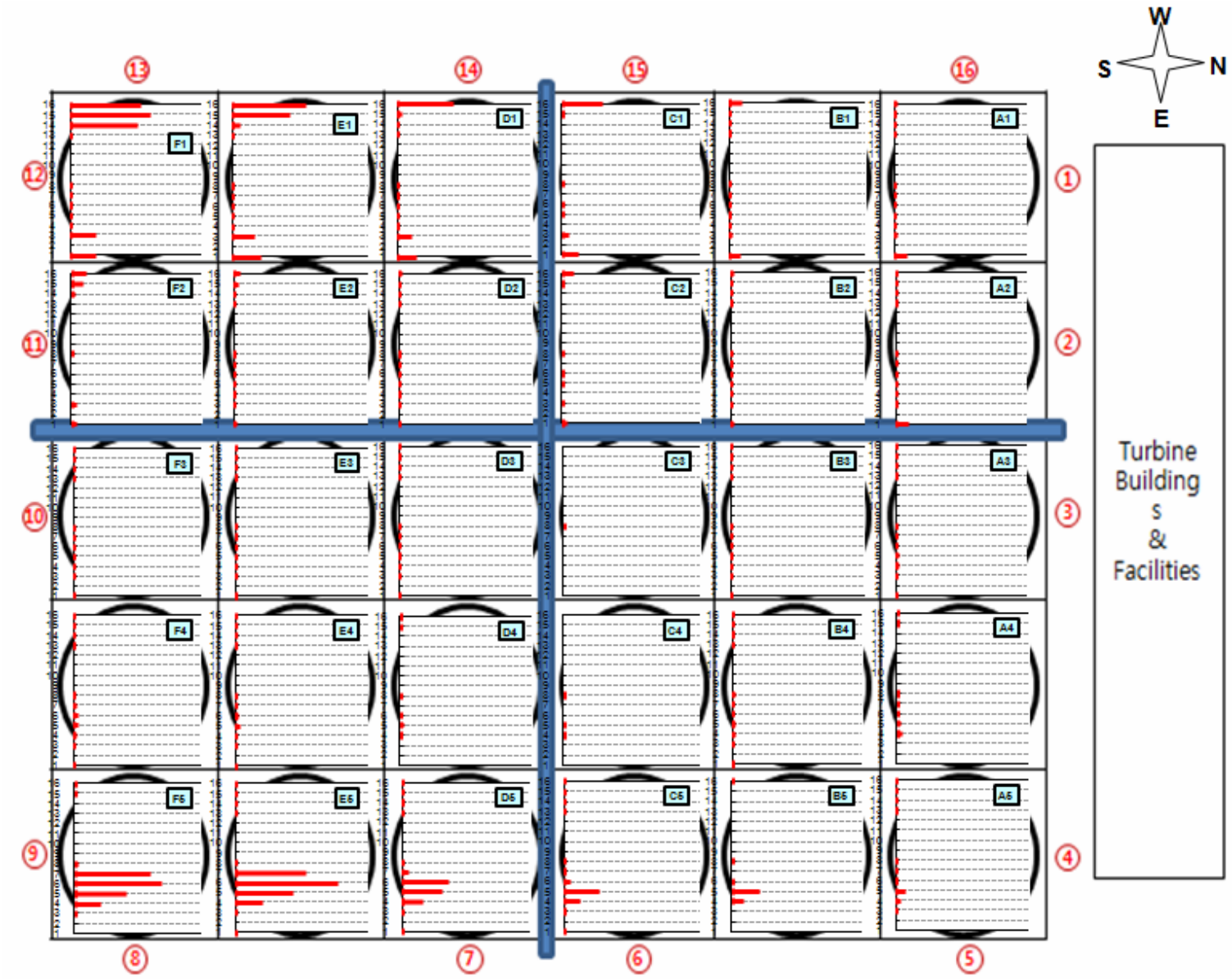

(a) Plan 1, 15 ft horiziontal skirt case

Figure 29 Individual Contributions of Each Fan, on ACC Platform, On Re-entrainment for Mitigation Plans

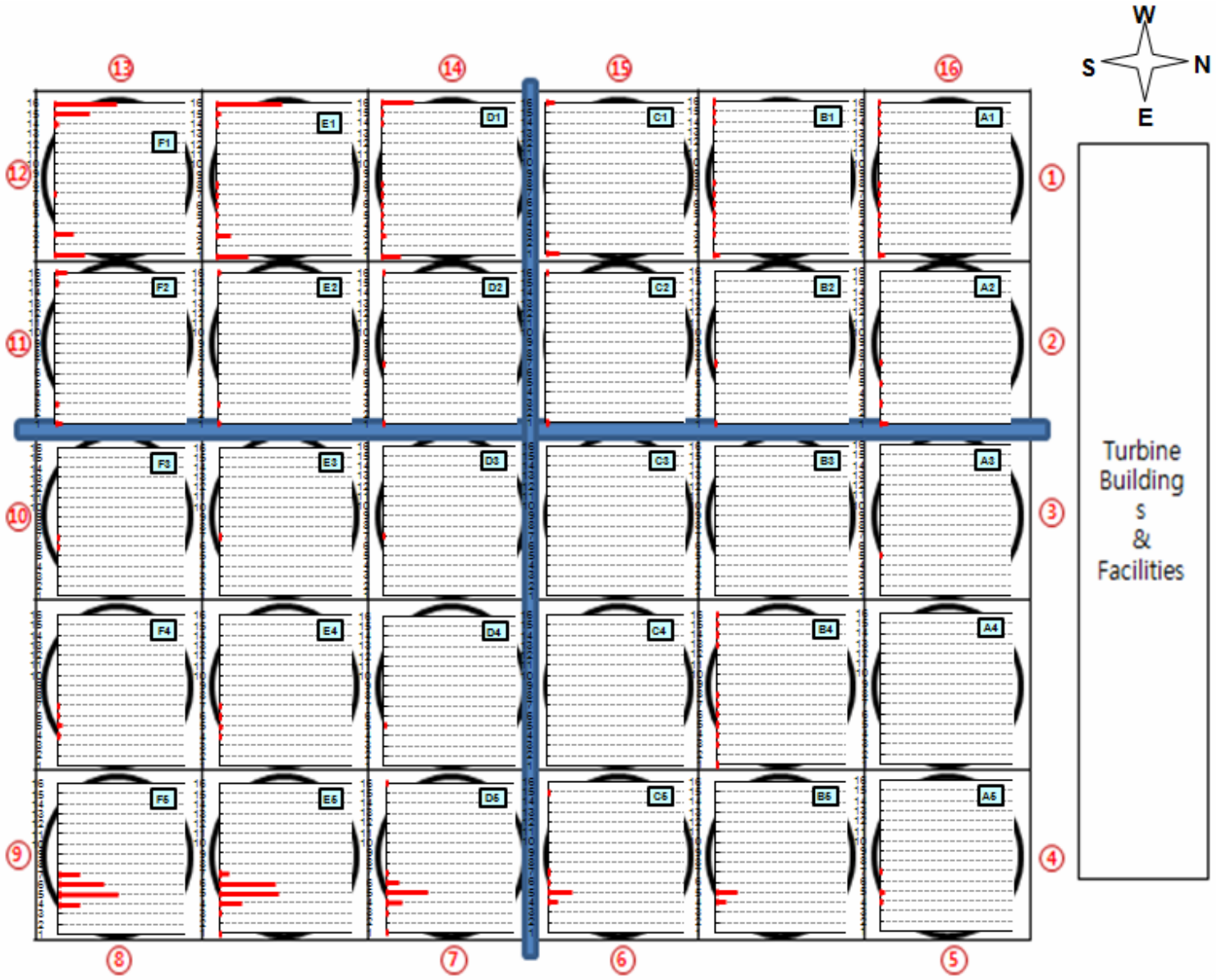

(b) Plan 2, 15 ft vertical hanger case

Figure 29 Individual Contributions of Each Fan, on ACC Platform, On Re-entrainment for Mitigation Plans

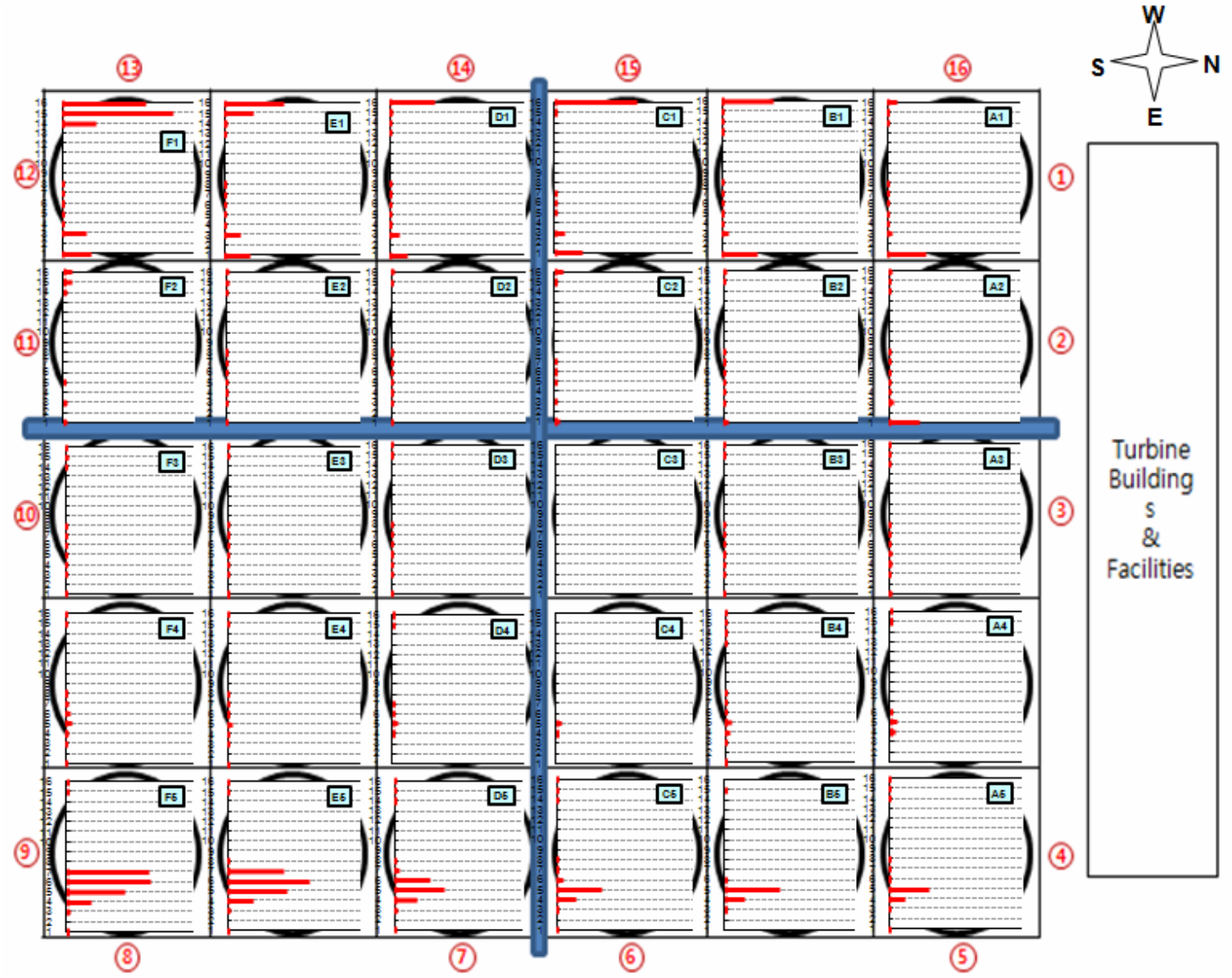

(c) Plan 3, 70 degree slanted wall atop the platform case

Figure 29 Individual Contributions of Each Fan, on ACC Platform, On Re-entrainment for Mitigation Plans

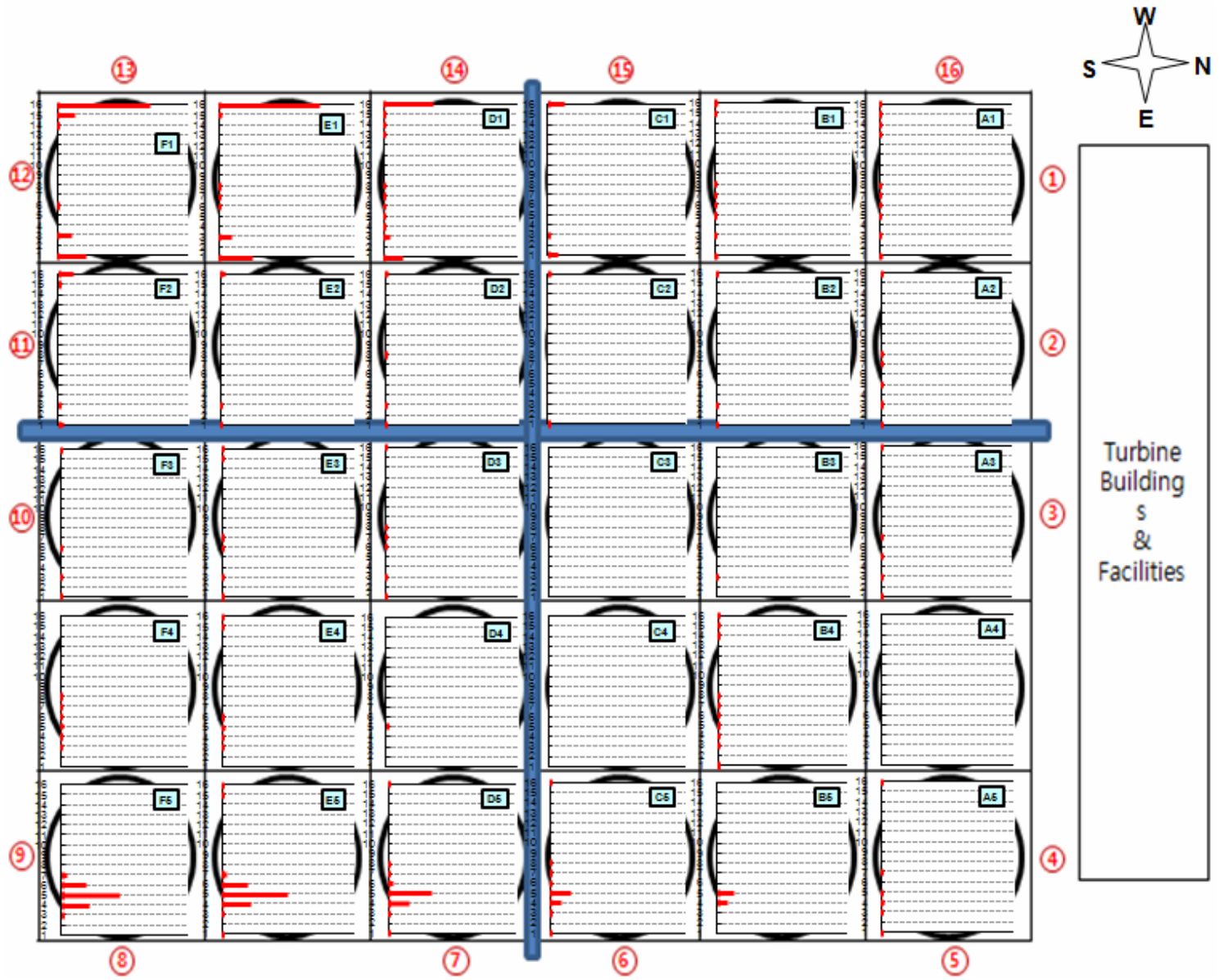

(d) Plan 4, 9 ft vertical hanger case

Figure 29 Individual Contributions of Each Fan, on ACC Platform, On Re-entrainment for Mitigation Plans

The characteristics of all four mitigation plans were similar to the existing case, which was shown in Figure 26 and explained previously. Among the four plans, the two vertical hanger cases showed the largest decrease in overall re-entrainment. It was found that regardless of the case, the largest re-entrainment came into the two outside back fans from the two front edge fans.

In order to quantitatively evaluate the effect of the mitigation plans on the re-entrainment rates, Figure 30 is presented. All six cases in Figure 30 are tested in southerly "mild" wind with the same configurations except the attachment of each mitigation plan. The front five purple bars in the figure indicate the summation of the individual contributions of all thirty fans, while the burgundy bar behind shows the existing result with all thirty nozzles releasing ethane gas simultaneously. It is found that the slanted wall of Plan 3 does not decrease the re-entrainment. The effect of the horizontal skirt in Plan 1 does not significantly decrease the re-entrainment. However, the vertical hangers in Plan 2 and Plan 4 decreased the total re-entrainment rate by over 40%. The effect of the vertical hangers is also shown in Figure 29 and Figure 30.

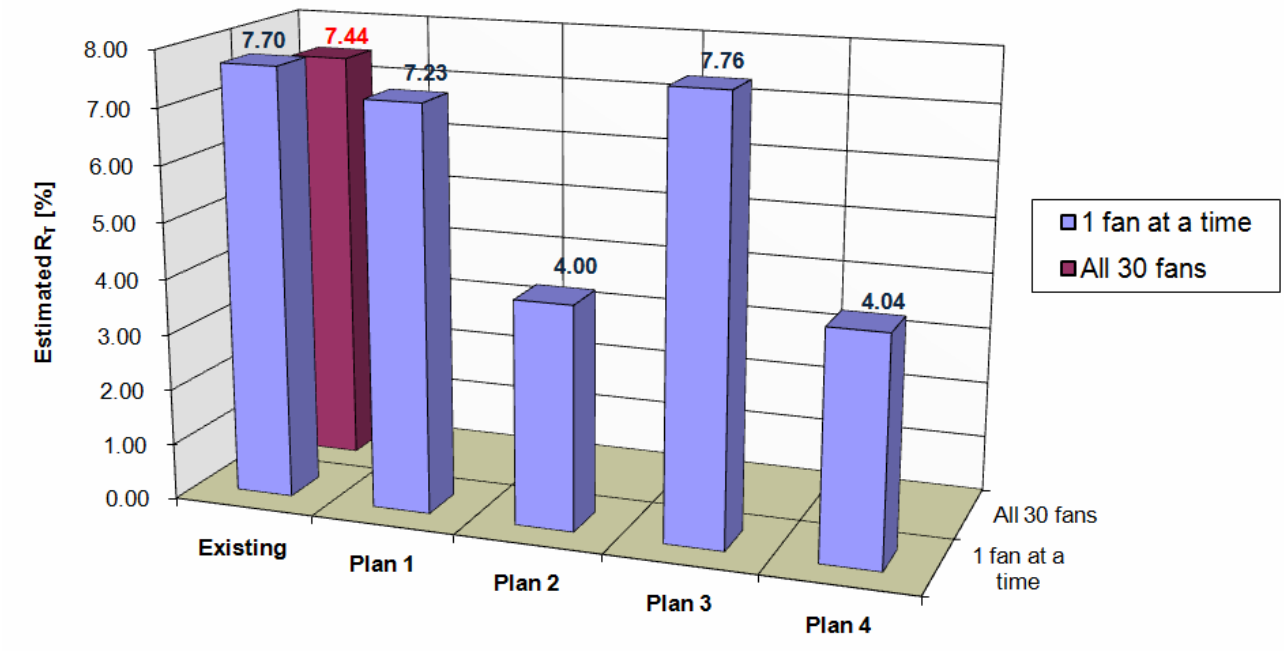

Figure 30 Total Re-entrainment Rate Comparison Between Existing Condition and Mitigation Plans

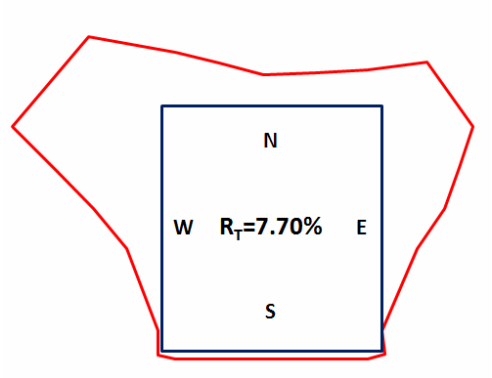

(a) Existing condition case

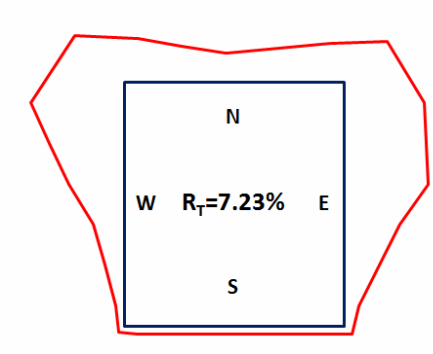

(b) Plan 1

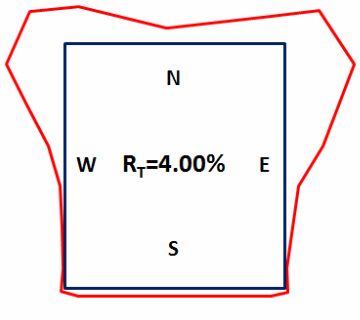

(c) Plan 2

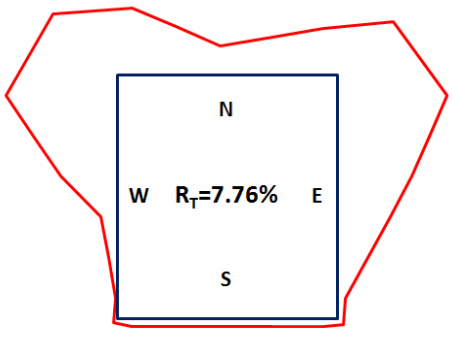

(d) Plan 3

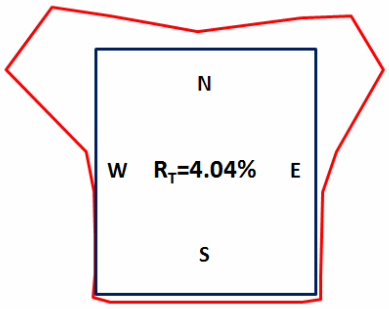

(d) Plan 4

Figure 31 Total Re-entrainment Rate and Local Distribution Along ACC Platform for Existing and Mitigation Plan Conditions

DUAL UNIT MODEL ANALYSIS

Previous chapters in this report present the wind-tunnel modeling procedure of a power plant and ACC and the application's methodology and results of re-entrainment rate. The previous wind-tunnel model was designed after the El Dorado power plant, although showed good potential to simulate similar case at any other location as long as accurate meteorological data is available. The design of the wind-tunnel model allowed for modification of the height of the ACC platform, the speed of each fan row, the porosity and configuration of the wind-screen beneath the platform, and the dimension and shape of the windbreak atop the platform in order to evaluate the effect of those parameters on the ACC flow. However, the distance between ACC and the adjacent buildings was fixed. The correlation between multiple ACC units in proximity to each other is another interesting issue as many power plant sites have multiple units. In order to gain insight into these various design parameters a separate dual ACC model was developed in the present study.

The basic geometry and configuration of this dual model was adopted from the single unit ACC model. However, simply doubling the ACC platforms with the other factors remaining the same would result in unrealistically large condensers versus the capacity of the power plant. To retain the correct balance, each ACC in the dual model was reduced to twelve fans arrayed in a 3x4 grid. Figure 32 shows the dual model.

Figure 32 Planar View of Dual ACC Model

The dual ACC model is capable of shifting the position of both ACC units and the power plant buildings. Figure 33 shows the nine total settings with three different ACC to ACC distances and three different ACCs to building distances. The gaps of each case in Figure 33 were set to multiples of the fan diameter. Testing of the dual ACC model was conducted for (a), (d), and (g) settings, seen in Figure 33. The testing wind condition used was a moderate northerly wind as the base single ACC model had the highest re-entrainment at this condition. Ethane gas was released through all 24 nozzles simultaneously. Due to the similarity between ACC units, only one unit was tested for re-entrainment rates.

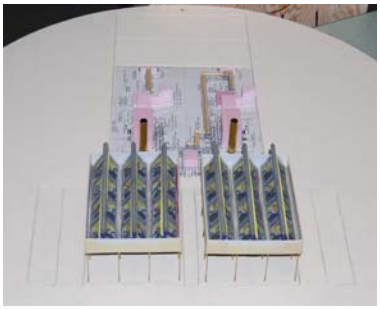

(a) fan-near & bldg.-near

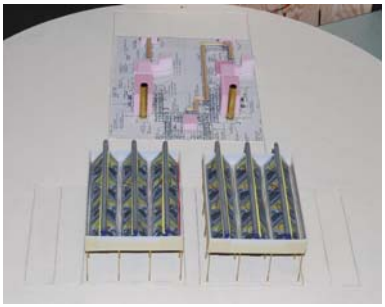

(b) fan-near & bldg.-mid.

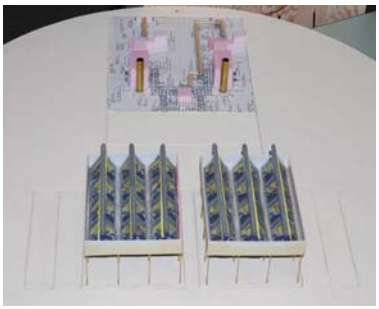

(c) fan-near & bldg.-far

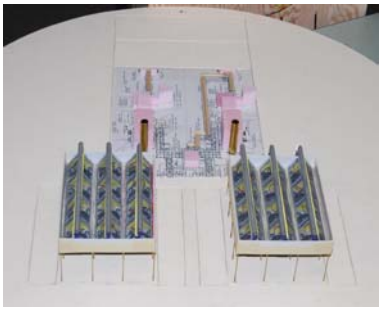

(d) fan-mid. & bldg.-near

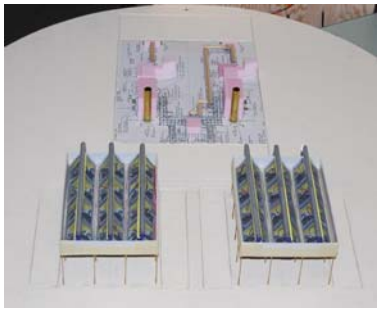

(e) fan-mid. & bldg.-mid.

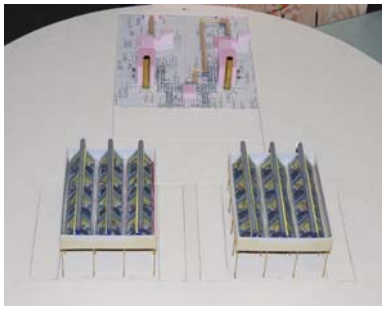

(f) fan-mid. & bldg.-far

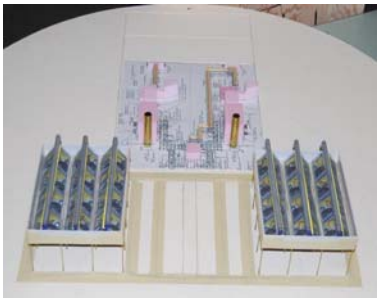

(g) fan-far & bldg.-near

(h) fan-far & bldg.-mid.

(i) fan-far & bldg.-far

Figure 33 Settings of Dual ACC Wind Tunnel Model

Figure 34 shows the schematics of the dual ACC model with the configuration of fan cells and testing locations. Unlike the single ACC model, wind screens under the platforms were not installed for the dual ACC model. Measurements were made at all 14 surfaces beneath all of the edge fans and the identification numbers of the testing surfaces are indicated in Figure 34.

Detailed results of the testing are presented as worksheets in Appendix-B. Figure 35 shows the local distribution of re-entrainments rate for three different ACC-to-ACC distance settings. Asymmetric distributions of re-entrainment rates were found for all three testing cases. The presence of another ACC unit makes the space between ACCs relatively limited compared to the open space on the opposite side and accordingly entrains more exhausted air downward than from the open side of ACC platform. This effect is most evident with the nearest ACC-to-ACC gap setting. However, the magnitude of local re-entrainment rate for the farthest and medium gap cases becomes similar, which indicates no significant influence of ACC-to-ACC distance beyond the medium gap. Figure 36 presents the total re-entrainment rates for the three testing conditions. The nearest ACC-to-ACC case bears very high R_T values and the medium gap decreased this rate significantly. The farthest gap case resulted in the lowest re-entrainment rate, however was only minimally better than the middle distance setting.

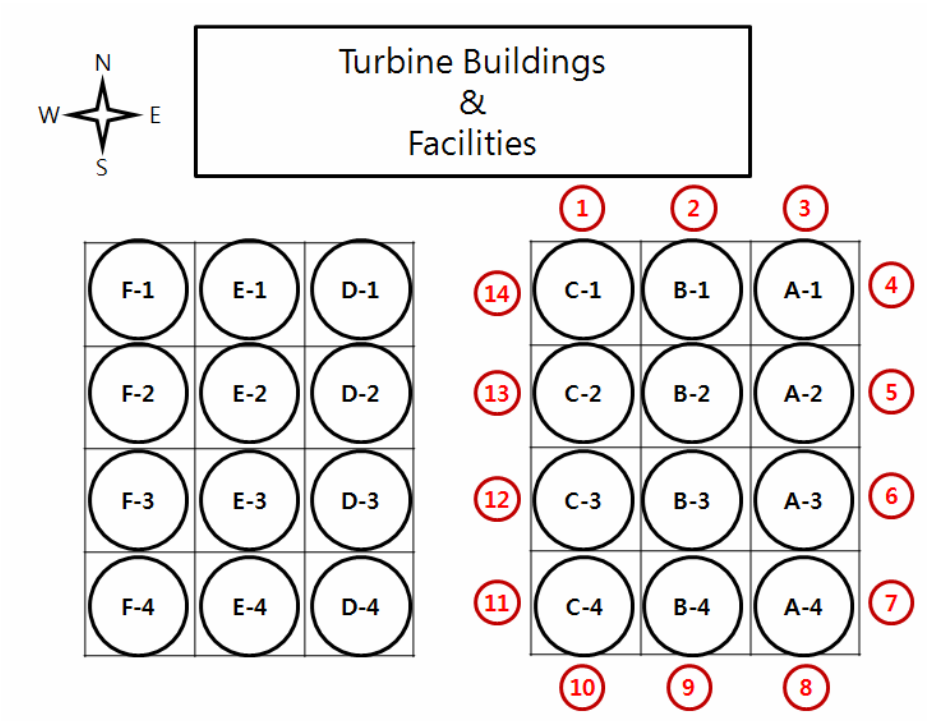

Figure 34 Dual ACC Model Configuration and Testing Locations

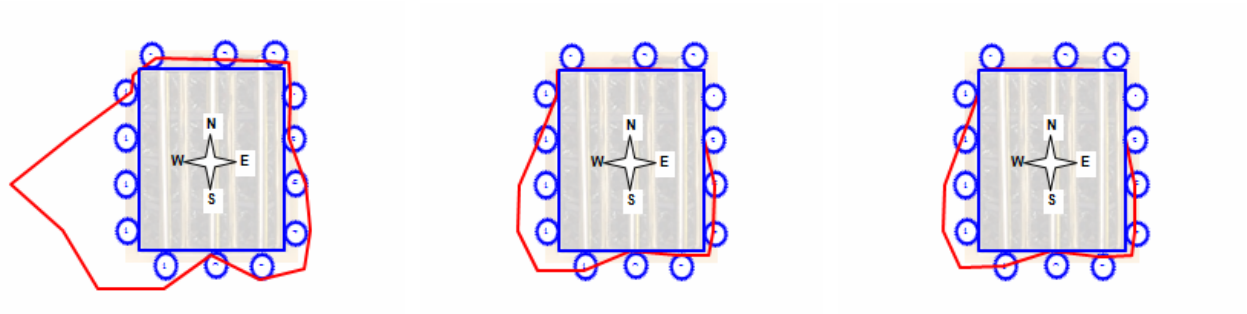

(a) nearest ACC gaps (b) medium ACC gaps (c) farthest ACC gaps

Figure 35 Dual ACC Model Distribution of Re-entrainment Rates

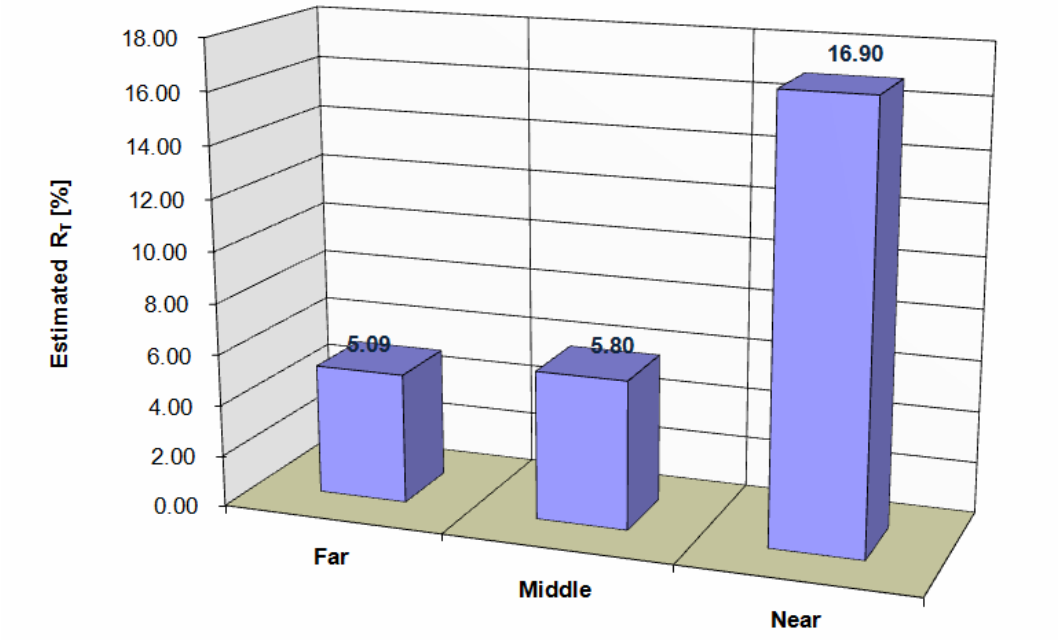

Figure 36 The Effect of the Gap Between ACC Platforms on the Total Re-entrainment Rate

CONCLUSION

Two wind-tunnel models were developed to simulate the wind effect on power plant air cooling condensers (ACC). The El Dorado power plant in Nevada was chosen to be modeled. The wind-tunnel models simulate a single ACC unit power plant and a power plant with adjacent dual ACCs. The models were mounted in the wind tunnel under various testing settings with combinations of upcoming wind speeds and directions. Flow patterns, over the ACC platform, were measured with a hot-wire sensor using constant temperature anemometry to evaluate the uniformity of upward flow from each fan cell. The suction of air flow through the open spaces beneath the ACC platform also was measured. In order to evaluate the effect of the wind on the ACCs, ethane gas was released from nozzles atop each fan and the concentration level of the ethane was measured at the inlet to the fans. The flow speed data and the concentration levels were then combined to determine the local re-entrainment rate at each testing point. The local re-entrainment rate also was examined with only one nozzle issuing the ethane gas at a time in order to evaluate the individual contribution of each fan cell to the re-entrainment rate distribution. The total of the individual contributions was found to well match the result of all the nozzles issuing the ethane gas simultaneously.

The re-entrainment rate was highest with the wind coming over the adjacent buildings. The opposite wind direction had second highest effect on the re-entrainment rate followed by the wind direction perpendicular to the axis that runs through the buildings and the ACC. The wind coming diagonally from the side of the ACC and buildings showed the least effect. However, applying the meteorological data collected from the site showed completely different patterns of the wind's effect on the site. Since the southerly wind is dominant at the El Dorado site while the northerly wind is rare, the overall effect of the wind on the ACC re-entrainment was highest with southerly wind followed by the diagonal wind.

Four mitigation plans were tested to find if the re-entrainment rate could be decreased. Vertical hanging walls at the outer edge of the ACC platform decreased the re-entrainment rate to almost half of the existing condition. Two different lengths, 15 ft and 9 ft, walls were tested, although the results were not significantly different.

A dual unit model was tested with three gap distances between the two ACC models and the findings showed that the nearest gap had the highest re-entrainment rate. Beyond a certain point, the distance between ACC does not significantly affect the ACC re-entrainment.

ACKNOWLEDGEMENTS

The authors are deeply grateful to Dr. Charles McGowin of EPRI for his generous support and patience for last two years of project. We wish to acknowledge that Dr. John Maulbetsch of Maulbetsch Consulting has been providing very helpful discussion and his field measurement experience. The meteorology data and plant conditions of El Dorado site were provided by Dr. Maulbetsch and Mr. Michael Spaulding, a former Plant Engineer of El Dorado Energy LLC. Mr. Franck David of EdF (Électricité de France) has shared his computational simulation results of single and dual air cooling condenser units with us. Dr. Robert Goldstein and other great researchers of EPRI have given us valuable comments so we could analyze the results more appropriately. Miss Bethany Kuspa, a former manager of U.C. Davis ABLWT laboratory, deserves special appreciation for her effort at the beginning stage of this project. U.C. Davis students Mr. Ashishkumar Patel and Mr. Justin Tucker have been great helpers to conduct huge hours of modeling and testing. Mrs. Yoke Dellenback, Mrs. Sharon Holgerson, and Mrs. Denyse Miller in Department of Mechanical and Aerospace Engineering of U.C. Davis have handled various administrative affairs smoothly and allowed us to concentrate on the engineering work of this project. The authors sincerely thank to each of these colleagues and friends.

REFERENCES

Rafat **Al-Waked** and Masud Behnia, "The performance of natural draft dry cooling towers under crosswind: CFD study," Int. J. Energy Research, Vol. 28, pp. 147-161, 2004

T.J. **Bender**, D.J. Bergstrom, and K.S. Rezhallah, "A study on the effects of wind on the air intake flow rate of a cooling tower: Part 2. Wind wall study," J. Wind Engineering and Industrial Aerodynamics, Vol. 64, pp.61-72, 1996a

T.J. **Bender**, D.J. Bergstrom, and K.S. Rezhallah, "A study on the effects of wind on the air intake flow rate of a cooling tower: Part 3. Numerical study," J. Wind Engineering and Industrial Aerodynamics, Vol. 64, pp.73-88, 1996b

R.B. **Bornoff** and M.R. Mokhtarzadeh-Dehghan, "A numerical study of interacting buoyant cooling-tower plumes," Atmospheric Environment, Vol.35, pp.589-598, 2001

D. **Derksen**, K.S. Rezhallah, and D.J. Bergstron, "A wind tunnel study of the effect of wind on the air intake of a cooling tower," ASME Measurement and Modeling of Environmental Flows, FED-Vol.143/HTD-Vol.232, pp. 171-176, 1992

D.D. **Derksen**, T.J. Bender, D.J. Bergstrom, and K.S. Rezhallah, "A study on the effects of wind on the air intake flow rate of a cooling tower: Part 1. Wind tunnel study," J. Wind Engineering and Industrial Aerodynamics, Vol. 64, pp.47-59, 1996

A.F. **du Preez** and D.G. Kröger, "Effect of wind on performance of a dry-cooling tower," Heat Recovery systems & CHP, Vol. 13, No.2, pp.139-146, 1993

A.F. **du Preez** and D.G. Kröger, "Effect of the shape of the tower supports and walls on the performance of a dry -cooling tower subjected to cross winds," Heat Transfer Engineering, Vol. 16, No.2, pp.42-49, 1995

A.F. **du Preez** and D.G. Kröger, "The effect of the heat exchanger arrangement and wind-break walls on the performance of natural draft dry-cooling towers subjected to cross-winds," J. Wind Engineering and Industrial Aerodynamics, Vol. 58, pp.293-303, 1995

K. **Duvenhage** and D.G. Kröger, "The influence of wind on the performance of forced draught air-cooled heat exchangers," J. Wind Engineering and Industrial Aerodynamics, Vol. 62, pp.259-277, 1996

Zhifu **Gu**, Hui Li, Wenhong Zhang, Yan Li, and Jiye Peng, "Wind tunnel simulation on re-circulation of air-cooled condensers of a power plant," J. Wind Engineering and Industrial Aerodynamics, Vol.93, pp.509-520, 2005

Zhifu **Gu**, Xuerei Chen, William Lubitz, Yan Li, and Wenlin Luo, "Wind tunnel simulation of exhaust recirculation in an air-cooling system at a large power plant," Int. J. Thermal Sciences, V.46, No.3, pp.308-317, 2007

G.J. **Hitchman** and P.R. Slawson, “An experimental investigation of recirculation and interference on modeled forced-draft round cooling towers,” J. Engineering for Gas Turbines and Power, Vol.109, pp.124-125, 1987

N. **Isymov** and H. Tanaka, “Wind tunnel modeling of stack gas dispersion – Difficulties and approximations,” Proceedings of Fifth Int. Conf. on Wind Engineering July 8-14 1979, Colorado State University, Vol. II, pp.VIII-3-1 to 15.

M. **Jensen**, “The model-law for phenomena in natural wind,” *Ingeniøren (International Edition)* , Vol. 2, No. 4, 1958

C.G. **Justus** and Amir Mikhail, “Height variation of wind speed and wind distributions statistics,” Geophysical Research Letters, Vol. 3, No. 5, pp.261-264, 1976

John F. **Kennedy** and Homer Fordyce, “Plume recirculation and interference in mechanical-draft cooling towers,” Proceedings of Cooling Tower Environment-1974 Symposium March 4-6, pp.58-87, 1974

Detlev G. **Kröger**, “Air-cooled heat exchangers and cooling towers; Thermal-flow performance evaluation and design,” Volume II, 2004

John S. **Maulbetsch**, personal communication and field measurement data, 2008

P. R. **Slawson** and H. F. Sullivan, “Model studies on the design and arrangement of forced draft cooling towers to minimize recirculation and interference,” Waste heat, utilization and management, Proceeding of Miami Beach Conference May 11-13, 1981, pp. 235- proceeding, 1981

William H. **Snyder**, “Guideline for fluid modeling of atmospheric diffusion,” US EPA Report No.EPA-600/8-81-009, 1981

M.D. **Su**, G.F. Tang, and S. Fu, “Numerical simulation of fluid flow and thermal performance of a dry-cooling tower under cross wind condition,” J. Wind Engineering and Industrial Aerodynamics, Vol. 79, pp. 289-306, 1999

O.G. **Sutton**, “Atmospheric Turbulence,” 1949

Q. **Wei**, B. Zhang, K.Liu, X. Du, and X. Meng, “A study of the unfavorable effects of wind on the cooling efficiency of dry cooling towers,” J. Wind Engineering and Industrial Aerodynamics, Vol. 54/55, pp. 633-643, 1995

Z. **Zhai** and S. Fu, “Improving cooling efficiency of dry-cooling towers under cross-wind conditions by using wind-break methods,” Applied Thermal Engineering, Vol. 26, pp. 1008-1017, 2006

APPENDIX

Appendix –A Testing Results of the Single Unit Base Model

Wind Strength	Calm			Wind Direction	S		Ethan Purity	12.6							
	X	Y	width	Concentration [PPM]			Speed [m/s]			Flux (times million)			Re-Entrainment Rate (%)			
	[cm]	[cm]	[cm]	T	M	B	T	M	B	T	M	B	T	M	B	SUM
1	0	-1.77	5.5	63.80	36.81	5.18	0.64	0.53	0.46	0.0557	0.0267	0.0032	0.5944	0.2849	0.0347	0.9140
2	0	-7.27	5.5	71.85	32.67	3.90	0.73	0.65	0.27	0.0715	0.0288	0.0015	0.7628	0.3077	0.0155	1.0860
3	0	-12.77	5.5	62.16	32.40	4.80	0.74	0.33	0.21	0.0621	0.0144	0.0014	0.6629	0.1543	0.0146	0.8318
3-4	0	-19.25	5.5	68.58	32.34	5.50	0.68	0.44	0.37	0.0637	0.0194	0.0028	0.6801	0.2071	0.0296	0.9168
4	0	-25.73	5.5	74.99	32.27	6.20	0.63	0.56	0.53	0.0644	0.0243	0.0045	0.6877	0.2598	0.0478	0.9953
5	-2.7	-27.5	5.4	85.93	29.40	5.59	0.60	0.52	0.52	0.0684	0.0205	0.0039	0.7299	0.2189	0.0411	0.9899
5-6	-8.1	-27.5	5.4	81.23	21.66	3.32	0.69	0.61	0.57	0.0750	0.0176	0.0025	0.8006	0.1876	0.0271	1.0153
6	-13.5	-27.5	5.4	76.53	13.92	1.05	0.79	0.69	0.63	0.0804	0.0129	0.0009	0.8585	0.1375	0.0094	1.0054
7	-18.9	-27.5	5.4	25.75	1.94	2.05	0.78	0.69	0.61	0.0266	0.0018	0.0017	0.2838	0.0191	0.0178	0.3208
7-8	-24.3	-27.5	5.4	14.71	2.06	2.08	0.70	0.63	0.56	0.0137	0.0017	0.0015	0.1465	0.0184	0.0165	0.1814
8	-29.7	-27.5	5.4	3.66	2.19	2.10	0.63	0.56	0.51	0.0031	0.0016	0.0014	0.0326	0.0174	0.0151	0.0651
9	-32.4	-25.73	5.5	1.05	1.13	2.08	0.54	0.47	0.41	0.0008	0.0007	0.0012	0.0082	0.0077	0.0125	0.0283
9-10	-32.4	-19.25	5.5	9.08	2.61	2.00	0.61	0.55	0.51	0.0075	0.0019	0.0014	0.0803	0.0208	0.0147	0.1159
10	-32.4	-12.77	5.5	17.10	4.09	1.91	0.68	0.63	0.60	0.0158	0.0035	0.0016	0.1689	0.0375	0.0167	0.2231
11	-32.4	-7.27	5.5	12.83	3.72	2.00	0.58	0.52	0.49	0.0101	0.0026	0.0013	0.1075	0.0281	0.0143	0.1499
12	-32.4	-1.77	5.5	1.32	0.84	0.99	0.52	0.48	0.40	0.0009	0.0005	0.0005	0.0100	0.0058	0.0057	0.0215
13	-29.7	0	5.4	1.68	0.92	0.90	0.59	0.55	0.49	0.0013	0.0007	0.0006	0.0141	0.0072	0.0063	0.0276
13-14	-24.3	0	5.4	27.24	5.50	0.78	0.66	0.60	0.54	0.0240	0.0044	0.0006	0.2567	0.0470	0.0061	0.3098
14	-18.9	0	5.4	52.80	10.08	0.66	0.73	0.66	0.60	0.0517	0.0088	0.0005	0.5516	0.0941	0.0056	0.6513
15	-13.5	0	5.4	44.87	8.06	0.45	0.75	0.65	0.59	0.0447	0.0070	0.0003	0.4769	0.0743	0.0037	0.5550
15-16	-8.1	0	5.4	45.31	10.00	1.27	0.69	0.61	0.54	0.0415	0.0081	0.0009	0.4432	0.0864	0.0097	0.5393
16	-2.7	0	5.4	45.75	11.93	2.09	0.63	0.57	0.49	0.0383	0.0090	0.0014	0.4088	0.0962	0.0145	0.5195
		height		6.2	3.7	1.2	6.2	3.7	1.2				Total Re-Entrainment (%)			11.46

* Inlet area is 63' (74mm in model scale) tall and 45, 46' (54, 55mm) wide

Vertical Distributions of Re-Entrainment Rate

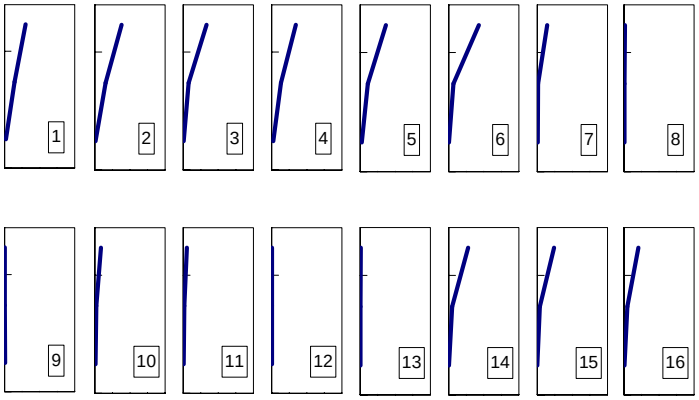

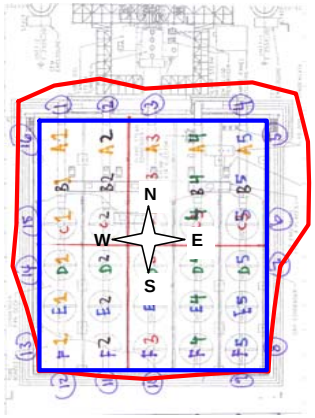

Re-entrainment Level along ACC Boundary

Estimated Contour of R

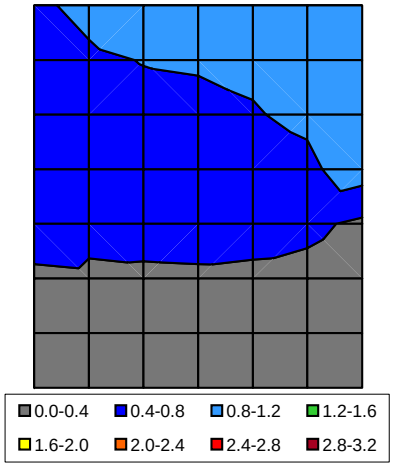

Wind Strength	Mild			Wind Direction	N		Ethan Purity	98.5							
	X	Y	width	Concentration [PPM]			Speed [m/s]			Flux (times million)			Re-Entrainment Rate (%)			
	[cm]	[cm]	[cm]	T	M	B	T	M	B	T	M	B	T	M	B	SUM
1	0	-1.77	5.5	1.03	0.60	0.44	1.87	1.62	1.44	0.0026	0.0013	0.0009	0.0036	0.0018	0.0012	0.0066
2	0	-7.27	5.5	26.48	0.54	0.40	2.13	1.93	0.32	0.0764	0.0014	0.0002	0.1044	0.0019	0.0002	0.1065
3	0	-12.77	5.5	6.79	3.60	3.69	2.27	1.71	0.39	0.0209	0.0084	0.0019	0.0285	0.0114	0.0026	0.0426
3-4	0	-19.25	5.5	6.71	4.88	4.79	1.96	1.50	0.78	0.0179	0.0099	0.0051	0.0244	0.0136	0.0069	0.0449
4	0	-25.73	5.5	6.63	6.15	5.89	1.66	1.29	1.17	0.0149	0.0108	0.0093	0.0204	0.0147	0.0128	0.0479
5	-2.7	-27.5	5.4	12.70	8.16	6.94	1.17	0.76	0.83	0.0197	0.0083	0.0077	0.0270	0.0113	0.0105	0.0488
5-6	-8.1	-27.5	5.4	83.68	8.75	8.40	1.33	0.99	0.93	0.1487	0.0115	0.0104	0.2030	0.0157	0.0142	0.2330
6	-13.5	-27.5	5.4	154.66	9.35	9.87	1.50	1.21	1.03	0.3092	0.0151	0.0136	0.4222	0.0206	0.0185	0.4613
7	-18.9	-27.5	5.4	445.44	61.72	9.52	1.76	1.67	1.58	1.0462	0.1370	0.0201	1.4287	0.1871	0.0274	1.6433
7-8	-24.3	-27.5	5.4	612.08	260.86	25.83	1.55	1.58	1.52	1.2611	0.5500	0.0524	1.7222	0.7511	0.0716	2.5449
8	-29.7	-27.5	5.4	778.72	460.00	42.13	1.33	1.50	1.47	1.3799	0.9185	0.0823	1.8844	1.2543	0.1124	3.2511
9	-32.4	-25.73	5.5	589.18	526.61	137.26	0.83	0.53	0.77	0.6672	0.3807	0.1438	0.9111	0.5199	0.1964	1.6274
9-10	-32.4	-19.25	5.5	475.78	421.37	166.88	0.77	0.60	0.62	0.4979	0.3445	0.1403	0.6799	0.4705	0.1917	1.3420
10	-32.4	-12.77	5.5	362.38	316.13	196.49	0.71	0.67	0.47	0.3481	0.2884	0.1246	0.4753	0.3938	0.1702	1.0393
11	-32.4	-7.27	5.5	338.77	257.52	179.17	0.68	0.57	0.42	0.3138	0.1995	0.1017	0.4285	0.2724	0.1388	0.8397
12	-32.4	-1.77	5.5	474.53	363.77	182.20	0.57	0.74	0.88	0.3650	0.3636	0.2168	0.4984	0.4966	0.2960	1.2910
13	-29.7	0	5.4	574.65	407.55	132.64	1.32	1.43	1.28	1.0095	0.7779	0.2254	1.3786	1.0624	0.3078	2.7488
13-14	-24.3	0	5.4	571.58	348.59	85.91	1.38	1.42	1.26	1.0480	0.6601	0.1446	1.4312	0.9015	0.1974	2.5301
14	-18.9	0	5.4	568.50	289.63	39.17	1.43	1.41	1.25	1.0860	0.5441	0.0653	1.4831	0.7431	0.0892	2.3153
15	-13.5	0	5.4	413.27	180.08	18.01	1.34	1.16	0.90	0.7400	0.2793	0.0216	1.0105	0.3815	0.0294	1.4214
15-16	-8.1	0	5.4	217.22	98.92	17.92	1.15	0.88	0.83	0.3334	0.1155	0.0198	0.4553	0.1577	0.0271	0.6402
16	-2.7	0	5.4	21.17	17.76	17.82	0.96	0.59	0.76	0.0271	0.0139	0.0181	0.0370	0.0190	0.0248	0.0808
		height		6.2	3.7	1.2	6.2	3.7	1.2				Total Re-Entrainment (%)		24.31	

* Inlet area is 63' (74mm in model scale) tall and 45, 46' (54, 55mm) wide

Vertical Distributions of Re-Entrainment Rate

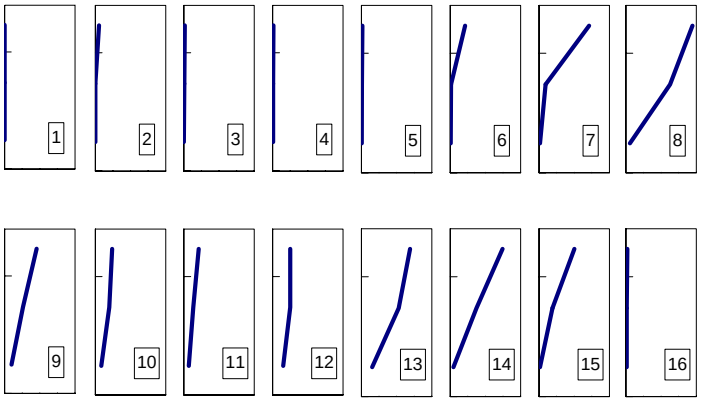

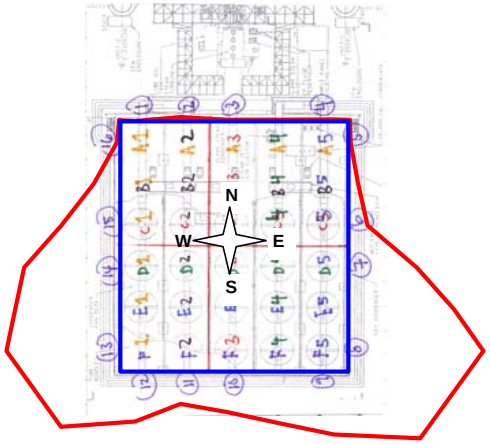

Re-entrainment Level along ACC Boundary

Estimated Contour of R

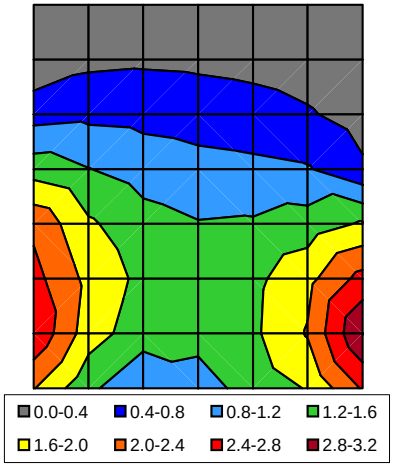

Wind Strength	Calm					Wind Direction	SW				Ethan Purity	10.01			
	X	Y	width	Concentration [PPM]			Speed [m/s]			Flux (times million)			Re-Entrainment Rate (%)			
	[cm]	[cm]	[cm]	T	M	B	T	M	B	T	M	B	T	M	B	SUM
1	0	-1.77	5.5	2.91	0.46	0.67	0.31	0.27	0.28	0.0012	0.0002	0.0003	0.0165	0.0023	0.0034	0.0222
2	0	-7.27	5.5	4.67	0.25	2.14	0.41	0.40	0.14	0.0026	0.0001	0.0004	0.0350	0.0018	0.0056	0.0424
3	0	-12.77	5.5	13.71	0.45	1.26	0.54	0.47	0.31	0.0100	0.0003	0.0005	0.1350	0.0039	0.0071	0.1460
3-4	0	-19.25	5.5	17.98	8.63	7.41	0.42	0.35	0.26	0.0102	0.0042	0.0026	0.1376	0.0558	0.0345	0.2279
4	0	-25.73	5.5	22.25	16.80	13.56	0.30	0.24	0.20	0.0090	0.0055	0.0037	0.1215	0.0743	0.0493	0.2452
5	-2.7	-27.5	5.4	33.03	24.74	15.35	0.30	0.31	0.22	0.0131	0.0102	0.0046	0.1755	0.1370	0.0614	0.3739
5-6	-8.1	-27.5	5.4	47.18	24.11	9.65	0.40	0.38	0.27	0.0252	0.0121	0.0035	0.3393	0.1632	0.0473	0.5498
6	-13.5	-27.5	5.4	61.34	23.48	3.95	0.51	0.45	0.32	0.0414	0.0140	0.0017	0.5562	0.1879	0.0229	0.7671
7	-18.9	-27.5	5.4	59.15	30.29	1.39	0.48	0.36	0.27	0.0379	0.0147	0.0005	0.5088	0.1977	0.0066	0.7132
7-8	-24.3	-27.5	5.4	36.22	15.56	2.12	0.42	0.30	0.23	0.0203	0.0061	0.0007	0.2728	0.0824	0.0089	0.3642
8	-29.7	-27.5	5.4	13.29	0.82	2.86	0.36	0.23	0.20	0.0064	0.0002	0.0008	0.0859	0.0034	0.0103	0.0996
9	-32.4	-25.73	5.5	4.06	0.78	0.81	0.49	0.44	0.28	0.0027	0.0005	0.0003	0.0362	0.0062	0.0042	0.0466
9-10	-32.4	-19.25	5.5	3.40	0.86	1.22	0.53	0.49	0.34	0.0024	0.0006	0.0006	0.0329	0.0077	0.0075	0.0482
10	-32.4	-12.77	5.5	2.75	0.95	1.62	0.57	0.55	0.40	0.0021	0.0007	0.0009	0.0286	0.0094	0.0117	0.0498
11	-32.4	-7.27	5.5	4.27	0.61	0.52	0.48	0.42	0.26	0.0028	0.0003	0.0002	0.0373	0.0046	0.0024	0.0444
12	-32.4	-1.77	5.5	0.68	1.39	5.96	0.40	0.36	0.25	0.0004	0.0007	0.0020	0.0050	0.0090	0.0268	0.0409
13	-29.7	0	5.4	0.84	0.58	0.65	0.44	0.35	0.23	0.0005	0.0003	0.0002	0.0066	0.0036	0.0027	0.0129
13-14	-24.3	0	5.4	4.44	4.25	1.65	0.50	0.39	0.25	0.0030	0.0022	0.0006	0.0398	0.0294	0.0074	0.0767
14	-18.9	0	5.4	8.04	7.93	2.65	0.56	0.42	0.27	0.0060	0.0045	0.0010	0.0805	0.0599	0.0129	0.1533
15	-13.5	0	5.4	1.56	0.81	2.30	0.57	0.47	0.34	0.0012	0.0005	0.0011	0.0160	0.0068	0.0142	0.0371
15-16	-8.1	0	5.4	2.58	0.70	2.11	0.51	0.43	0.29	0.0017	0.0004	0.0008	0.0235	0.0053	0.0111	0.0399
16	-2.7	0	5.4	3.61	0.58	1.92	0.44	0.38	0.24	0.0021	0.0003	0.0006	0.0285	0.0040	0.0083	0.0408
		height		6.2	3.7	1.2	6.2	3.7	1.2					Total Re-Entrainment (%)		4.14

* Inlet area is 63' (74mm in model scale) tall and 45,46' (54,55mm) wide

Vertical Distributions of Re-Entrainment Rate

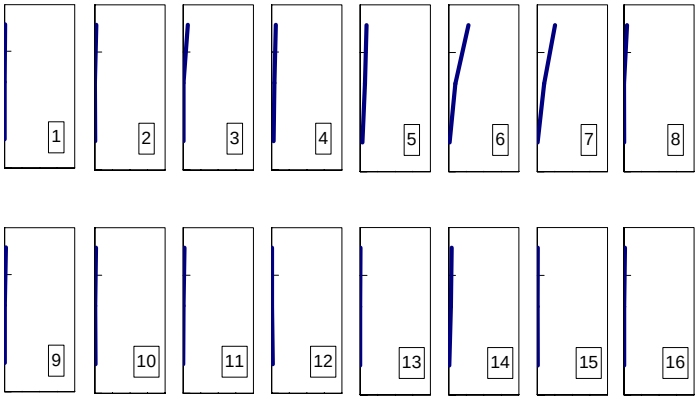

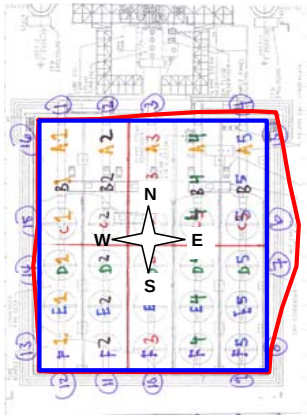

Re-entrainment Level along ACC Boundary

Estimated Contour of R

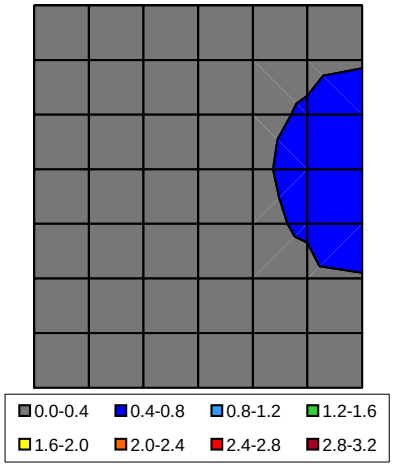

Wind Strength	Calm			Wind Direction	W		Ethan Purity	12.6							
	X	Y	width	Concentration [PPM]			Speed [m/s]			Flux (times million)			Re-Entrainment Rate (%)			
	[cm]	[cm]	[cm]	T	M	B	T	M	B	T	M	B	T	M	B	SUM
1	0	-1.77	5.5	3.60	2.75	2.75	0.47	0.42	0.39	0.0023	0.0016	0.0014	0.0247	0.0168	0.0154	0.0568
2	0	-7.27	5.5	4.10	2.17	2.72	0.60	0.53	0.13	0.0033	0.0016	0.0005	0.0354	0.0166	0.0053	0.0572
3	0	-12.77	5.5	7.32	3.28	1.94	0.54	0.53	0.47	0.0053	0.0024	0.0012	0.0569	0.0252	0.0133	0.0954
3-4	0	-19.25	5.5	9.66	3.24	2.12	0.43	0.41	0.37	0.0056	0.0018	0.0011	0.0600	0.0194	0.0115	0.0909
4	0	-25.73	5.5	12.00	3.21	2.31	0.32	0.29	0.28	0.0052	0.0013	0.0009	0.0560	0.0136	0.0092	0.0788
5	-2.7	-27.5	5.4	30.39	4.42	2.39	0.55	0.45	0.34	0.0221	0.0026	0.0011	0.2362	0.0281	0.0114	0.2757
5-6	-8.1	-27.5	5.4	47.60	28.21	10.58	0.64	0.52	0.41	0.0409	0.0194	0.0058	0.4363	0.2076	0.0622	0.7061
6	-13.5	-27.5	5.4	64.80	52.00	18.78	0.74	0.59	0.49	0.0641	0.0408	0.0123	0.6844	0.4350	0.1311	1.2506
7	-18.9	-27.5	5.4	61.50	58.85	32.17	0.75	0.61	0.51	0.0618	0.0476	0.0220	0.6599	0.5081	0.2352	1.4033
7-8	-24.3	-27.5	5.4	71.19	34.44	16.81	0.66	0.54	0.45	0.0625	0.0246	0.0100	0.6668	0.2626	0.1067	1.0362
8	-29.7	-27.5	5.4	80.87	10.03	1.44	0.56	0.47	0.38	0.0606	0.0062	0.0007	0.6473	0.0663	0.0078	0.7214
9	-32.4	-25.73	5.5	47.19	15.84	0.98	0.41	0.35	0.30	0.0262	0.0075	0.0004	0.2798	0.0797	0.0043	0.3638
9-10	-32.4	-19.25	5.5	30.08	10.20	1.01	0.48	0.42	0.36	0.0196	0.0058	0.0005	0.2088	0.0614	0.0053	0.2755
10	-32.4	-12.77	5.5	12.97	4.55	1.04	0.55	0.48	0.42	0.0097	0.0030	0.0006	0.1032	0.0320	0.0063	0.1414
11	-32.4	-7.27	5.5	2.65	1.17	1.24	0.48	0.45	0.41	0.0017	0.0007	0.0007	0.0185	0.0077	0.0073	0.0336
12	-32.4	-1.77	5.5	5.05	1.69	1.69	0.38	0.38	0.33	0.0026	0.0009	0.0007	0.0275	0.0094	0.0080	0.0448
13	-29.7	0	5.4	16.89	1.85	2.14	0.49	0.35	0.31	0.0110	0.0009	0.0009	0.1174	0.0091	0.0095	0.1359
13-14	-24.3	0	5.4	11.10	2.70	2.27	0.55	0.42	0.37	0.0082	0.0015	0.0011	0.0874	0.0162	0.0118	0.1154
14	-18.9	0	5.4	5.30	3.56	2.40	0.62	0.50	0.42	0.0044	0.0023	0.0014	0.0466	0.0251	0.0144	0.0861
15	-13.5	0	5.4	1.96	1.92	2.95	0.68	0.53	0.45	0.0018	0.0013	0.0018	0.0191	0.0143	0.0187	0.0521
15-16	-8.1	0	5.4	8.57	1.91	2.44	0.61	0.48	0.39	0.0070	0.0012	0.0013	0.0747	0.0132	0.0136	0.1014
16	-2.7	0	5.4	15.17	1.91	1.93	0.54	0.44	0.34	0.0110	0.0011	0.0009	0.1174	0.0120	0.0092	0.1386
		height		6.2	3.7	1.2	6.2	3.7	1.2				Total Re-Entrainment (%)			7.26

* Inlet area is 63' (74mm in model scale) tall and 45, 46' (54, 55mm) wide

Vertical Distributions of Re-Entrainment Rate

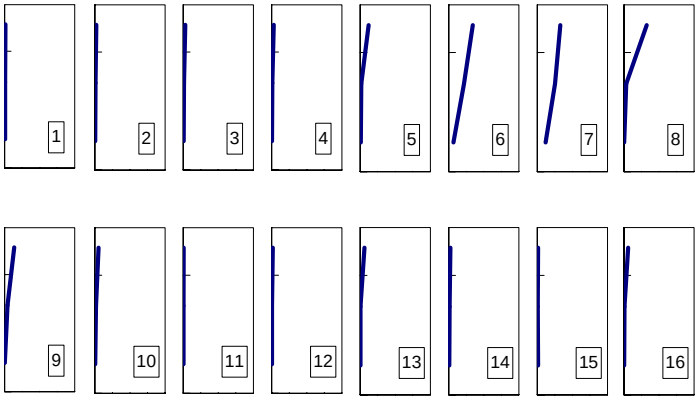

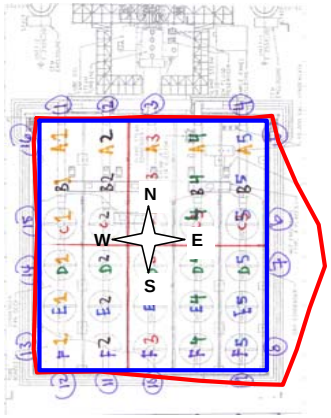

Re-entrainment Level along ACC Boundary

Estimated Contour of R

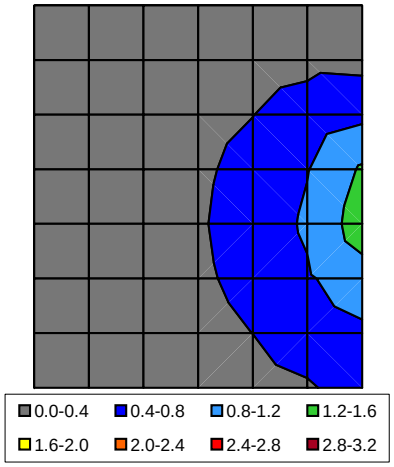

Wind Strength	Calm			Wind Direction	N		Ethan Purity	12.6								
	X	Y	width	Concentration [PPM]			Speed [m/s]			Flux (times million)			Re-Entrainment Rate (%)			
	[cm]	[cm]	[cm]	T	M	B	T	M	B	T	M	B	T	M	B	SUM
1	0	-1.77	5.5	1.88	1.56	2.38	0.51	0.39	0.38	0.0013	0.0008	0.0012	0.0139	0.0087	0.0130	0.0357
2	0	-7.27	5.5	1.90	1.56	1.91	0.57	0.48	0.28	0.0015	0.0010	0.0007	0.0156	0.0108	0.0078	0.0343
3	0	-12.77	5.5	1.32	1.58	1.72	0.66	0.57	0.05	0.0012	0.0012	0.0001	0.0126	0.0131	0.0012	0.0269
3-4	0	-19.25	5.5	0.89	1.01	1.25	0.59	0.49	0.22	0.0007	0.0007	0.0004	0.0076	0.0072	0.0039	0.0187
4	0	-25.73	5.5	0.46	0.44	0.78	0.52	0.41	0.39	0.0003	0.0002	0.0004	0.0034	0.0026	0.0044	0.0104
5	-2.7	-27.5	5.4	11.23	0.61	0.80	0.43	0.38	0.33	0.0064	0.0003	0.0004	0.0679	0.0033	0.0037	0.0750
5-6	-8.1	-27.5	5.4	33.58	0.81	0.97	0.51	0.44	0.38	0.0228	0.0005	0.0005	0.2429	0.0050	0.0052	0.2532
6	-13.5	-27.5	5.4	55.93	1.00	1.13	0.59	0.49	0.43	0.0441	0.0007	0.0006	0.4710	0.0070	0.0069	0.4849
7	-18.9	-27.5	5.4	39.78	6.29	1.03	0.64	0.55	0.45	0.0341	0.0046	0.0006	0.3644	0.0490	0.0067	0.4201
7-8	-24.3	-27.5	5.4	60.50	16.79	0.72	0.56	0.45	0.39	0.0448	0.0100	0.0004	0.4780	0.1067	0.0040	0.5887
8	-29.7	-27.5	5.4	81.22	27.30	0.41	0.47	0.35	0.33	0.0505	0.0126	0.0002	0.5394	0.1344	0.0019	0.6758
9	-32.4	-25.73	5.5	70.61	42.52	5.16	0.36	0.41	0.32	0.0344	0.0239	0.0022	0.3670	0.2553	0.0238	0.6461
9-10	-32.4	-19.25	5.5	66.08	45.16	6.67	0.48	0.47	0.38	0.0433	0.0289	0.0034	0.4619	0.3089	0.0368	0.8077
10	-32.4	-12.77	5.5	61.54	47.79	8.19	0.61	0.53	0.44	0.0506	0.0344	0.0049	0.5406	0.3670	0.0525	0.9601
11	-32.4	-7.27	5.5	56.20	37.03	10.46	0.50	0.44	0.36	0.0383	0.0221	0.0051	0.4094	0.2359	0.0544	0.6998
12	-32.4	-1.77	5.5	80.52	44.22	5.41	0.42	0.37	0.29	0.0455	0.0221	0.0021	0.4854	0.2358	0.0226	0.7439
13	-29.7	0	5.4	94.34	40.31	1.52	0.46	0.32	0.27	0.0573	0.0169	0.0005	0.6113	0.1806	0.0057	0.7975
13-14	-24.3	0	5.4	74.90	24.10	1.46	0.52	0.38	0.32	0.0516	0.0123	0.0006	0.5513	0.1312	0.0066	0.6892
14	-18.9	0	5.4	55.47	7.89	1.41	0.58	0.45	0.37	0.0428	0.0047	0.0007	0.4571	0.0506	0.0075	0.5152
15	-13.5	0	5.4	50.42	4.97	2.18	0.67	0.51	0.42	0.0447	0.0034	0.0012	0.4774	0.0363	0.0131	0.5267
15-16	-8.1	0	5.4	27.80	3.42	2.01	0.56	0.41	0.36	0.0207	0.0019	0.0010	0.2207	0.0199	0.0102	0.2509
16	-2.7	0	5.4	5.17	1.88	1.84	0.45	0.31	0.29	0.0031	0.0008	0.0007	0.0332	0.0082	0.0077	0.0490
		height		6.2	3.7	1.2	6.2	3.7	1.2						Total Re-Entrainment (%)	9.31

* Inlet area is 63' (74mm in model scale) tall and 45, 46' (54, 55mm) wide

Vertical Distributions of Re-Entrainment Rate

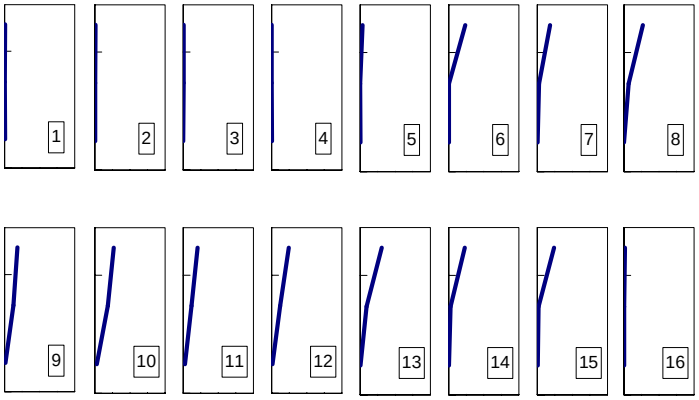

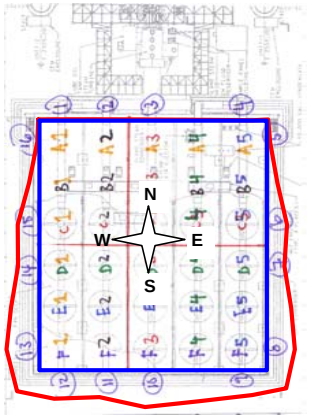

Re-entrainment Level along ACC Boundary

Estimated Contour of R

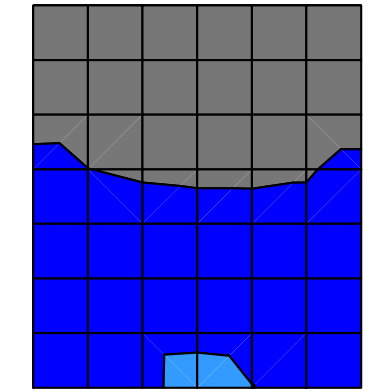

Wind Strength	Mild					Wind Direction	S				Ethan Purity	98.5			
	X	Y	width	Concentration [PPM]			Speed [m/s]			Flux (times million)			Re-Entrainment Rate (%)			
	[cm]	[cm]	[cm]	T	M	B	T	M	B	T	M	B	T	M	B	SUM
1	0	-1.77	5.5	375.98	217.28	50.58	0.60	0.44	0.33	0.3045	0.1293	0.0224	0.4159	0.1765	0.0306	0.6230
2	0	-7.27	5.5	228.32	138.03	41.98	0.47	0.56	0.37	0.1455	0.1043	0.0213	0.1987	0.1425	0.0291	0.3702
3	0	-12.77	5.5	191.78	139.19	62.83	0.63	0.71	0.62	0.1630	0.1342	0.0530	0.2226	0.1833	0.0723	0.4782
3-4	0	-19.25	5.5	267.22	184.91	67.04	0.53	0.60	0.48	0.1924	0.1510	0.0433	0.2628	0.2062	0.0592	0.5282
4	0	-25.73	5.5	342.65	230.63	71.25	0.44	0.49	0.33	0.2023	0.1543	0.0320	0.2763	0.2107	0.0438	0.5307
5	-2.7	-27.5	5.4	403.84	233.29	40.28	1.22	1.30	1.09	0.6564	0.4028	0.0586	0.8963	0.5501	0.0801	1.5265
5-6	-8.1	-27.5	5.4	401.80	174.87	36.42	1.25	1.22	1.09	0.6713	0.2852	0.0528	0.9168	0.3895	0.0722	1.3784
6	-13.5	-27.5	5.4	399.77	116.45	32.56	1.29	1.15	1.09	0.6861	0.1788	0.0471	0.9369	0.2441	0.0643	1.2454
7	-18.9	-27.5	5.4	298.18	55.33	34.28	1.04	0.90	0.75	0.4113	0.0666	0.0342	0.5617	0.0909	0.0467	0.6993
7-8	-24.3	-27.5	5.4	168.76	44.93	33.57	1.04	0.82	0.68	0.2340	0.0492	0.0303	0.3195	0.0672	0.0413	0.4280
8	-29.7	-27.5	5.4	39.33	34.54	32.85	1.05	0.74	0.60	0.0548	0.0341	0.0264	0.0748	0.0466	0.0361	0.1575
9	-32.4	-25.73	5.5	12.98	33.80	33.26	1.76	1.52	1.31	0.0311	0.0699	0.0591	0.0424	0.0955	0.0808	0.2187
9-10	-32.4	-19.25	5.5	13.56	23.79	23.10	1.89	1.65	1.41	0.0347	0.0532	0.0442	0.0474	0.0727	0.0604	0.1805
10	-32.4	-12.77	5.5	14.14	13.78	12.94	2.01	1.77	1.51	0.0386	0.0332	0.0265	0.0526	0.0453	0.0362	0.1342
11	-32.4	-7.27	5.5	14.57	13.65	14.07	1.79	1.66	1.43	0.0354	0.0307	0.0272	0.0483	0.0419	0.0372	0.1274
12	-32.4	-1.77	5.5	15.53	14.51	14.48	1.68	1.52	1.34	0.0355	0.0300	0.0264	0.0484	0.0410	0.0361	0.1255
13	-29.7	0	5.4	20.53	14.76	16.72	0.80	0.59	0.50	0.0220	0.0116	0.0111	0.0300	0.0159	0.0152	0.0610
13-14	-24.3	0	5.4	70.60	14.41	15.45	0.95	0.70	0.58	0.0889	0.0134	0.0120	0.1214	0.0182	0.0163	0.1559
14	-18.9	0	5.4	120.66	14.07	14.18	1.09	0.80	0.66	0.1747	0.0150	0.0125	0.2386	0.0205	0.0171	0.2762
15	-13.5	0	5.4	275.16	26.18	14.26	1.33	1.22	1.14	0.4884	0.0424	0.0217	0.6670	0.0579	0.0296	0.7545
15-16	-8.1	0	5.4	371.26	119.87	17.41	1.37	1.31	1.19	0.6787	0.2095	0.0275	0.9268	0.2860	0.0375	1.2503
16	-2.7	0	5.4	467.37	213.56	20.56	1.41	1.41	1.23	0.8791	0.4005	0.0337	1.2005	0.5469	0.0460	1.7934
		height		6.2	3.7	1.2	6.2	3.7	1.2						Total Re-Entrainment (%)	13.04

* Inlet area is 63' (74mm in model scale) tall and 45, 46' (54, 55mm) wide

Vertical Distributions of Re-Entrainment Rate

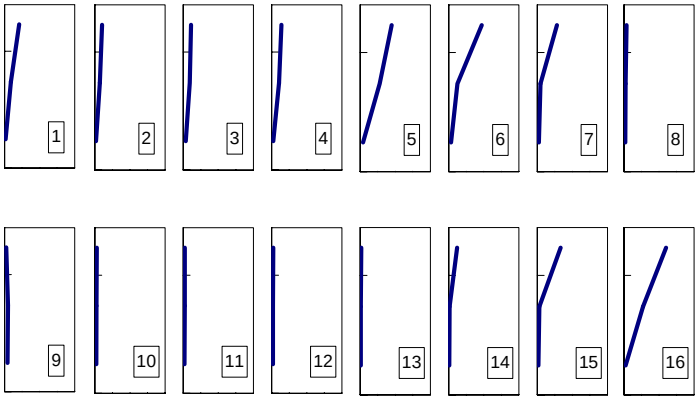

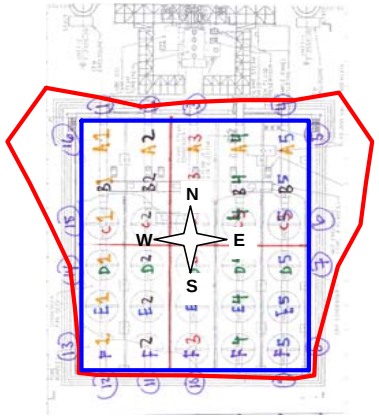

Re-entrainment Level along ACC Boundary

Estimated Contour of R

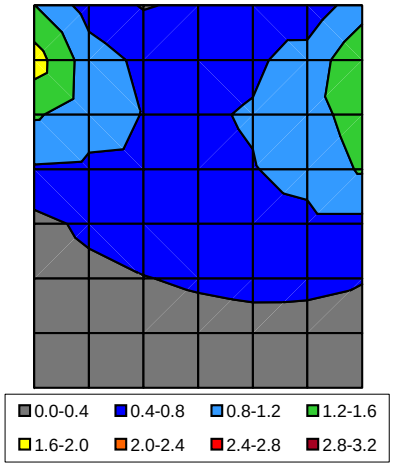

Wind Strength	Mild			Wind Direction	SW		Ethan Purity	98.5								
	X	Y	width	Concentration [PPM]			Speed [m/s]			Flux (times million)			Re-Entrainment Rate (%)			
	[cm]	[cm]	[cm]	T	M	B	T	M	B	T	M	B	T	M	B	SUM
1	0	-1.77	5.5	59.65	2.01	2.02	0.37	0.48	0.41	0.0297	0.0013	0.0011	0.0406	0.0018	0.0015	0.0439
2	0	-7.27	5.5	26.45	4.20	3.34	0.44	0.55	0.49	0.0156	0.0032	0.0022	0.0213	0.0043	0.0030	0.0287
3	0	-12.77	5.5	13.70	10.39	13.60	0.81	0.74	0.52	0.0150	0.0104	0.0095	0.0205	0.0142	0.0130	0.0477
3-4	0	-19.25	5.5	95.44	99.22	46.63	0.62	0.57	0.38	0.0805	0.0761	0.0238	0.1100	0.1039	0.0325	0.2464
4	0	-25.73	5.5	177.17	188.04	79.66	0.43	0.39	0.24	0.1045	0.1007	0.0255	0.1428	0.1376	0.0349	0.3152
5	-2.7	-27.5	5.4	268.53	217.01	94.37	1.13	1.04	0.89	0.4055	0.3000	0.1115	0.5537	0.4096	0.1522	1.1156
5-6	-8.1	-27.5	5.4	308.63	217.67	80.40	1.09	0.89	0.76	0.4470	0.2571	0.0810	0.6105	0.3511	0.1106	1.0721
6	-13.5	-27.5	5.4	348.72	218.32	66.42	1.04	0.74	0.63	0.4837	0.2139	0.0553	0.6606	0.2921	0.0755	1.0282
7	-18.9	-27.5	5.4	374.57	198.98	49.16	0.86	0.55	0.48	0.4298	0.1468	0.0318	0.5869	0.2004	0.0434	0.8307
7-8	-24.3	-27.5	5.4	375.21	115.06	32.03	0.73	0.52	0.50	0.3654	0.0790	0.0212	0.4991	0.1079	0.0289	0.6359
8	-29.7	-27.5	5.4	375.84	31.14	14.91	0.60	0.48	0.51	0.3009	0.0198	0.0101	0.4109	0.0270	0.0138	0.4517
9	-32.4	-25.73	5.5	54.84	19.22	17.19	1.72	1.56	1.38	0.1276	0.0406	0.0322	0.1743	0.0554	0.0440	0.2737
9-10	-32.4	-19.25	5.5	36.89	19.15	18.00	1.85	1.64	1.46	0.0925	0.0426	0.0355	0.1264	0.0581	0.0485	0.2330
10	-32.4	-12.77	5.5	18.94	19.07	18.80	1.98	1.72	1.53	0.0509	0.0445	0.0390	0.0696	0.0608	0.0533	0.1836
11	-32.4	-7.27	5.5	19.38	19.37	18.37	1.54	1.31	1.07	0.0406	0.0344	0.0267	0.0554	0.0469	0.0364	0.1388
12	-32.4	-1.77	5.5	19.31	19.87	19.43	1.38	1.17	0.99	0.0361	0.0314	0.0261	0.0493	0.0429	0.0356	0.1278
13	-29.7	0	5.4	18.86	18.46	19.28	1.49	1.19	0.99	0.0374	0.0292	0.0255	0.0511	0.0399	0.0348	0.1257
13-14	-24.3	0	5.4	19.27	18.70	19.22	1.62	1.27	1.05	0.0416	0.0316	0.0270	0.0568	0.0431	0.0368	0.1368
14	-18.9	0	5.4	19.68	18.95	19.17	1.75	1.35	1.12	0.0459	0.0340	0.0285	0.0627	0.0465	0.0389	0.1481
15	-13.5	0	5.4	26.27	20.60	19.69	1.87	1.57	1.40	0.0656	0.0432	0.0368	0.0895	0.0590	0.0503	0.1988
15-16	-8.1	0	5.4	28.27	19.94	19.48	1.84	1.53	1.35	0.0692	0.0407	0.0350	0.0945	0.0556	0.0478	0.1978
16	-2.7	0	5.4	30.27	19.29	19.27	1.80	1.49	1.29	0.0727	0.0383	0.0331	0.0992	0.0523	0.0453	0.1967
		height		6.2	3.7	1.2	6.2	3.7	1.2				Total Re-Entrainment (%)			7.78

* Inlet area is 63' (74mm in model scale) tall and 45, 46' (54, 55mm) wide

Vertical Distributions of Re-Entrainment Rate

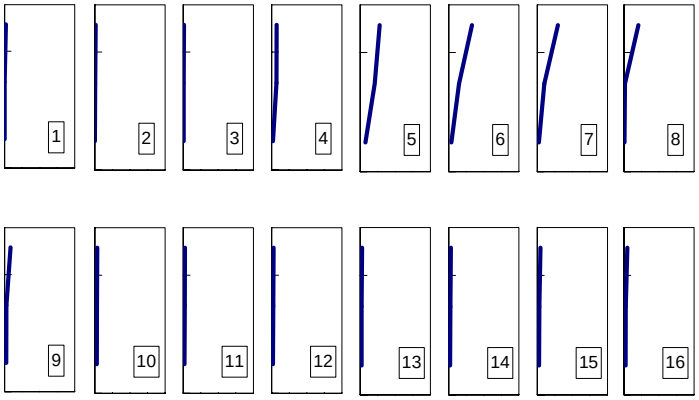

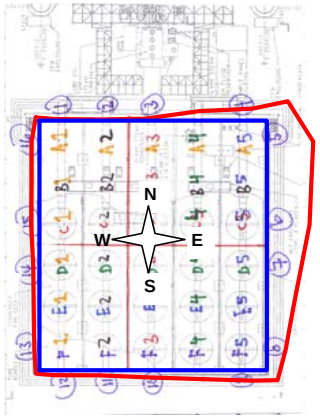

Re-entrainment Level along ACC Boundary

Estimated Contour of R

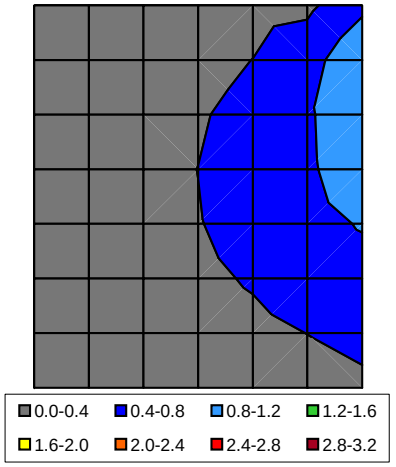

Wind Strength	Mild			Wind Direction	W		Ethan Purity	98.5								
	X	Y	width	Concentration [PPM]			Speed [m/s]			Flux (times million)			Re-Entrainment Rate (%)			
	[cm]	[cm]	[cm]	T	M	B	T	M	B	T	M	B	T	M	B	SUM
1	0	-1.77	5.5	1.47	1.26	0.73	1.10	0.89	0.81	0.0022	0.0015	0.0008	0.0030	0.0021	0.0011	0.0062
2	0	-7.27	5.5	172.39	27.95	2.09	1.14	1.16	0.54	0.2662	0.0441	0.0015	0.3636	0.0602	0.0021	0.4259
3	0	-12.77	5.5	105.10	6.27	5.27	1.60	1.37	1.35	0.2281	0.0116	0.0097	0.3116	0.0159	0.0132	0.3407
3-4	0	-19.25	5.5	260.96	163.00	69.46	1.12	0.90	0.88	0.3955	0.1996	0.0829	0.5400	0.2726	0.1132	0.9259
4	0	-25.73	5.5	416.82	319.74	133.64	0.63	0.44	0.41	0.3585	0.1894	0.0739	0.4896	0.2587	0.1009	0.8492
5	-2.7	-27.5	5.4	367.22	294.16	105.78	0.71	0.42	0.25	0.3455	0.1660	0.0352	0.4718	0.2266	0.0481	0.7465
5-6	-8.1	-27.5	5.4	290.90	238.78	129.68	0.81	0.69	0.56	0.3152	0.2186	0.0961	0.4304	0.2986	0.1312	0.8602
6	-13.5	-27.5	5.4	214.58	183.39	153.58	0.92	0.95	0.86	0.2631	0.2324	0.1764	0.3593	0.3174	0.2409	0.9176
7	-18.9	-27.5	5.4	244.34	202.44	115.15	0.85	0.72	0.57	0.2770	0.1935	0.0879	0.3782	0.2642	0.1200	0.7624
7-8	-24.3	-27.5	5.4	290.54	210.99	80.35	0.81	0.68	0.66	0.3127	0.1903	0.0706	0.4271	0.2599	0.0964	0.7834
8	-29.7	-27.5	5.4	336.75	219.54	45.56	0.77	0.64	0.75	0.3433	0.1862	0.0453	0.4688	0.2543	0.0618	0.7849
9	-32.4	-25.73	5.5	377.85	185.10	12.43	1.22	1.32	1.22	0.6250	0.3326	0.0205	0.8536	0.4543	0.0280	1.3359
9-10	-32.4	-19.25	5.5	238.72	96.01	9.34	1.26	1.25	1.15	0.4092	0.1622	0.0146	0.5588	0.2215	0.0199	0.8003
10	-32.4	-12.77	5.5	99.58	6.92	6.25	1.31	1.17	1.09	0.1767	0.0109	0.0092	0.2413	0.0149	0.0126	0.2688
11	-32.4	-7.27	5.5	26.83	6.77	6.80	0.77	0.60	0.50	0.0280	0.0055	0.0046	0.0383	0.0075	0.0063	0.0521
12	-32.4	-1.77	5.5	8.65	5.96	6.69	0.73	0.52	0.46	0.0086	0.0042	0.0042	0.0117	0.0057	0.0057	0.0232
13	-29.7	0	5.4	7.06	7.32	7.03	1.92	1.58	1.34	0.0180	0.0154	0.0125	0.0246	0.0210	0.0171	0.0627
13-14	-24.3	0	5.4	8.00	8.08	7.86	1.99	1.68	1.43	0.0212	0.0180	0.0149	0.0290	0.0246	0.0204	0.0740
14	-18.9	0	5.4	8.94	8.84	8.69	2.06	1.77	1.52	0.0245	0.0209	0.0176	0.0335	0.0285	0.0240	0.0860
15	-13.5	0	5.4	10.01	8.98	8.42	2.14	1.73	1.47	0.0286	0.0207	0.0165	0.0390	0.0283	0.0225	0.0897
15-16	-8.1	0	5.4	9.32	8.71	8.72	1.99	1.64	1.39	0.0247	0.0190	0.0161	0.0337	0.0260	0.0220	0.0816
16	-2.7	0	5.4	8.64	8.44	9.01	1.83	1.55	1.30	0.0211	0.0174	0.0156	0.0288	0.0238	0.0214	0.0739
		height		6.2	3.7	1.2	6.2	3.7	1.2				Total Re-Entrainment (%)			10.35

* Inlet area is 63' (74mm in model scale) tall and 45, 46' (54, 55mm) wide

Vertical Distributions of Re-Entrainment Rate

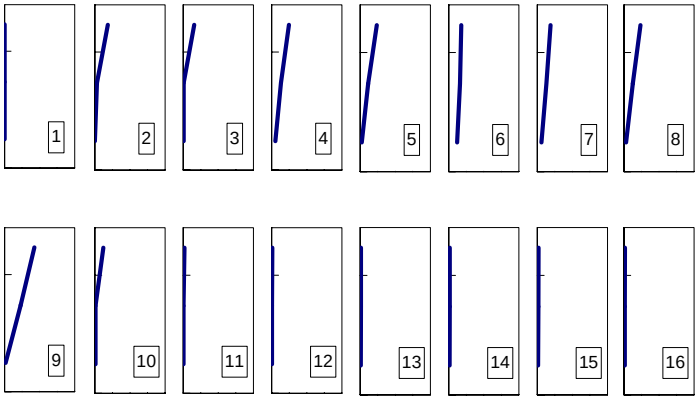

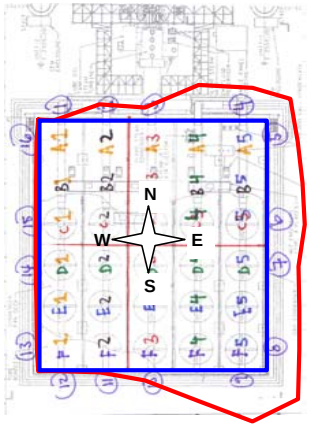

Re-entrainment Level along ACC Boundary

Estimated Contour of R

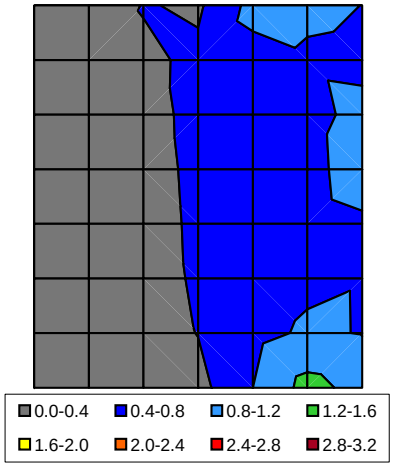

Wind Strength	Mild			Wind Direction	N		Ethan Purity	98.5								
	X	Y	width	Concentration [PPM]			Speed [m/s]			Flux (times million)			Re-Entrainment Rate (%)			
	[cm]	[cm]	[cm]	T	M	B	T	M	B	T	M	B	T	M	B	SUM
1	0	-1.77	5.5	1.03	0.60	0.44	1.87	1.62	1.44	0.0026	0.0013	0.0009	0.0036	0.0018	0.0012	0.0066
2	0	-7.27	5.5	26.48	0.54	0.40	2.13	1.93	0.32	0.0764	0.0014	0.0002	0.1044	0.0019	0.0002	0.1065
3	0	-12.77	5.5	6.79	3.60	3.69	2.27	1.71	0.39	0.0209	0.0084	0.0019	0.0285	0.0114	0.0026	0.0426
3-4	0	-19.25	5.5	6.71	4.88	4.79	1.96	1.50	0.78	0.0179	0.0099	0.0051	0.0244	0.0136	0.0069	0.0449
4	0	-25.73	5.5	6.63	6.15	5.89	1.66	1.29	1.17	0.0149	0.0108	0.0093	0.0204	0.0147	0.0128	0.0479
5	-2.7	-27.5	5.4	12.70	8.16	6.94	1.17	0.76	0.83	0.0197	0.0083	0.0077	0.0270	0.0113	0.0105	0.0488
5-6	-8.1	-27.5	5.4	83.68	8.75	8.40	1.33	0.99	0.93	0.1487	0.0115	0.0104	0.2030	0.0157	0.0142	0.2330
6	-13.5	-27.5	5.4	154.66	9.35	9.87	1.50	1.21	1.03	0.3092	0.0151	0.0136	0.4222	0.0206	0.0185	0.4613
7	-18.9	-27.5	5.4	445.44	61.72	9.52	1.76	1.67	1.58	1.0462	0.1370	0.0201	1.4287	0.1871	0.0274	1.6433
7-8	-24.3	-27.5	5.4	612.08	260.86	25.83	1.55	1.58	1.52	1.2611	0.5500	0.0524	1.7222	0.7511	0.0716	2.5449
8	-29.7	-27.5	5.4	778.72	460.00	42.13	1.33	1.50	1.47	1.3799	0.9185	0.0823	1.8844	1.2543	0.1124	3.2511
9	-32.4	-25.73	5.5	589.18	526.61	137.26	0.83	0.53	0.77	0.6672	0.3807	0.1438	0.9111	0.5199	0.1964	1.6274
9-10	-32.4	-19.25	5.5	475.78	421.37	166.88	0.77	0.60	0.62	0.4979	0.3445	0.1403	0.6799	0.4705	0.1917	1.3420
10	-32.4	-12.77	5.5	362.38	316.13	196.49	0.71	0.67	0.47	0.3481	0.2884	0.1246	0.4753	0.3938	0.1702	1.0393
11	-32.4	-7.27	5.5	338.77	257.52	179.17	0.68	0.57	0.42	0.3138	0.1995	0.1017	0.4285	0.2724	0.1388	0.8397
12	-32.4	-1.77	5.5	474.53	363.77	182.20	0.57	0.74	0.88	0.3650	0.3636	0.2168	0.4984	0.4966	0.2960	1.2910
13	-29.7	0	5.4	574.65	407.55	132.64	1.32	1.43	1.28	1.0095	0.7779	0.2254	1.3786	1.0624	0.3078	2.7488
13-14	-24.3	0	5.4	571.58	348.59	85.91	1.38	1.42	1.26	1.0480	0.6601	0.1446	1.4312	0.9015	0.1974	2.5301
14	-18.9	0	5.4	568.50	289.63	39.17	1.43	1.41	1.25	1.0860	0.5441	0.0653	1.4831	0.7431	0.0892	2.3153
15	-13.5	0	5.4	413.27	180.08	18.01	1.34	1.16	0.90	0.7400	0.2793	0.0216	1.0105	0.3815	0.0294	1.4214
15-16	-8.1	0	5.4	217.22	98.92	17.92	1.15	0.88	0.83	0.3334	0.1155	0.0198	0.4553	0.1577	0.0271	0.6402
16	-2.7	0	5.4	21.17	17.76	17.82	0.96	0.59	0.76	0.0271	0.0139	0.0181	0.0370	0.0190	0.0248	0.0808
		height		6.2	3.7	1.2	6.2	3.7	1.2				Total Re-Entrainment (%)			24.31

* Inlet area is 63' (74mm in model scale) tall and 45,46' (54,55mm) wide

Vertical Distributions of Re-Entrainment Rate

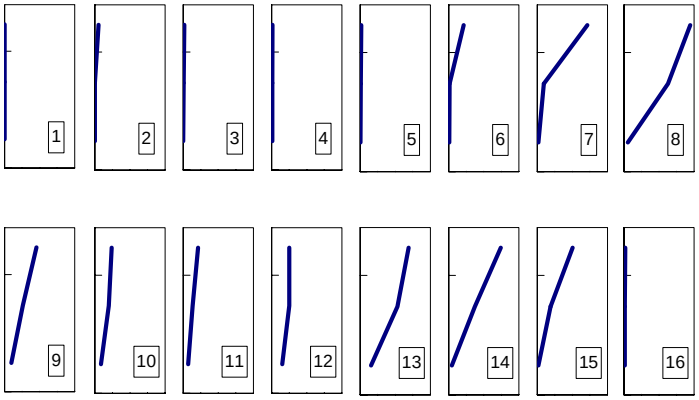

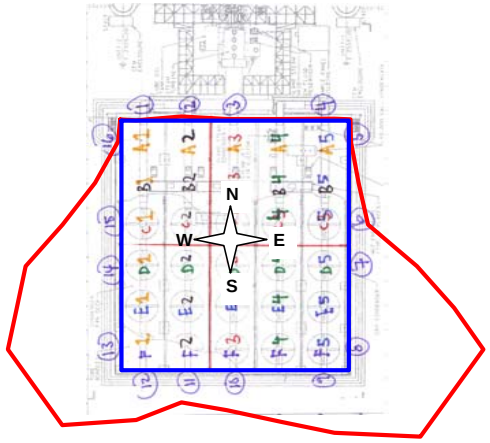

Re-entrainment Level along ACC Boundary

Estimated Contour of R

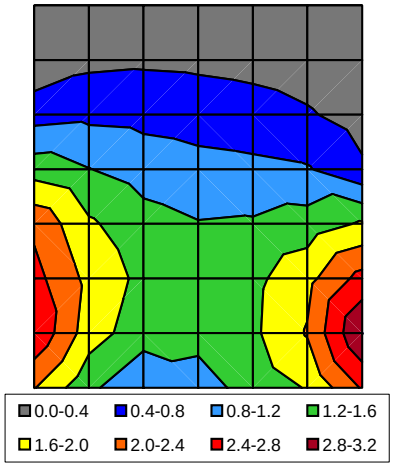

Wind Strength Moderate **Wind Direction** S **Ethan Purity** 98.5

	X	Y	width	Concentration [PPM]			Speed [m/s]			Flux (times million)			Re-Entrainment Rate (%)			
	[cm]	[cm]	[cm]	T	M	B	T	M	B	T	M	B	T	M	B	SUM
1	0	-1.77	5.5	351.12	141.93	6.10	0.65	0.90	0.63	0.3091	0.1733	0.0052	0.4222	0.2367	0.0072	0.6660
2	0	-7.27	5.5	228.29	99.68	14.38	0.68	0.76	0.59	0.2107	0.1031	0.0115	0.2877	0.1409	0.0157	0.4442
3	0	-12.77	5.5	116.97	56.75	25.29	0.99	1.00	0.81	0.1571	0.0767	0.0277	0.2146	0.1048	0.0379	0.3572
3-4	0	-19.25	5.5	196.26	109.29	27.13	0.81	1.04	0.77	0.2161	0.1537	0.0282	0.2951	0.2099	0.0385	0.5435
4	0	-25.73	5.5	275.55	161.83	28.96	0.63	1.08	0.72	0.2366	0.2365	0.0284	0.3231	0.3230	0.0388	0.6849
5	-2.7	-27.5	5.4	328.59	169.36	16.81	1.26	1.45	1.27	0.5520	0.3274	0.0284	0.7539	0.4471	0.0387	1.2397
5-6	-8.1	-27.5	5.4	267.69	95.66	14.58	1.20	1.24	1.15	0.4282	0.1586	0.0222	0.5848	0.2166	0.0304	0.8318
6	-13.5	-27.5	5.4	206.80	21.96	12.35	1.14	1.04	1.02	0.3142	0.0304	0.0168	0.4291	0.0415	0.0230	0.4935
7	-18.9	-27.5	5.4	159.72	16.16	14.49	0.98	0.72	0.61	0.2082	0.0156	0.0117	0.2843	0.0213	0.0159	0.3215
7-8	-24.3	-27.5	5.4	87.33	15.24	14.25	0.98	0.69	0.60	0.1143	0.0141	0.0114	0.1560	0.0192	0.0156	0.1908
8	-29.7	-27.5	5.4	14.93	14.31	14.02	0.99	0.66	0.60	0.0196	0.0126	0.0112	0.0268	0.0172	0.0153	0.0593
9	-32.4	-25.73	5.5	15.14	15.70	15.45	2.23	2.01	1.73	0.0458	0.0428	0.0362	0.0625	0.0585	0.0494	0.1704
9-10	-32.4	-19.25	5.5	15.18	15.56	15.38	2.32	2.09	1.81	0.0479	0.0441	0.0378	0.0654	0.0602	0.0517	0.1772
10	-32.4	-12.77	5.5	15.21	15.43	15.30	2.42	2.16	1.90	0.0500	0.0453	0.0395	0.0682	0.0619	0.0539	0.1840
11	-32.4	-7.27	5.5	16.16	15.60	14.89	2.28	2.09	1.81	0.0500	0.0442	0.0366	0.0683	0.0603	0.0500	0.1786
12	-32.4	-1.77	5.5	17.36	17.21	16.90	2.13	1.98	1.70	0.0501	0.0461	0.0389	0.0685	0.0630	0.0531	0.1846
13	-29.7	0	5.4	33.28	17.28	16.54	0.80	0.61	0.58	0.0353	0.0141	0.0127	0.0482	0.0193	0.0174	0.0849
13-14	-24.3	0	5.4	95.52	17.80	17.20	0.94	0.68	0.58	0.1195	0.0161	0.0132	0.1631	0.0220	0.0181	0.2031
14	-18.9	0	5.4	157.76	18.33	17.86	1.08	0.74	0.58	0.2271	0.0181	0.0137	0.3102	0.0248	0.0188	0.3537
15	-13.5	0	5.4	238.22	22.79	18.47	1.43	1.23	1.18	0.4533	0.0373	0.0289	0.6190	0.0509	0.0395	0.7094
15-16	-8.1	0	5.4	339.79	96.76	18.23	1.50	1.46	1.34	0.6795	0.1885	0.0325	0.9280	0.2575	0.0444	1.2299
16	-2.7	0	5.4	441.37	170.73	17.98	1.57	1.70	1.50	0.9255	0.3861	0.0360	1.2639	0.5272	0.0492	1.8403
		height		6.2	3.7	1.2	6.2	3.7	1.2					Total Re-Entrainment (%)		11.15

* Inlet area is 63' (74mm in model scale) tall and 45, 46' (54, 55mm) wide

Vertical Distributions of Re-Entrainment Rate

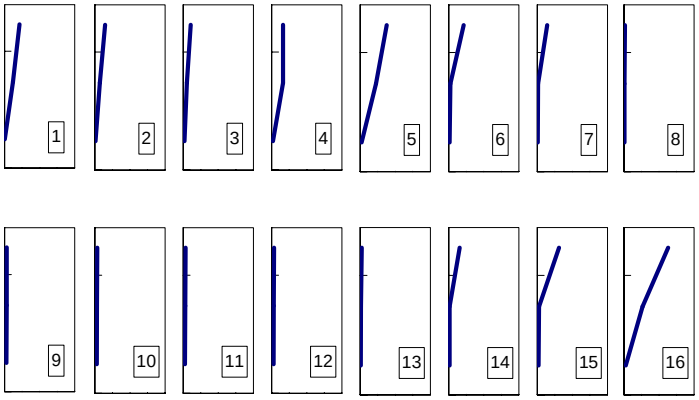

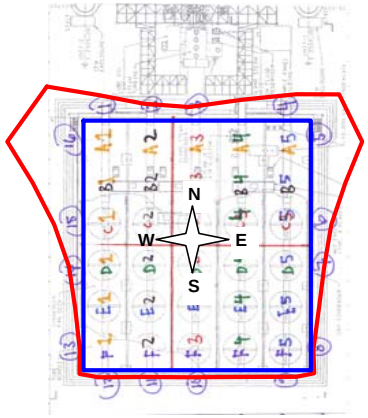

Re-entrainment Level along ACC Boundary

Estimated Contour of R

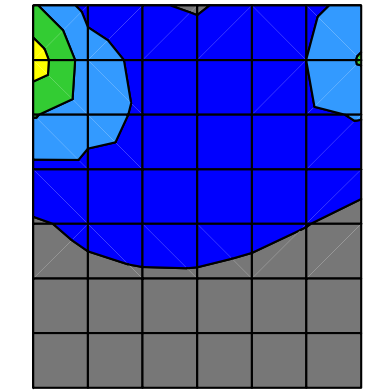

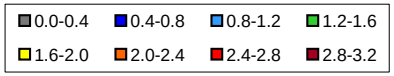

Wind Strength Moderate **Wind Direction** SW **Ethan Purity** 98.5

	X	Y	width	Concentration [PPM]			Speed [m/s]			Flux (times million)			Re-Entrainment Rate (%)			
	[cm]	[cm]	[cm]	T	M	B	T	M	B	T	M	B	T	M	B	SUM
1	0	-1.77	5.5	27.68	0.49	0.94	0.63	0.67	0.47	0.0236	0.0004	0.0006	0.0322	0.0006	0.0008	0.0337
2	0	-7.27	5.5	14.38	3.09	3.19	0.75	0.69	0.48	0.0146	0.0029	0.0021	0.0199	0.0039	0.0028	0.0267
3	0	-12.77	5.5	37.04	6.33	6.88	0.81	1.13	0.75	0.0405	0.0097	0.0070	0.0553	0.0133	0.0096	0.0782
3-4	0	-19.25	5.5	101.34	76.18	60.35	0.65	0.88	0.63	0.0889	0.0914	0.0516	0.1214	0.1248	0.0705	0.3168
4	0	-25.73	5.5	165.63	146.03	113.81	0.49	0.64	0.51	0.1096	0.1262	0.0787	0.1496	0.1723	0.1075	0.4294
5	-2.7	-27.5	5.4	232.50	184.86	101.47	1.12	1.06	0.93	0.3466	0.2612	0.1257	0.4734	0.3567	0.1716	1.0017
5-6	-8.1	-27.5	5.4	155.85	113.03	58.95	0.95	0.77	0.79	0.1974	0.1153	0.0620	0.2696	0.1574	0.0847	0.5118
6	-13.5	-27.5	5.4	79.19	41.21	16.42	0.78	0.47	0.65	0.0826	0.0258	0.0142	0.1128	0.0353	0.0194	0.1675
7	-18.9	-27.5	5.4	116.45	72.06	13.78	0.67	0.80	0.80	0.1041	0.0770	0.0146	0.1422	0.1052	0.0200	0.2674
7-8	-24.3	-27.5	5.4	217.12	43.12	12.68	0.72	0.90	0.92	0.2077	0.0516	0.0155	0.2837	0.0705	0.0211	0.3753
8	-29.7	-27.5	5.4	317.79	14.18	11.58	0.77	1.00	1.04	0.3239	0.0188	0.0160	0.4423	0.0257	0.0218	0.4898
9	-32.4	-25.73	5.5	19.87	11.45	12.04	2.08	1.94	1.71	0.0562	0.0302	0.0280	0.0767	0.0412	0.0382	0.1561
9-10	-32.4	-19.25	5.5	16.11	11.56	11.66	2.14	1.94	1.71	0.0469	0.0305	0.0270	0.0640	0.0416	0.0368	0.1425
10	-32.4	-12.77	5.5	12.35	11.67	11.28	2.21	1.94	1.70	0.0369	0.0308	0.0260	0.0504	0.0420	0.0355	0.1280
11	-32.4	-7.27	5.5	12.73	11.08	12.15	1.66	1.48	1.18	0.0287	0.0222	0.0195	0.0392	0.0303	0.0266	0.0960
12	-32.4	-1.77	5.5	11.71	11.54	11.73	1.67	1.41	1.19	0.0265	0.0221	0.0189	0.0362	0.0302	0.0258	0.0922
13	-29.7	0	5.4	13.19	13.16	12.59	1.81	1.45	1.21	0.0317	0.0254	0.0202	0.0433	0.0347	0.0276	0.1056
13-14	-24.3	0	5.4	15.62	13.57	12.43	1.85	1.45	1.20	0.0385	0.0262	0.0198	0.0525	0.0358	0.0271	0.1154
14	-18.9	0	5.4	18.05	13.98	12.27	1.89	1.45	1.19	0.0455	0.0270	0.0194	0.0621	0.0369	0.0265	0.1255
15	-13.5	0	5.4	27.30	14.73	13.33	2.10	1.84	1.65	0.0762	0.0362	0.0294	0.1041	0.0494	0.0401	0.1936
15-16	-8.1	0	5.4	22.26	14.29	14.05	2.16	1.88	1.66	0.0640	0.0357	0.0311	0.0875	0.0488	0.0425	0.1787
16	-2.7	0	5.4	17.23	13.85	14.76	2.22	1.91	1.67	0.0510	0.0353	0.0328	0.0697	0.0482	0.0448	0.1627
		height		6.2	3.7	1.2	6.2	3.7	1.2				Total Re-Entrainment (%)			5.19

* Inlet area is 63' (74mm in model scale) tall and 45, 46' (54, 55mm) wide

Vertical Distributions of Re-Entrainment Rate

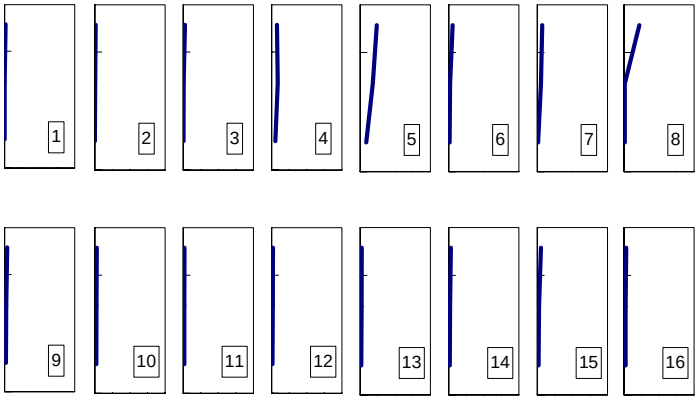

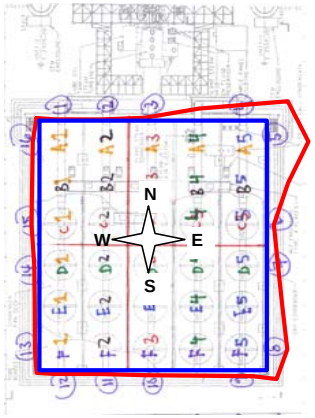

Re-entrainment Level along ACC Boundary

Estimated Contour of R

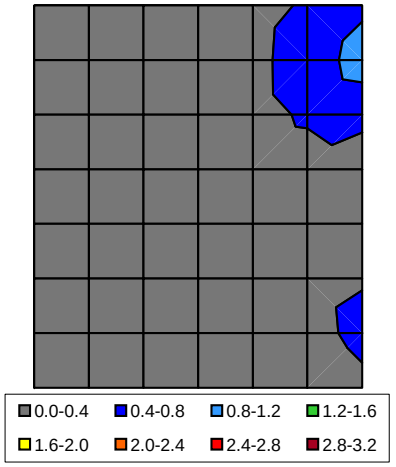

Wind Strength Moderate **Wind Direction** W **Ethan Purity** 98.5

	X	Y	width	Concentration [PPM]			Speed [m/s]			Flux (times million)			Re-Entrainment Rate (%)			
	[cm]	[cm]	[cm]	T	M	B	T	M	B	T	M	B	T	M	B	SUM
1	0	-1.77	5.5	4.50	1.08	1.12	1.16	1.05	0.95	0.0071	0.0015	0.0014	0.0097	0.0021	0.0020	0.0138
2	0	-7.27	5.5	77.96	12.02	3.98	1.07	0.88	0.96	0.1131	0.0143	0.0052	0.1544	0.0195	0.0071	0.1810
3	0	-12.77	5.5	158.35	169.39	7.06	1.54	1.53	1.70	0.3302	0.3526	0.0162	0.4509	0.4815	0.0222	0.9546
3-4	0	-19.25	5.5	286.40	177.01	19.06	1.21	1.07	1.06	0.4700	0.2581	0.0273	0.6419	0.3525	0.0373	1.0317
4	0	-25.73	5.5	414.45	184.63	31.06	0.88	0.62	0.42	0.4962	0.1541	0.0176	0.6776	0.2105	0.0241	0.9121
5	-2.7	-27.5	5.4	282.01	189.15	105.96	0.54	0.53	0.36	0.2018	0.1340	0.0505	0.2756	0.1830	0.0690	0.5276
5-6	-8.1	-27.5	5.4	273.04	187.15	124.58	0.69	0.62	0.50	0.2498	0.1535	0.0822	0.3411	0.2097	0.1123	0.6630
6	-13.5	-27.5	5.4	264.07	185.15	143.20	0.84	0.70	0.63	0.2941	0.1726	0.1207	0.4017	0.2357	0.1649	0.8023
7	-18.9	-27.5	5.4	318.99	245.18	77.20	1.04	0.89	0.69	0.4404	0.2911	0.0713	0.6015	0.3975	0.0973	1.0964
7-8	-24.3	-27.5	5.4	359.51	210.07	50.22	0.88	0.96	0.99	0.4211	0.2684	0.0663	0.5750	0.3665	0.0905	1.0320
8	-29.7	-27.5	5.4	400.03	174.96	23.24	0.72	1.03	1.29	0.3847	0.2393	0.0399	0.5253	0.3267	0.0545	0.9066
9	-32.4	-25.73	5.5	261.42	92.22	17.72	1.24	1.40	1.29	0.4413	0.1746	0.0311	0.6027	0.2385	0.0424	0.8836
9-10	-32.4	-19.25	5.5	158.43	55.53	18.41	1.10	1.12	1.05	0.2371	0.0845	0.0262	0.3238	0.1153	0.0358	0.4749
10	-32.4	-12.77	5.5	55.44	18.83	19.11	0.96	0.85	0.80	0.0723	0.0216	0.0209	0.0988	0.0295	0.0285	0.1568
11	-32.4	-7.27	5.5	46.04	17.76	18.62	0.62	0.63	0.63	0.0387	0.0152	0.0160	0.0528	0.0208	0.0218	0.0954
12	-32.4	-1.77	5.5	27.19	20.71	19.58	0.68	0.60	0.60	0.0252	0.0169	0.0159	0.0345	0.0231	0.0217	0.0792
13	-29.7	0	5.4	21.14	21.34	20.78	2.25	1.96	1.60	0.0635	0.0557	0.0444	0.0867	0.0761	0.0606	0.2234
13-14	-24.3	0	5.4	21.88	21.95	21.56	2.28	2.00	1.66	0.0666	0.0585	0.0476	0.0909	0.0799	0.0650	0.2358
14	-18.9	0	5.4	22.62	22.57	22.34	2.31	2.04	1.71	0.0697	0.0613	0.0509	0.0952	0.0837	0.0695	0.2485
15	-13.5	0	5.4	22.53	22.31	23.25	2.27	2.01	1.68	0.0680	0.0597	0.0521	0.0929	0.0815	0.0711	0.2455
15-16	-8.1	0	5.4	22.54	23.27	23.56	2.21	1.96	1.60	0.0663	0.0607	0.0504	0.0905	0.0829	0.0688	0.2422
16	-2.7	0	5.4	22.54	24.23	23.87	2.15	1.91	1.53	0.0646	0.0617	0.0486	0.0882	0.0842	0.0664	0.2387
		height		6.2	3.7	1.2	6.2	3.7	1.2				Total Re-Entrainment (%)			11.25

* Inlet area is 63' (74mm in model scale) tall and 45, 46' (54, 55mm) wide

Vertical Distributions of Re-Entrainment Rate

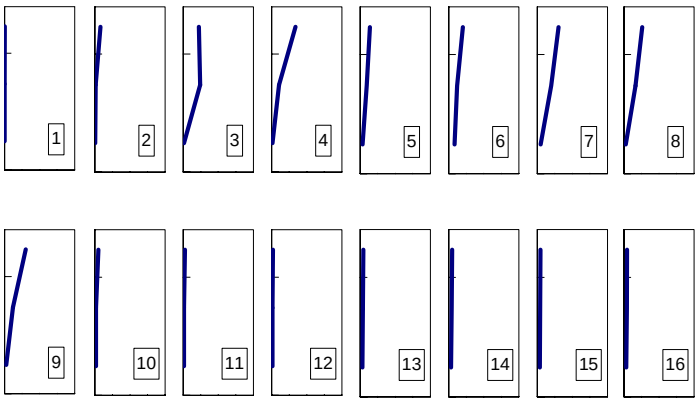

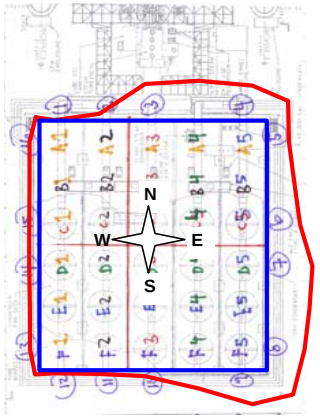

Re-entrainment Level along ACC Boundary

Estimated Contour of R

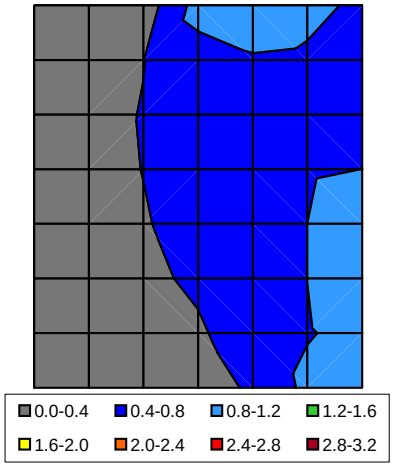

Wind Strength Moderate **Wind Direction** N **Ethan Purity** 98.5

	X	Y	width	Concentration [PPM]			Speed [m/s]			Flux (times million)			Re-Entrainment Rate (%)			
	[cm]	[cm]	[cm]	T	M	B	T	M	B	T	M	B	T	M	B	SUM
1	0	-1.77	5.5	1.90	0.40	0.15	2.38	1.82	1.63	0.0061	0.0010	0.0003	0.0084	0.0014	0.0004	0.0102
2	0	-7.27	5.5	10.21	3.04	2.84	2.69	2.35	0.58	0.0373	0.0097	0.0022	0.0509	0.0132	0.0030	0.0672
3	0	-12.77	5.5	8.41	6.51	6.79	2.72	2.11	0.75	0.0310	0.0186	0.0069	0.0424	0.0254	0.0095	0.0773
3-4	0	-19.25	5.5	8.54	7.52	7.73	2.19	1.62	1.02	0.0254	0.0165	0.0107	0.0347	0.0225	0.0146	0.0718
4	0	-25.73	5.5	8.68	8.53	8.66	1.66	1.12	1.29	0.0196	0.0130	0.0151	0.0268	0.0177	0.0207	0.0652
5	-2.7	-27.5	5.4	13.52	9.35	8.60	1.14	0.59	0.72	0.0205	0.0074	0.0083	0.0280	0.0101	0.0113	0.0494
5-6	-8.1	-27.5	5.4	145.38	11.96	9.26	1.38	0.90	0.82	0.2678	0.0143	0.0101	0.3657	0.0195	0.0138	0.3990
6	-13.5	-27.5	5.4	277.24	14.57	9.91	1.63	1.20	0.92	0.6008	0.0233	0.0121	0.8205	0.0318	0.0165	0.8688
7	-18.9	-27.5	5.4	404.40	50.95	10.50	1.77	1.66	1.48	0.9526	0.1124	0.0207	1.3009	0.1534	0.0282	1.4825
7-8	-24.3	-27.5	5.4	624.72	215.80	23.64	1.62	1.67	1.53	1.3488	0.4810	0.0481	1.8419	0.6568	0.0656	2.5644
8	-29.7	-27.5	5.4	845.04	380.66	36.78	1.47	1.69	1.58	1.6583	0.8573	0.0772	2.2646	1.1707	0.1054	3.5407
9	-32.4	-25.73	5.5	626.68	491.96	89.69	0.75	0.81	1.27	0.6347	0.5421	0.1540	0.8667	0.7403	0.2103	1.8173
9-10	-32.4	-19.25	5.5	480.32	379.20	131.36	0.76	0.79	0.89	0.4964	0.4074	0.1592	0.6779	0.5564	0.2174	1.4517
10	-32.4	-12.77	5.5	333.97	266.45	173.04	0.78	0.77	0.52	0.3521	0.2790	0.1222	0.4809	0.3810	0.1669	1.0288
11	-32.4	-7.27	5.5	300.50	222.23	155.13	1.12	0.89	0.51	0.4551	0.2675	0.1083	0.6214	0.3653	0.1479	1.1346
12	-32.4	-1.77	5.5	500.26	372.23	159.71	0.65	1.09	1.25	0.4381	0.5509	0.2703	0.5983	0.7523	0.3691	1.7197
13	-29.7	0	5.4	585.45	366.91	85.35	1.36	1.66	1.49	1.0604	0.8090	0.1693	1.4481	1.1047	0.2311	2.7839
13-14	-24.3	0	5.4	495.00	291.56	58.08	1.45	1.60	1.39	0.9560	0.6203	0.1073	1.3055	0.8471	0.1466	2.2992
14	-18.9	0	5.4	404.55	216.21	30.81	1.54	1.54	1.29	0.8298	0.4433	0.0528	1.1332	0.6054	0.0721	1.8107
15	-13.5	0	5.4	352.96	113.08	19.06	1.31	1.19	0.93	0.6140	0.1787	0.0237	0.8385	0.2440	0.0324	1.1149
15-16	-8.1	0	5.4	190.55	62.66	16.51	1.18	0.84	0.77	0.2993	0.0704	0.0169	0.4087	0.0961	0.0231	0.5280
16	-2.7	0	5.4	28.15	12.25	13.95	1.05	0.50	0.61	0.0395	0.0082	0.0113	0.0539	0.0111	0.0154	0.0804
		height		6.2	3.7	1.2	6.2	3.7	1.2				Total Re-Entrainment (%)			24.97

* Inlet area is 63' (74mm in model scale) tall and 45, 46' (54, 55mm) wide

Vertical Distributions of Re-Entrainment Rate

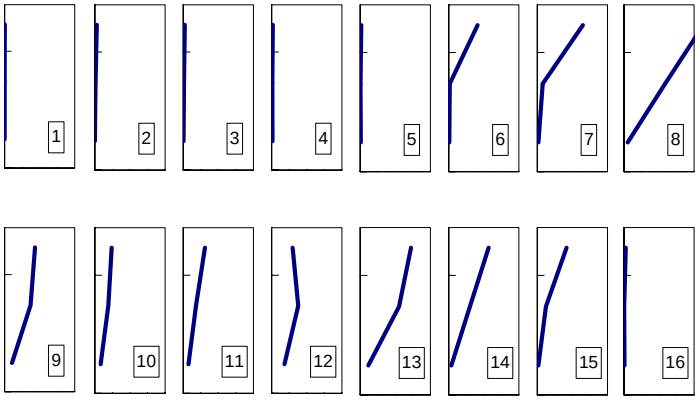

Re-entrainment Level along ACC Boundary

Estimated Contour of R

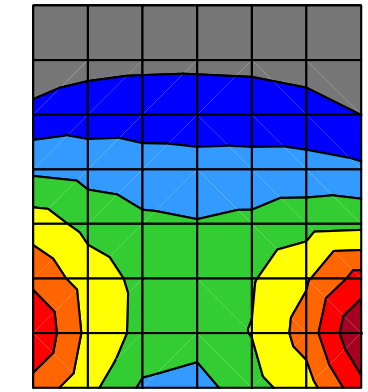

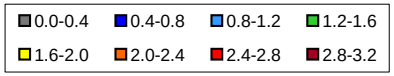

Wind Strength	Strong			Wind Direction	S		Ethan Purity	98.5								
	X	Y	width	Concentration [PPM]			Speed [m/s]			Flux (times million)			Re-Entrainment Rate (%)			
	[cm]	[cm]	[cm]	T	M	B	T	M	B	T	M	B	T	M	B	SUM
1	0	-1.77	5.5	223.38	70.13	2.45	1.56	2.31	1.39	0.4730	0.2203	0.0046	0.6459	0.3008	0.0063	0.9530
2	0	-7.27	5.5	251.53	45.18	8.05	1.01	0.79	0.75	0.3447	0.0482	0.0082	0.4707	0.0658	0.0113	0.5478
3	0	-12.77	5.5	218.34	140.02	52.06	1.29	1.28	1.39	0.3812	0.2434	0.0981	0.5205	0.3323	0.1340	0.9869
3-4	0	-19.25	5.5	167.02	82.29	30.77	1.62	1.55	1.35	0.3674	0.1728	0.0566	0.5017	0.2360	0.0772	0.8149
4	0	-25.73	5.5	115.71	24.55	9.49	1.96	1.81	1.32	0.3070	0.0605	0.0170	0.4193	0.0826	0.0232	0.5250
5	-2.7	-27.5	5.4	99.20	19.08	10.67	1.76	1.54	1.48	0.2331	0.0393	0.0210	0.3184	0.0536	0.0287	0.4007
5-6	-8.1	-27.5	5.4	74.50	16.19	10.96	1.53	1.15	1.16	0.1520	0.0247	0.0169	0.2076	0.0337	0.0231	0.2643
6	-13.5	-27.5	5.4	49.80	13.29	11.26	1.30	0.75	0.83	0.0861	0.0132	0.0125	0.1176	0.0181	0.0171	0.1528
7	-18.9	-27.5	5.4	112.57	15.22	12.45	1.03	0.89	0.84	0.1551	0.0180	0.0139	0.2118	0.0245	0.0190	0.2553
7-8	-24.3	-27.5	5.4	92.37	13.91	12.52	1.22	0.91	0.84	0.1500	0.0169	0.0141	0.2048	0.0231	0.0192	0.2472
8	-29.7	-27.5	5.4	72.17	12.59	12.58	1.40	0.94	0.85	0.1350	0.0158	0.0142	0.1843	0.0216	0.0194	0.2253
9	-32.4	-25.73	5.5	13.15	14.21	12.71	3.24	3.08	2.70	0.0579	0.0593	0.0466	0.0791	0.0810	0.0636	0.2236
9-10	-32.4	-19.25	5.5	13.40	14.15	13.29	3.22	3.08	2.68	0.0586	0.0592	0.0482	0.0800	0.0809	0.0659	0.2267
10	-32.4	-12.77	5.5	13.65	14.10	13.87	3.20	3.09	2.65	0.0592	0.0591	0.0499	0.0808	0.0807	0.0681	0.2297
11	-32.4	-7.27	5.5	14.28	14.35	14.26	3.10	3.05	2.61	0.0602	0.0594	0.0506	0.0821	0.0811	0.0690	0.2323
12	-32.4	-1.77	5.5	14.11	14.22	14.04	3.05	2.95	2.64	0.0585	0.0569	0.0502	0.0798	0.0777	0.0686	0.2262
13	-29.7	0	5.4	47.50	13.71	14.25	1.19	1.00	0.96	0.0752	0.0183	0.0182	0.1026	0.0251	0.0248	0.1525
13-14	-24.3	0	5.4	76.72	17.93	14.34	1.06	0.98	0.98	0.1085	0.0234	0.0187	0.1481	0.0319	0.0255	0.2056
14	-18.9	0	5.4	105.95	22.16	14.43	0.93	0.95	1.00	0.1319	0.0282	0.0192	0.1801	0.0384	0.0262	0.2448
15	-13.5	0	5.4	74.81	21.96	15.09	1.16	0.74	0.53	0.1156	0.0217	0.0107	0.1579	0.0296	0.0146	0.2022
15-16	-8.1	0	5.4	133.18	40.97	15.61	1.53	1.27	1.10	0.2715	0.0695	0.0228	0.3708	0.0949	0.0311	0.4969
16	-2.7	0	5.4	191.56	59.99	16.14	1.90	1.81	1.66	0.4850	0.1442	0.0357	0.6624	0.1970	0.0487	0.9081
		height		6.2	3.7	1.2	6.2	3.7	1.2					Total Re-Entrainment (%)		8.72

* Inlet area is 63' (74mm in model scale) tall and 45, 46' (54, 55mm) wide

Vertical Distributions of Re-Entrainment Rate

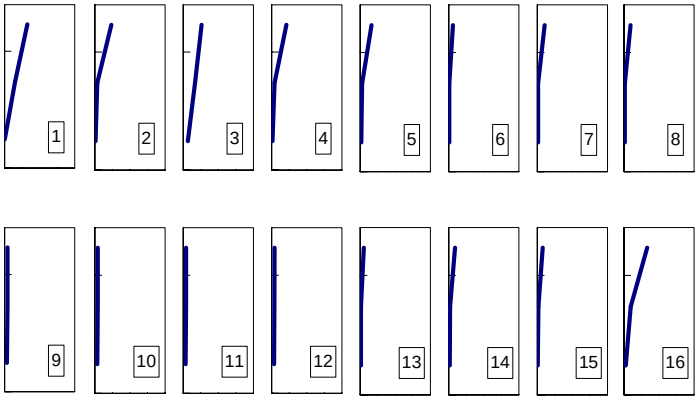

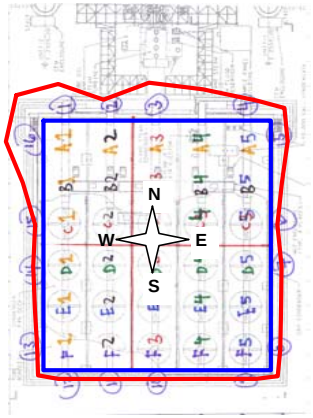

Re-entrainment Level along ACC Boundary

Estimated Contour of R

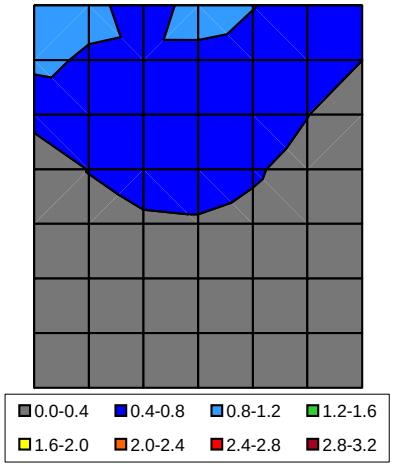

Wind Strength Strong **Wind Direction** SW **Ethan Purity** 98.5

	X	Y	width	Concentration [PPM]			Speed [m/s]			Flux (times million)			Re-Entrainment Rate (%)			
	[cm]	[cm]	[cm]	T	M	B	T	M	B	T	M	B	T	M	B	SUM
1	0	-1.77	5.5	3.93	1.25	1.14	1.62	1.81	1.26	0.0086	0.0031	0.0019	0.0118	0.0042	0.0027	0.0186
2	0	-7.27	5.5	9.81	4.17	3.78	1.75	1.32	0.93	0.0233	0.0075	0.0048	0.0318	0.0102	0.0065	0.0485
3	0	-12.77	5.5	100.13	16.73	6.57	0.62	1.31	0.65	0.0843	0.0298	0.0058	0.1151	0.0407	0.0079	0.1637
3-4	0	-19.25	5.5	86.20	39.62	33.82	0.68	1.02	0.72	0.0797	0.0550	0.0329	0.1088	0.0751	0.0449	0.2289
4	0	-25.73	5.5	72.27	62.51	61.08	0.74	0.73	0.79	0.0728	0.0621	0.0652	0.0994	0.0848	0.0891	0.2732
5	-2.7	-27.5	5.4	78.66	84.32	84.43	1.01	0.82	0.65	0.1058	0.0922	0.0733	0.1444	0.1259	0.1000	0.3704
5-6	-8.1	-27.5	5.4	102.40	100.00	84.45	0.86	0.78	0.60	0.1177	0.1037	0.0675	0.1607	0.1416	0.0921	0.3944
6	-13.5	-27.5	5.4	126.15	115.69	84.48	0.72	0.74	0.55	0.1203	0.1134	0.0617	0.1643	0.1548	0.0842	0.4034
7	-18.9	-27.5	5.4	18.09	15.02	14.28	1.84	1.92	1.88	0.0444	0.0385	0.0357	0.0606	0.0526	0.0488	0.1620
7-8	-24.3	-27.5	5.4	80.55	15.30	14.96	1.56	2.02	1.98	0.1672	0.0411	0.0395	0.2284	0.0562	0.0540	0.3386
8	-29.7	-27.5	5.4	143.00	15.59	15.64	1.28	2.11	2.09	0.2430	0.0439	0.0436	0.3318	0.0599	0.0595	0.4512
9	-32.4	-25.73	5.5	18.59	17.28	17.06	2.97	2.91	2.70	0.0750	0.0683	0.0624	0.1024	0.0933	0.0853	0.2809
9-10	-32.4	-19.25	5.5	18.14	17.73	17.83	2.96	2.83	2.60	0.0727	0.0681	0.0630	0.0993	0.0930	0.0860	0.2784
10	-32.4	-12.77	5.5	17.68	18.19	18.60	2.94	2.75	2.51	0.0705	0.0678	0.0634	0.0963	0.0926	0.0866	0.2754
11	-32.4	-7.27	5.5	19.54	17.89	17.86	2.34	2.08	1.67	0.0620	0.0504	0.0405	0.0846	0.0688	0.0553	0.2087
12	-32.4	-1.77	5.5	19.78	18.76	17.89	2.30	2.18	1.84	0.0617	0.0555	0.0446	0.0843	0.0759	0.0609	0.2210
13	-29.7	0	5.4	18.76	19.34	18.91	2.19	1.92	1.59	0.0547	0.0493	0.0401	0.0748	0.0674	0.0548	0.1969
13-14	-24.3	0	5.4	19.58	19.65	19.45	2.15	1.82	1.47	0.0560	0.0476	0.0380	0.0765	0.0650	0.0519	0.1934
14	-18.9	0	5.4	20.40	19.96	20.00	2.11	1.72	1.34	0.0572	0.0457	0.0358	0.0781	0.0624	0.0488	0.1894
15	-13.5	0	5.4	20.82	20.89	20.31	2.30	2.13	1.90	0.0638	0.0593	0.0514	0.0871	0.0810	0.0703	0.2383
15-16	-8.1	0	5.4	21.19	20.97	20.80	2.42	2.27	1.99	0.0683	0.0633	0.0552	0.0932	0.0864	0.0754	0.2550
16	-2.7	0	5.4	21.57	21.05	21.29	2.54	2.40	2.08	0.0729	0.0673	0.0591	0.0996	0.0919	0.0807	0.2721
		height		6.2	3.7	1.2	6.2	3.7	1.2				Total Re-Entrainment (%)			5.46

* Inlet area is 63' (74mm in model scale) tall and 45, 46' (54, 55mm) wide

Vertical Distributions of Re-Entrainment Rate

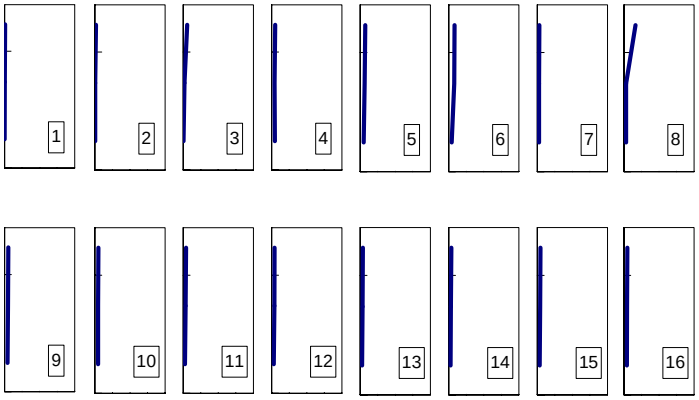

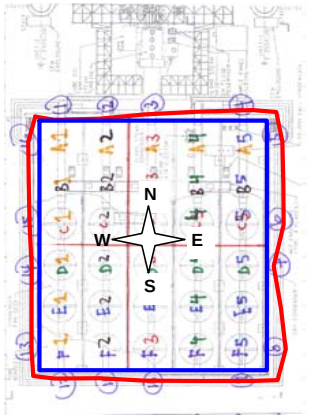

Re-entrainment Level along ACC Boundary

Estimated Contour of R

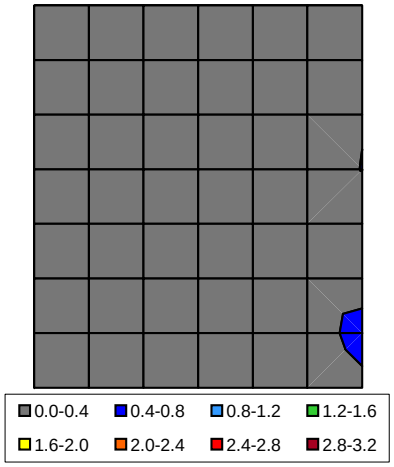

Wind Strength	Strong			Wind Direction	W		Ethan Purity	98.5								
	X	Y	width	Concentration [PPM]			Speed [m/s]			Flux (times million)			Re-Entrainment Rate (%)			
	[cm]	[cm]	[cm]	T	M	B	T	M	B	T	M	B	T	M	B	SUM
1	0	-1.77	5.5	15.06	6.68	5.32	1.17	1.16	0.94	0.0238	0.0105	0.0068	0.0325	0.0143	0.0093	0.0562
2	0	-7.27	5.5	33.61	8.37	8.07	1.00	0.93	0.88	0.0458	0.0106	0.0097	0.0625	0.0144	0.0132	0.0901
3	0	-12.77	5.5	34.31	9.99	9.96	1.49	1.60	1.78	0.0695	0.0217	0.0240	0.0949	0.0296	0.0328	0.1573
3-4	0	-19.25	5.5	101.34	13.53	9.95	1.23	1.38	1.32	0.1691	0.0253	0.0178	0.2309	0.0345	0.0243	0.2897
4	0	-25.73	5.5	168.37	17.08	9.95	0.97	1.15	0.86	0.2208	0.0267	0.0117	0.3015	0.0364	0.0159	0.3538
5	-2.7	-27.5	5.4	66.73	17.65	13.51	0.86	1.44	0.96	0.0764	0.0339	0.0172	0.1043	0.0463	0.0235	0.1742
5-6	-8.1	-27.5	5.4	114.76	24.50	15.64	0.86	1.25	1.40	0.1312	0.0408	0.0291	0.1792	0.0558	0.0397	0.2747
6	-13.5	-27.5	5.4	162.80	31.35	17.77	0.86	1.06	1.84	0.1859	0.0443	0.0435	0.2538	0.0605	0.0594	0.3737
7	-18.9	-27.5	5.4	115.81	73.03	59.93	1.51	1.13	1.27	0.2323	0.1104	0.1017	0.3172	0.1507	0.1389	0.6068
7-8	-24.3	-27.5	5.4	135.47	75.50	53.26	1.34	1.22	1.03	0.2421	0.1227	0.0732	0.3306	0.1675	0.1000	0.5981
8	-29.7	-27.5	5.4	155.12	77.96	46.60	1.18	1.31	0.79	0.2433	0.1355	0.0490	0.3323	0.1851	0.0669	0.5843
9	-32.4	-25.73	5.5	71.55	20.46	16.34	1.29	1.15	1.03	0.1247	0.0320	0.0229	0.1704	0.0436	0.0312	0.2452
9-10	-32.4	-19.25	5.5	47.24	18.00	15.93	1.26	1.10	0.90	0.0806	0.0268	0.0195	0.1100	0.0366	0.0266	0.1732
10	-32.4	-12.77	5.5	22.94	15.53	15.52	1.23	1.05	0.77	0.0383	0.0221	0.0162	0.0522	0.0301	0.0221	0.1045
11	-32.4	-7.27	5.5	31.96	14.98	14.92	1.12	1.26	1.36	0.0487	0.0256	0.0275	0.0665	0.0349	0.0375	0.1390
12	-32.4	-1.77	5.5	18.47	15.09	14.78	1.16	1.17	1.14	0.0290	0.0239	0.0230	0.0395	0.0327	0.0313	0.1036
13	-29.7	0	5.4	15.16	14.98	14.99	3.00	2.91	2.43	0.0605	0.0580	0.0485	0.0826	0.0792	0.0662	0.2280
13-14	-24.3	0	5.4	15.07	14.92	14.97	3.02	2.84	2.43	0.0607	0.0564	0.0485	0.0828	0.0770	0.0662	0.2260
14	-18.9	0	5.4	14.99	14.86	14.96	3.04	2.77	2.43	0.0608	0.0548	0.0485	0.0830	0.0748	0.0662	0.2240
15	-13.5	0	5.4	15.53	15.33	14.99	2.94	2.71	2.31	0.0608	0.0554	0.0462	0.0830	0.0756	0.0631	0.2217
15-16	-8.1	0	5.4	15.19	15.05	14.85	2.92	2.75	2.31	0.0591	0.0551	0.0457	0.0806	0.0752	0.0624	0.2183
16	-2.7	0	5.4	14.85	14.77	14.72	2.90	2.78	2.31	0.0574	0.0548	0.0452	0.0783	0.0748	0.0617	0.2148
		height		6.2	3.7	1.2	6.2	3.7	1.2				Total Re-Entrainment (%)			5.66

* Inlet area is 63' (74mm in model scale) tall and 45, 46' (54, 55mm) wide

Vertical Distributions of Re-Entrainment Rate

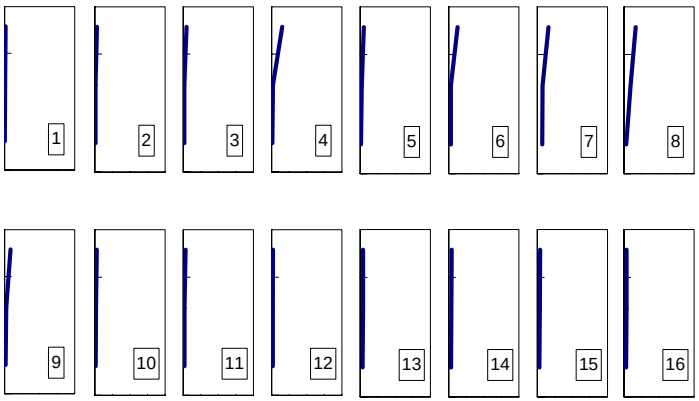

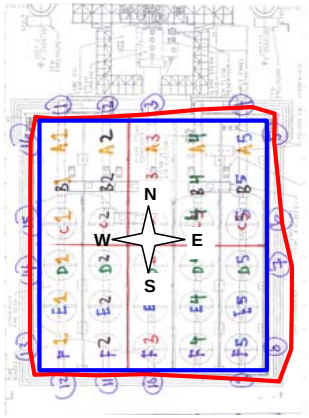

Re-entrainment Level along ACC Boundary

Estimated Contour of R

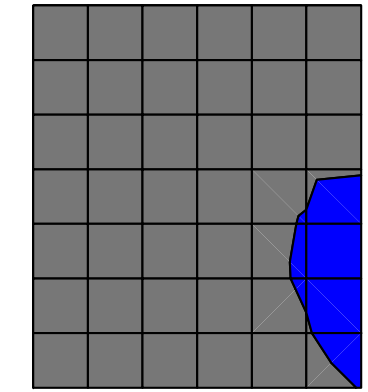

Wind Strength	Strong			Wind Direction	N		Ethan Purity	98.5								
	X	Y	width	Concentration [PPM]			Speed [m/s]			Flux (times million)			Re-Entrainment Rate (%)			
	[cm]	[cm]	[cm]	T	M	B	T	M	B	T	M	B	T	M	B	SUM
1	0	-1.77	5.5	1.06	1.36	0.02	2.40	0.83	2.07	0.0035	0.0015	0.0001	0.0047	0.0021	0.0001	0.0069
2	0	-7.27	5.5	4.34	2.64	3.02	3.33	3.11	0.96	0.0196	0.0111	0.0039	0.0268	0.0152	0.0053	0.0473
3	0	-12.77	5.5	5.73	5.95	5.92	3.09	2.08	1.86	0.0240	0.0168	0.0149	0.0328	0.0229	0.0204	0.0761
3-4	0	-19.25	5.5	6.16	5.99	6.00	2.43	1.63	1.62	0.0203	0.0132	0.0132	0.0277	0.0180	0.0180	0.0637
4	0	-25.73	5.5	6.59	6.03	6.07	1.76	1.18	1.39	0.0157	0.0096	0.0114	0.0215	0.0131	0.0156	0.0502
5	-2.7	-27.5	5.4	61.33	9.51	7.34	0.92	0.59	0.72	0.0751	0.0075	0.0070	0.1025	0.0102	0.0096	0.1223
5-6	-8.1	-27.5	5.4	156.73	52.97	9.49	1.17	0.78	0.86	0.2452	0.0550	0.0109	0.3349	0.0752	0.0149	0.4249
6	-13.5	-27.5	5.4	252.13	96.42	11.64	1.43	0.97	1.00	0.4803	0.1247	0.0156	0.6559	0.1703	0.0213	0.8475
7	-18.9	-27.5	5.4	246.93	92.15	15.93	2.02	1.73	1.64	0.6632	0.2119	0.0349	0.9057	0.2894	0.0476	1.2426
7-8	-24.3	-27.5	5.4	358.45	149.83	21.99	2.05	1.99	1.82	0.9783	0.3978	0.0533	1.3359	0.5432	0.0727	1.9519
8	-29.7	-27.5	5.4	469.98	207.52	28.04	2.08	2.26	2.00	1.3030	0.6247	0.0745	1.7794	0.8531	0.1018	2.7342
9	-32.4	-25.73	5.5	542.75	288.96	74.86	0.82	1.91	2.11	0.6022	0.7483	0.2144	0.8224	1.0219	0.2927	2.1370
9-10	-32.4	-19.25	5.5	378.19	212.98	84.40	0.92	1.42	1.46	0.4700	0.4100	0.1672	0.6418	0.5599	0.2283	1.4300
10	-32.4	-12.77	5.5	213.62	137.01	93.95	1.01	0.93	0.81	0.2939	0.1727	0.1032	0.4013	0.2358	0.1410	0.7781
11	-32.4	-7.27	5.5	213.30	171.81	119.48	1.27	1.43	1.14	0.3675	0.3332	0.1845	0.5019	0.4550	0.2519	1.2087
12	-32.4	-1.77	5.5	382.51	270.67	124.86	0.83	1.59	2.06	0.4310	0.5855	0.3489	0.5886	0.7996	0.4765	1.8647
13	-29.7	0	5.4	368.64	214.35	75.46	1.66	1.92	1.75	0.8173	0.5486	0.1762	1.1161	0.7491	0.2406	2.1059
13-14	-24.3	0	5.4	272.68	153.78	50.54	1.54	1.61	1.51	0.5607	0.3304	0.1018	0.7657	0.4512	0.1390	1.3559
14	-18.9	0	5.4	176.72	93.21	25.62	1.42	1.30	1.27	0.3350	0.1620	0.0433	0.4575	0.2212	0.0592	0.7379
15	-13.5	0	5.4	171.93	89.71	18.66	1.04	0.81	0.75	0.2392	0.0970	0.0187	0.3266	0.1325	0.0255	0.4846
15-16	-8.1	0	5.4	137.20	53.55	17.11	0.97	0.66	0.65	0.1773	0.0470	0.0147	0.2422	0.0642	0.0201	0.3265
16	-2.7	0	5.4	102.48	17.39	15.56	0.90	0.51	0.54	0.1224	0.0117	0.0112	0.1671	0.0160	0.0153	0.1984
		height		6.2	3.7	1.2	6.2	3.7	1.2					Total Re-Entrainment (%)		20.20

* Inlet area is 63' (74mm in model scale) tall and 45, 46' (54, 55mm) wide

Vertical Distributions of Re-Entrainment Rate

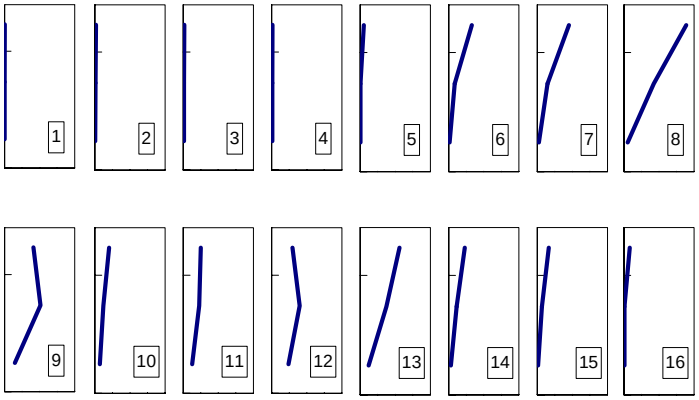

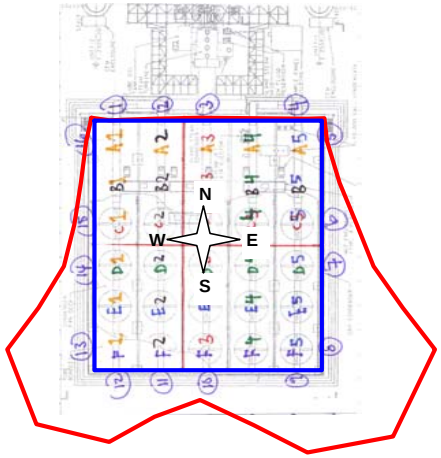

Re-entrainment Level along ACC Boundary

Estimated Contour of R

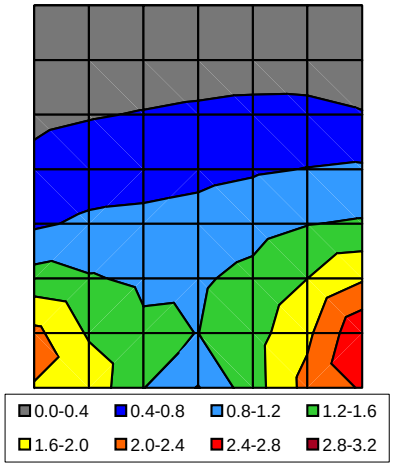

Wind Strength Extreme **Wind Direction** S **Ethan Purity** 98.5

	X	Y	width	Concentration [PPM]			Speed [m/s]			Flux (times million)			Re-Entrainment Rate (%)			
	[cm]	[cm]	[cm]	T	M	B	T	M	B	T	M	B	T	M	B	SUM
1	0	-1.77	5.5	401.38	272.75	184.29	0.32	0.89	0.16	0.1732	0.3291	0.0398	0.2365	0.4494	0.0544	0.7403
2	0	-7.27	5.5	526.42	341.50	163.91	0.42	0.45	0.27	0.2968	0.2094	0.0611	0.4053	0.2860	0.0834	0.7747
3	0	-12.77	5.5	306.60	133.97	114.94	0.46	2.14	0.26	0.1902	0.3895	0.0413	0.2597	0.5319	0.0564	0.8480
3-4	0	-19.25	5.5	232.70	128.90	85.85	0.49	1.39	0.34	0.1558	0.2433	0.0394	0.2128	0.3322	0.0538	0.5988
4	0	-25.73	5.5	158.79	123.83	56.76	0.53	0.64	0.41	0.1142	0.1074	0.0317	0.1559	0.1466	0.0433	0.3458
5	-2.7	-27.5	5.4	126.69	50.23	23.57	0.50	0.41	0.39	0.0838	0.0272	0.0123	0.1144	0.0372	0.0168	0.1683
5-6	-8.1	-27.5	5.4	76.68	32.68	17.97	0.55	0.34	0.34	0.0560	0.0148	0.0081	0.0764	0.0202	0.0111	0.1078
6	-13.5	-27.5	5.4	26.66	15.13	12.38	0.60	0.27	0.29	0.0213	0.0055	0.0048	0.0291	0.0075	0.0065	0.0431
7	-18.9	-27.5	5.4	128.13	22.46	13.76	0.79	0.87	1.11	0.1356	0.0261	0.0203	0.1852	0.0357	0.0278	0.2487
7-8	-24.3	-27.5	5.4	112.16	17.90	14.47	0.85	0.82	0.89	0.1266	0.0196	0.0171	0.1729	0.0268	0.0233	0.2230
8	-29.7	-27.5	5.4	96.20	13.34	15.19	0.90	0.77	0.66	0.1153	0.0138	0.0134	0.1575	0.0188	0.0183	0.1945
9	-32.4	-25.73	5.5	15.54	13.25	15.53	2.21	2.09	1.54	0.0466	0.0376	0.0324	0.0637	0.0513	0.0442	0.1592
9-10	-32.4	-19.25	5.5	15.08	14.17	15.33	2.16	2.06	1.49	0.0442	0.0396	0.0311	0.0604	0.0540	0.0424	0.1569
10	-32.4	-12.77	5.5	14.62	15.08	15.13	2.11	2.03	1.45	0.0419	0.0414	0.0298	0.0572	0.0566	0.0407	0.1546
11	-32.4	-7.27	5.5	16.33	15.77	16.16	2.06	2.01	1.39	0.0457	0.0431	0.0305	0.0624	0.0588	0.0416	0.1629
12	-32.4	-1.77	5.5	18.81	16.87	16.40	2.13	2.02	1.38	0.0544	0.0461	0.0306	0.0743	0.0630	0.0418	0.1791
13	-29.7	0	5.4	54.98	17.38	17.53	0.80	0.73	0.65	0.0589	0.0170	0.0152	0.0805	0.0232	0.0208	0.1245
13-14	-24.3	0	5.4	81.18	18.78	17.03	0.78	0.80	0.91	0.0846	0.0200	0.0206	0.1155	0.0273	0.0281	0.1709
14	-18.9	0	5.4	107.38	20.18	16.53	0.76	0.87	1.16	0.1086	0.0233	0.0255	0.1484	0.0318	0.0349	0.2150
15	-13.5	0	5.4	38.89	17.98	18.05	0.40	0.25	0.20	0.0205	0.0060	0.0048	0.0280	0.0082	0.0066	0.0428
15-16	-8.1	0	5.4	117.93	66.32	71.99	0.47	0.28	0.25	0.0737	0.0251	0.0244	0.1007	0.0343	0.0334	0.1683
16	-2.7	0	5.4	196.98	114.67	125.92	0.54	0.32	0.31	0.1424	0.0485	0.0519	0.1944	0.0662	0.0709	0.3315
		height		6.2	3.7	1.2	6.2	3.7	1.2				Total Re-Entrainment (%)			6.16

* Inlet area is 63' (74mm in model scale) tall and 45,46' (54,55mm) wide

Vertical Distributions of Re-Entrainment Rate

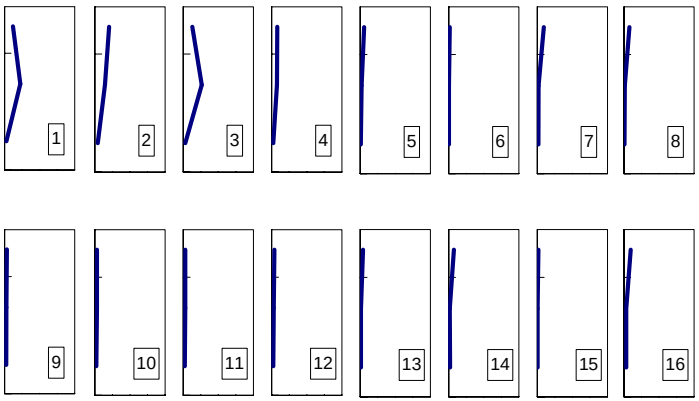

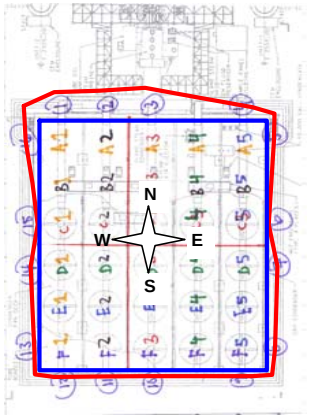

Re-entrainment Level along ACC Boundary

Estimated Contour of R

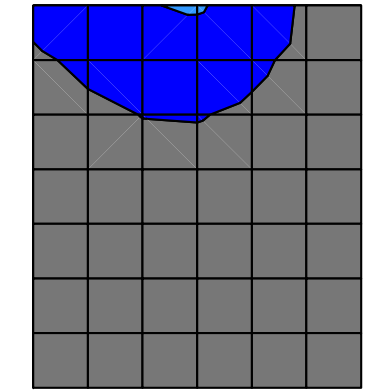

Wind Strength Extreme **Wind Direction** SW **Ethan Purity** 98.5

	X	Y	width	Concentration [PPM]			Speed [m/s]			Flux (times million)			Re-Entrainment Rate (%)			
	[cm]	[cm]	[cm]	T	M	B	T	M	B	T	M	B	T	M	B	SUM
1	0	-1.77	5.5	3.08	1.86	0.30	1.32	1.47	1.19	0.0055	0.0037	0.0005	0.0075	0.0051	0.0007	0.0132
2	0	-7.27	5.5	7.06	5.09	3.45	1.50	1.23	0.78	0.0144	0.0085	0.0037	0.0196	0.0116	0.0050	0.0362
3	0	-12.77	5.5	85.29	9.67	6.23	0.37	0.42	0.88	0.0427	0.0055	0.0075	0.0584	0.0075	0.0102	0.0761
3-4	0	-19.25	5.5	73.34	21.53	28.54	0.57	0.64	0.61	0.0563	0.0188	0.0236	0.0768	0.0257	0.0322	0.1347
4	0	-25.73	5.5	61.39	33.39	50.85	0.76	0.87	0.33	0.0635	0.0392	0.0229	0.0866	0.0535	0.0313	0.1715
5	-2.7	-27.5	5.4	90.65	34.69	25.45	0.38	0.51	0.41	0.0458	0.0234	0.0140	0.0625	0.0319	0.0191	0.1135
5-6	-8.1	-27.5	5.4	166.19	64.76	37.90	0.45	0.49	0.38	0.1003	0.0423	0.0193	0.1370	0.0577	0.0263	0.2211
6	-13.5	-27.5	5.4	241.73	94.84	50.35	0.53	0.47	0.35	0.1698	0.0599	0.0235	0.2319	0.0818	0.0321	0.3459
7	-18.9	-27.5	5.4	23.36	10.34	8.78	1.22	1.49	1.61	0.0380	0.0205	0.0188	0.0520	0.0280	0.0257	0.1056
7-8	-24.3	-27.5	5.4	87.05	9.91	9.10	1.12	1.87	1.90	0.1303	0.0247	0.0230	0.1780	0.0337	0.0314	0.2432
8	-29.7	-27.5	5.4	150.74	9.48	9.42	1.03	2.26	2.19	0.2059	0.0285	0.0275	0.2812	0.0389	0.0375	0.3576
9	-32.4	-25.73	5.5	2.74	10.27	11.00	2.04	1.98	1.79	0.0076	0.0277	0.0267	0.0104	0.0378	0.0364	0.0845
9-10	-32.4	-19.25	5.5	3.62	7.73	7.51	1.92	1.87	1.64	0.0094	0.0196	0.0168	0.0129	0.0268	0.0229	0.0625
10	-32.4	-12.77	5.5	4.50	5.18	4.02	1.80	1.76	1.50	0.0110	0.0123	0.0082	0.0150	0.0169	0.0112	0.0430
11	-32.4	-7.27	5.5	6.70	6.52	5.35	1.42	1.27	0.95	0.0129	0.0112	0.0069	0.0176	0.0153	0.0095	0.0424
12	-32.4	-1.77	5.5	8.33	6.95	8.07	1.52	1.47	1.11	0.0171	0.0138	0.0122	0.0234	0.0189	0.0166	0.0589
13	-29.7	0	5.4	8.24	9.50	9.66	1.62	1.47	1.18	0.0177	0.0186	0.0151	0.0242	0.0254	0.0207	0.0702
13-14	-24.3	0	5.4	9.69	9.44	9.99	1.49	1.32	0.97	0.0192	0.0166	0.0130	0.0262	0.0227	0.0177	0.0666
14	-18.9	0	5.4	11.14	9.38	10.31	1.36	1.18	0.77	0.0201	0.0147	0.0106	0.0275	0.0201	0.0145	0.0620
15	-13.5	0	5.4	9.88	9.71	9.68	1.71	1.67	1.45	0.0225	0.0216	0.0187	0.0308	0.0295	0.0255	0.0857
15-16	-8.1	0	5.4	10.06	10.88	10.58	1.80	1.73	1.51	0.0241	0.0251	0.0212	0.0329	0.0343	0.0290	0.0961
16	-2.7	0	5.4	10.25	12.04	11.48	1.88	1.79	1.57	0.0257	0.0288	0.0239	0.0351	0.0393	0.0327	0.1071
		height		6.2	3.7	1.2	6.2	3.7	1.2				Total Re-Entrainment (%)			2.60

* Inlet area is 63' (74mm in model scale) tall and 45, 46' (54, 55mm) wide

Vertical Distributions of Re-Entrainment Rate

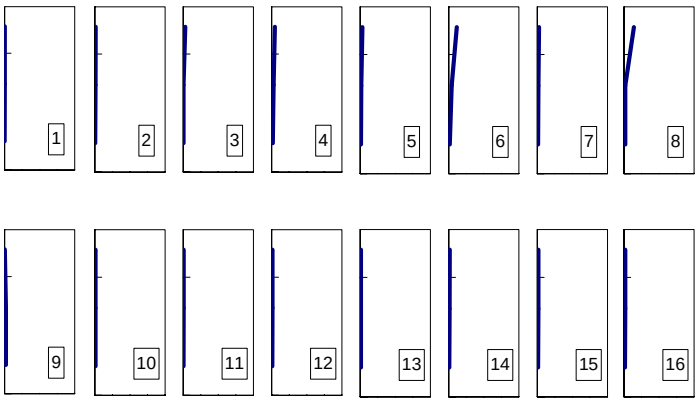

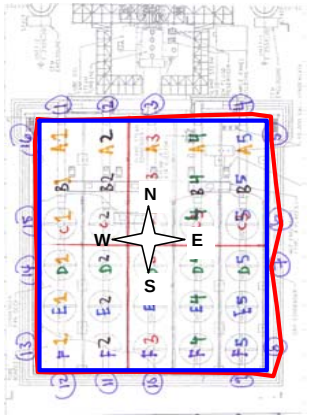

Re-entrainment Level along ACC Boundary

Estimated Contour of R

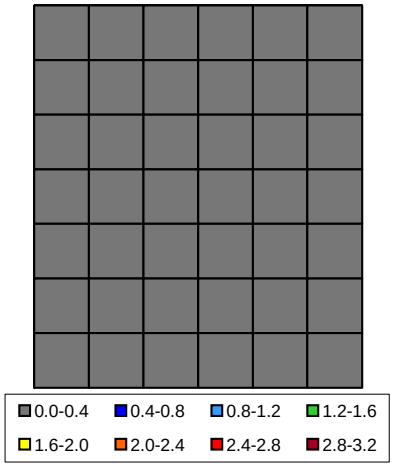

Wind Strength Extreme **Wind Direction** W **Ethan Purity** 98.5

	X	Y	width	Concentration [PPM]			Speed [m/s]			Flux (times million)			Re-Entrainment Rate (%)			
	[cm]	[cm]	[cm]	T	M	B	T	M	B	T	M	B	T	M	B	SUM
1	0	-1.77	5.5	4.41	2.65	1.03	0.64	0.72	0.61	0.0039	0.0026	0.0009	0.0053	0.0035	0.0012	0.0100
2	0	-7.27	5.5	16.64	6.69	4.58	0.73	0.65	0.51	0.0165	0.0059	0.0032	0.0225	0.0081	0.0043	0.0349
3	0	-12.77	5.5	21.88	9.91	7.23	0.71	0.85	0.82	0.0210	0.0114	0.0081	0.0287	0.0156	0.0110	0.0553
3-4	0	-19.25	5.5	106.09	10.91	8.71	0.56	0.81	0.69	0.0803	0.0120	0.0082	0.1096	0.0164	0.0111	0.1371
4	0	-25.73	5.5	190.30	11.91	10.19	0.41	0.77	0.56	0.1054	0.0125	0.0077	0.1440	0.0170	0.0105	0.1716
5	-2.7	-27.5	5.4	25.25	12.77	12.26	0.99	0.83	0.28	0.0334	0.0141	0.0046	0.0456	0.0192	0.0063	0.0711
5-6	-8.1	-27.5	5.4	132.90	41.66	16.09	0.71	0.79	0.97	0.1256	0.0437	0.0208	0.1715	0.0596	0.0285	0.2596
6	-13.5	-27.5	5.4	240.54	70.55	19.92	0.43	0.75	1.66	0.1365	0.0702	0.0441	0.1864	0.0959	0.0603	0.3426
7	-18.9	-27.5	5.4	596.64	412.82	265.34	0.50	0.40	0.36	0.3947	0.2190	0.1289	0.5390	0.2991	0.1760	1.0141
7-8	-24.3	-27.5	5.4	542.48	357.97	233.38	0.52	0.45	0.37	0.3743	0.2136	0.1156	0.5111	0.2917	0.1579	0.9607
8	-29.7	-27.5	5.4	488.32	303.12	201.42	0.54	0.50	0.38	0.3507	0.2009	0.1018	0.4790	0.2743	0.1390	0.8923
9	-32.4	-25.73	5.5	194.94	237.74	179.02	0.43	0.37	0.31	0.1148	0.1193	0.0747	0.1567	0.1629	0.1021	0.4217
9-10	-32.4	-19.25	5.5	110.16	133.36	103.43	0.47	0.33	0.25	0.0696	0.0602	0.0350	0.0951	0.0822	0.0479	0.2252
10	-32.4	-12.77	5.5	25.38	28.98	27.84	0.50	0.30	0.19	0.0171	0.0116	0.0072	0.0234	0.0159	0.0099	0.0492
11	-32.4	-7.27	5.5	31.29	16.63	18.11	1.00	0.98	1.10	0.0423	0.0220	0.0270	0.0578	0.0301	0.0369	0.1248
12	-32.4	-1.77	5.5	33.52	18.95	18.39	0.86	0.82	0.78	0.0392	0.0210	0.0196	0.0535	0.0287	0.0267	0.1089
13	-29.7	0	5.4	18.82	16.74	19.36	2.09	1.94	1.64	0.0524	0.0432	0.0422	0.0715	0.0591	0.0576	0.1882
13-14	-24.3	0	5.4	18.68	18.19	19.51	2.02	1.89	1.57	0.0503	0.0457	0.0407	0.0687	0.0625	0.0556	0.1867
14	-18.9	0	5.4	18.54	19.63	19.66	1.95	1.84	1.50	0.0483	0.0480	0.0392	0.0659	0.0656	0.0535	0.1850
15	-13.5	0	5.4	18.39	18.05	20.42	1.88	1.81	1.44	0.0461	0.0435	0.0391	0.0630	0.0594	0.0534	0.1758
15-16	-8.1	0	5.4	19.08	18.79	19.50	1.90	1.88	1.51	0.0482	0.0470	0.0393	0.0659	0.0641	0.0537	0.1837
16	-2.7	0	5.4	19.77	19.53	18.58	1.91	1.94	1.59	0.0504	0.0506	0.0393	0.0688	0.0691	0.0537	0.1916
		height		6.2	3.7	1.2	6.2	3.7	1.2				Total Re-Entrainment (%)			5.99

* Inlet area is 63' (74mm in model scale) tall and 45, 46' (54, 55mm) wide

Vertical Distributions of Re-Entrainment Rate

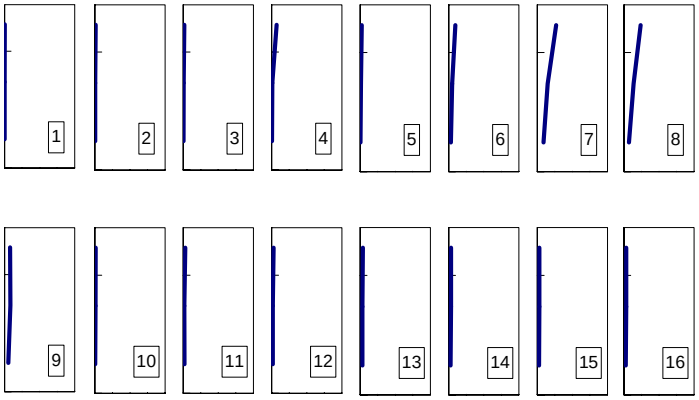

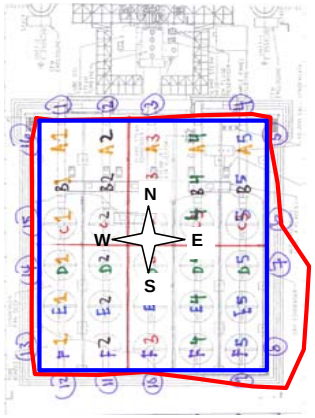

Re-entrainment Level along ACC Boundary

Estimated Contour of R

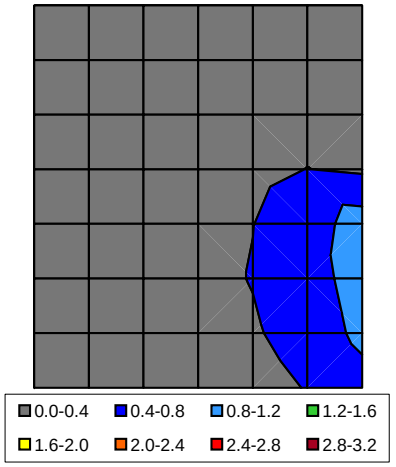

Wind Strength Extreme **Wind Direction** N **Ethan Purity** 98.5

	X	Y	width	Concentration [PPM]			Speed [m/s]			Flux (times million)			Re-Entrainment Rate (%)			
	[cm]	[cm]	[cm]	T	M	B	T	M	B	T	M	B	T	M	B	SUM
1	0	-1.77	5.5	3.40	1.64	0.56	1.24	0.55	1.11	0.0057	0.0012	0.0008	0.0078	0.0017	0.0011	0.0106
2	0	-7.27	5.5	5.97	4.99	3.65	2.22	2.09	0.51	0.0180	0.0141	0.0025	0.0246	0.0193	0.0035	0.0474
3	0	-12.77	5.5	8.64	8.39	8.51	2.00	1.53	1.12	0.0235	0.0174	0.0129	0.0320	0.0237	0.0177	0.0734
3-4	0	-19.25	5.5	10.03	9.76	9.70	1.38	1.14	0.98	0.0188	0.0151	0.0128	0.0257	0.0207	0.0175	0.0639
4	0	-25.73	5.5	11.42	11.14	10.88	0.76	0.76	0.83	0.0118	0.0115	0.0123	0.0161	0.0157	0.0168	0.0486
5	-2.7	-27.5	5.4	65.31	13.85	11.96	0.73	0.46	0.43	0.0633	0.0084	0.0068	0.0864	0.0115	0.0093	0.1072
5-6	-8.1	-27.5	5.4	103.95	21.04	13.31	0.60	0.48	0.44	0.0835	0.0133	0.0078	0.1140	0.0182	0.0107	0.1429
6	-13.5	-27.5	5.4	142.58	28.24	14.67	0.48	0.49	0.45	0.0909	0.0186	0.0089	0.1241	0.0254	0.0121	0.1616
7	-18.9	-27.5	5.4	137.00	34.06	16.79	0.61	0.51	0.60	0.1106	0.0232	0.0135	0.1511	0.0317	0.0184	0.2011
7-8	-24.3	-27.5	5.4	263.04	98.90	28.66	0.81	0.77	0.86	0.2840	0.1019	0.0329	0.3879	0.1392	0.0449	0.5719
8	-29.7	-27.5	5.4	389.09	163.74	40.54	1.02	1.04	1.12	0.5262	0.2260	0.0605	0.7185	0.3086	0.0826	1.1097
9	-32.4	-25.73	5.5	495.66	170.29	50.06	0.94	1.38	1.41	0.6327	0.3177	0.0955	0.8640	0.4338	0.1304	1.4281
9-10	-32.4	-19.25	5.5	440.20	222.25	77.42	0.87	1.09	1.08	0.5178	0.3289	0.1137	0.7071	0.4491	0.1552	1.3115
10	-32.4	-12.77	5.5	384.75	274.22	104.78	0.79	0.81	0.76	0.4140	0.3000	0.1079	0.5654	0.4096	0.1474	1.1224
11	-32.4	-7.27	5.5	510.67	243.03	56.72	0.57	0.49	0.40	0.3960	0.1600	0.0311	0.5408	0.2185	0.0424	0.8017
12	-32.4	-1.77	5.5	300.63	155.71	59.22	0.86	1.11	1.14	0.3512	0.2355	0.0913	0.4796	0.3216	0.1246	0.9259
13	-29.7	0	5.4	282.26	159.84	50.92	0.86	0.89	0.91	0.3221	0.1903	0.0620	0.4399	0.2598	0.0847	0.7843
13-14	-24.3	0	5.4	189.50	99.31	37.02	0.72	0.73	0.73	0.1817	0.0965	0.0360	0.2481	0.1318	0.0492	0.4291
14	-18.9	0	5.4	96.73	38.78	23.12	0.58	0.57	0.55	0.0751	0.0292	0.0169	0.1026	0.0399	0.0230	0.1655
15	-13.5	0	5.4	153.15	49.22	22.28	0.52	0.50	0.41	0.1052	0.0330	0.0121	0.1436	0.0451	0.0166	0.2053
15-16	-8.1	0	5.4	104.22	35.41	21.91	0.54	0.54	0.37	0.0755	0.0253	0.0107	0.1031	0.0346	0.0146	0.1523
16	-2.7	0	5.4	55.28	21.60	21.54	0.57	0.57	0.32	0.0421	0.0164	0.0093	0.0575	0.0224	0.0126	0.0926
		height		6.2	3.7	1.2	6.2	3.7	1.2				Total Re-Entrainment (%)			9.96

* Inlet area is 63' (74mm in model scale) tall and 45, 46' (54, 55mm) wide

Vertical Distributions of Re-Entrainment Rate

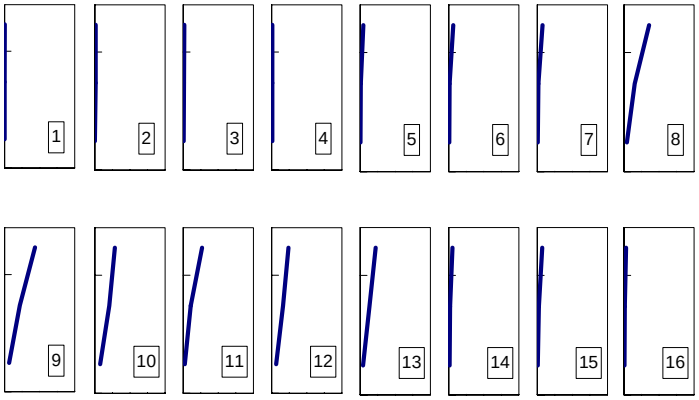

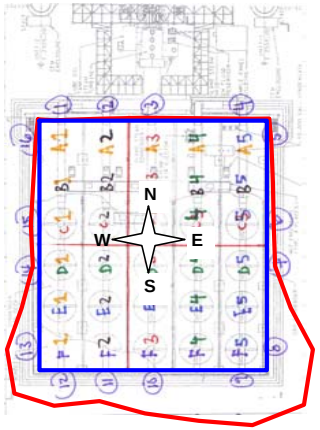

Re-entrainment Level along ACC Boundary

Estimated Contour of R

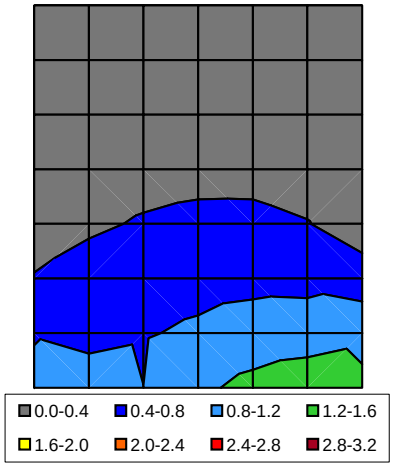

Appendix – B Testing Results of the Dual Unit Base Model

Wind Strength Moderate Unit Distance Near Ethan Purity 98.5

	X [cm]	Y [cm]	width [cm]	Concentration [PPM] T	M	B	Speed [m/s] T	M	B	Flux (times million) T	M	B	Re-Entrainment Rate (%) T	M	B	SUM
1	0	-1.905	5.4	31.56	20.94	38.95	2.30	2.12	1.91	0.0966	0.0592	0.0990	0.1609	0.0986	0.1648	0.4243
2	0	-8.895	5.4	32.38	21.30	38.30	2.31	1.87	1.25	0.0998	0.0530	0.0639	0.1662	0.0882	0.1064	0.3608
3	0	-14.295	5.4	23.88	23.04	34.00	2.13	1.59	1.80	0.0678	0.0487	0.0816	0.1130	0.0811	0.1358	0.3299
4	-2.75	-16.2	5.5	36.02	18.89	33.56	1.64	1.19	1.24	0.0802	0.0306	0.0566	0.1335	0.0509	0.0942	0.2787
5	-8.25	-16.2	5.5	48.15	14.74	33.11	1.15	0.80	0.69	0.0751	0.0160	0.0308	0.1250	0.0267	0.0513	0.2030
6	-13.75	-16.2	5.5	268.00	18.14	32.97	1.20	0.94	0.80	0.4366	0.0231	0.0357	0.7270	0.0384	0.0594	0.8248
7	-19.25	-16.2	5.5	299.25	42.35	34.73	1.17	1.20	1.08	0.4767	0.0690	0.0510	0.7938	0.1149	0.0850	0.9936
8	-21.6	-13.5	5.4	330.49	66.56	36.49	1.15	1.46	1.37	0.5052	0.1298	0.0665	0.8412	0.2161	0.1108	1.1681
9	-21.6	-8.1	5.4	31.19	19.02	38.00	1.10	1.16	1.06	0.0459	0.0295	0.0537	0.0764	0.0491	0.0894	0.2148
10	-21.6	-2.7	5.4	181.34	235.80	212.57	0.98	1.22	1.06	0.2367	0.3836	0.2996	0.3941	0.6387	0.4989	1.5318
11	-19.25	0	5.5	331.49	452.58	387.13	0.86	1.28	1.06	0.3850	0.7850	0.5548	0.6411	1.3072	0.9238	2.8720
12	-13.75	0	5.5	974.84	805.56	176.75	1.25	0.92	0.93	1.6550	1.0012	0.2230	2.7558	1.6671	0.3712	4.7942
13	-8.25	0	5.5	517.12	412.62	108.47	1.37	0.87	0.79	0.9637	0.4874	0.1156	1.6046	0.8116	0.1924	2.6086
14	-2.75	0	5.5	59.40	19.69	40.20	1.50	0.83	0.64	0.1205	0.0220	0.0349	0.2007	0.0367	0.0582	0.2956
		height		6.2	3.7	1.2	6.2	3.7	1.2				Total Re-Entrainment (%)			16.90

* Inlet area is 63' (74mm in model scale) tall and 45, 46' (54, 55mm) wide

Vertical Distributions of Re-Entrainment Rate

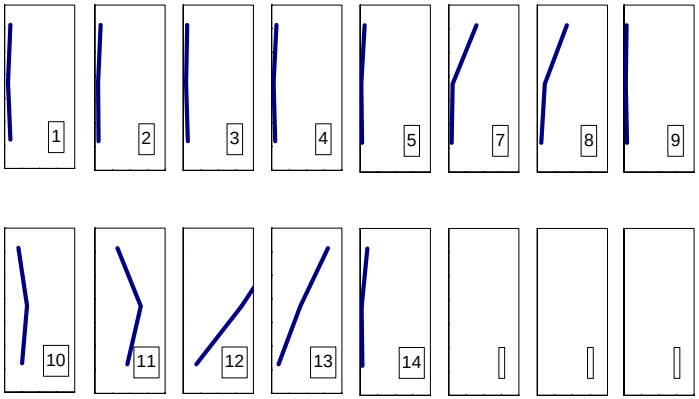

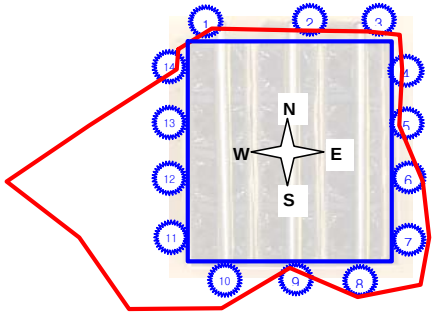

Re-entrainment Level along ACC Boundary

Estimated Contour or R

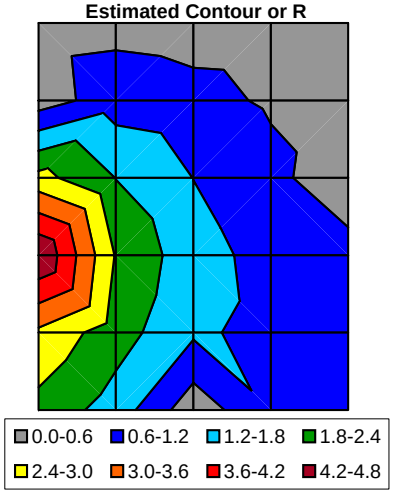

Wind Strength Moderate Unit Distance Middle Ethan Purity 98.5

	X [cm]	Y [cm]	width [cm]	Concentration [PPM] T	M	B	Speed [m/s] T	M	B	Flux (times million) T	M	B	Re-Entrainment Rate (%) T	M	B	SUM
1	0	-1.905	5.4	0.52	3.63	13.07	2.16	1.77	1.46	0.0015	0.0086	0.0254	0.0025	0.0142	0.0423	0.0591
2	0	-8.895	5.4	0.47	6.07	14.88	2.18	1.09	0.69	0.0014	0.0088	0.0137	0.0023	0.0147	0.0228	0.0398
3	0	-14.295	5.4	1.61	0.25	6.31	2.03	0.55	0.43	0.0043	0.0002	0.0036	0.0072	0.0003	0.0060	0.0136
4	-2.75	-16.2	5.5	1.74	0.18	8.28	1.61	0.70	0.57	0.0038	0.0002	0.0064	0.0063	0.0003	0.0107	0.0173
5	-8.25	-16.2	5.5	1.86	0.12	10.24	1.19	0.84	0.71	0.0030	0.0001	0.0099	0.0050	0.0002	0.0165	0.0218
6	-13.75	-16.2	5.5	154.68	0.08	9.31	1.19	0.93	0.81	0.2490	0.0001	0.0103	0.4146	0.0002	0.0171	0.4319
7	-19.25	-16.2	5.5	108.32	2.19	10.33	1.29	1.17	1.06	0.1896	0.0035	0.0149	0.3156	0.0058	0.0248	0.3462
8	-21.6	-13.5	5.4	61.96	4.29	11.35	1.39	1.40	1.31	0.1150	0.0080	0.0199	0.1914	0.0133	0.0331	0.2379
9	-21.6	-8.1	5.4	0.66	3.48	11.74	1.11	1.05	0.85	0.0010	0.0049	0.0133	0.0016	0.0081	0.0222	0.0319
10	-21.6	-2.7	5.4	208.24	113.98	21.85	1.03	1.10	0.91	0.2861	0.1664	0.0264	0.4764	0.2771	0.0440	0.7975
11	-19.25	0	5.5	415.82	224.47	31.95	0.95	1.14	0.96	0.5368	0.3475	0.0417	0.8939	0.5786	0.0694	1.5419
12	-13.75	0	5.5	453.60	108.77	13.09	1.14	1.15	0.94	0.7010	0.1699	0.0168	1.1672	0.2828	0.0279	1.4779
13	-8.25	0	5.5	226.95	57.21	13.54	1.17	0.96	0.81	0.3606	0.0744	0.0149	0.6004	0.1239	0.0248	0.7491
14	-2.75	0	5.5	0.30	5.65	14.00	1.20	0.77	0.68	0.0005	0.0059	0.0129	0.0008	0.0098	0.0215	0.0321
		height		6.2	3.7	1.2	6.2	3.7	1.2				Total Re-Entrainment (%)			5.80

* Inlet area is 63' (74mm in model scale) tall and 45,46' (54,55mm) wide

Vertical Distributions of Re-Entrainment Rate

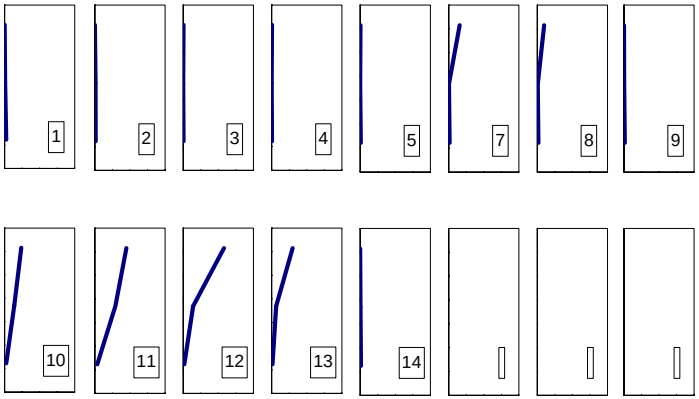

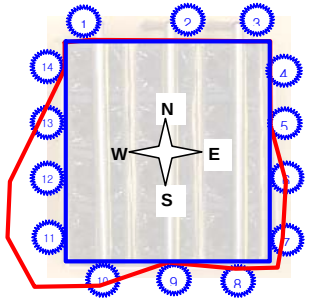

Re-entrainment Level along ACC Boundary

Estimated Contour or R

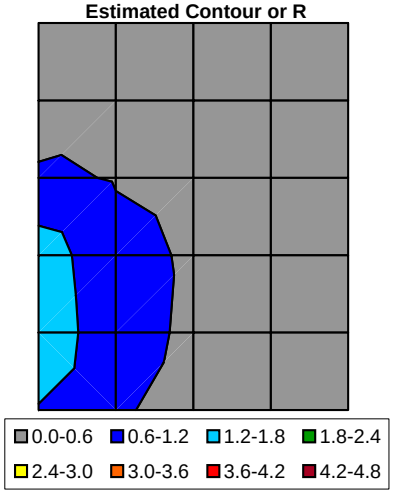

Wind Strength Moderate Unit Distance Far Ethan Purity 98.5

	X [cm]	Y [cm]	width [cm]	Concentration [PPM] T	M	B	Speed [m/s] T	M	B	Flux (times million) T	M	B	Re-Entrainment Rate (%) T	M	B	SUM
1	0	-1.905	5.4	3.61	4.53	6.92	2.14	1.56	1.49	0.0103	0.0094	0.0137	0.0172	0.0157	0.0228	0.0557
2	0	-8.895	5.4	4.88	4.44	5.08	2.27	0.84	0.51	0.0148	0.0049	0.0035	0.0246	0.0082	0.0058	0.0386
3	0	-14.295	5.4	0.88	0.93	0.88	1.92	0.58	0.39	0.0022	0.0007	0.0005	0.0037	0.0012	0.0008	0.0057
4	-2.75	-16.2	5.5	2.89	0.84	0.77	1.54	0.71	0.57	0.0060	0.0008	0.0006	0.0101	0.0013	0.0010	0.0124
5	-8.25	-16.2	5.5	4.91	0.75	0.65	1.16	0.84	0.75	0.0077	0.0009	0.0007	0.0129	0.0014	0.0011	0.0154
6	-13.75	-16.2	5.5	141.48	0.45	0.65	1.16	0.92	0.82	0.2219	0.0006	0.0007	0.3694	0.0009	0.0012	0.3716
7	-19.25	-16.2	5.5	116.71	1.64	0.44	1.30	1.17	1.06	0.2064	0.0026	0.0006	0.3436	0.0043	0.0010	0.3490
8	-21.6	-13.5	5.4	91.94	2.83	0.22	1.45	1.41	1.30	0.1777	0.0053	0.0004	0.2958	0.0089	0.0006	0.3053
9	-21.6	-8.1	5.4	1.55	1.30	0.00	1.19	1.09	0.93	0.0024	0.0019	0.0000	0.0041	0.0032	0.0000	0.0072
10	-21.6	-2.7	5.4	181.12	80.03	3.38	1.13	1.16	0.95	0.2729	0.1232	0.0043	0.4543	0.2052	0.0071	0.6667
11	-19.25	0	5.5	360.69	158.76	6.76	1.08	1.22	0.97	0.5269	0.2623	0.0089	0.8773	0.4367	0.0149	1.3289
12	-13.75	0	5.5	359.56	63.32	1.22	1.35	1.25	0.99	0.6598	0.1072	0.0016	1.0987	0.1784	0.0027	1.2798
13	-8.25	0	5.5	183.97	32.87	1.67	1.30	1.06	0.87	0.3238	0.0474	0.0020	0.5392	0.0789	0.0033	0.6214
14	-2.75	0	5.5	8.37	2.41	2.12	1.24	0.88	0.76	0.0141	0.0029	0.0022	0.0235	0.0048	0.0036	0.0319
	height			6.2	3.7	1.2	6.2	3.7	1.2				Total Re-Entrainmet (%)			5.09

* Inlet area is 63' (74mm in model scale) tall and 45, 46' (54, 55mm) wide

Vertical Distributions of Re-Entrainment Rate

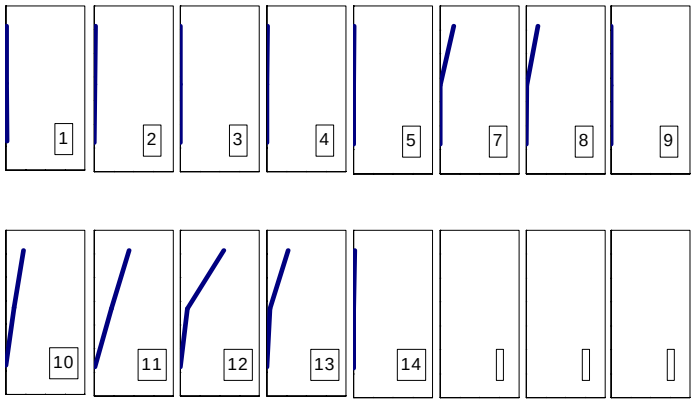

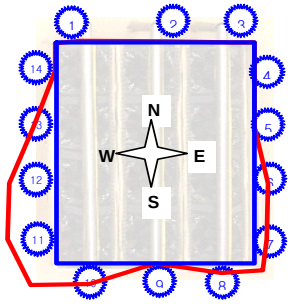

Re-entrainment Level along ACC Boundary

Estimated Contour or R